ISSN: 2764-5886
e-ISSN: 2764-622X

Volume 9· Nº 3 · March 2026

Journal of Bioengineering, Technologies and Health

An Official Publication of
SENAI CIMATEC

ISSN: 2764-5886 / e-ISSN 2764-622X

Volume 9 • Number 3 • March 2026

JOURNAL OF BIOENGINEERING TECHNOLOGIES AND HEALTH

An Official Publication of SENAI CIMATEC

PUBLISHED BY SENAI CIMATEC

Sistema FIEB | SENAI CIMATEC
PELO FUTURO DA INOVAÇÃO

March 2026
Printed in Brazil

JOURNAL OF BIOENGINEERING TECHNOLOGIES AND HEALTH

An Official Publication of SENAI CIMATEC

JOURNAL OF BIOENGINEERING TECHNOLOGIES AND HEALTH

Volume 9 • Number 3 **SUMMARY** *March 2026*

Original Articles

Systematic Review

Instructions for Authors

Statement of Editorial Policy

Checklist for Submitted Manuscripts

The Journal of Bioengineering, Technologies and Health (JBTH) is an official publication of the SENAI CIMATEC University (Serviço Nacional de Aprendizagem Industrial - Universidade Centro Integrado de Manufatura e Tecnologia). It is published montly (January to December) in English by SENAI CIMATEC University – Avenida Orlando Gomes, 1845, Piatã, Zip Code: 41650-010, Salvador-Bahia-Brazil; phone: (55 71) 3879-5501. The editorial offices are at SENAI CIMATEC University.

Editorial Office

Correspondence concerning subscriptions, advertisements, claims for missing issues, changes of address, and communications to the editors should be addressed to the Deputy Editor, Dr. Roberto Badaró, SENAI CIMATEC University (Journal of Bioengineering, Technologies and Health – JBTH) – Avenida Orlando Gomes, 1845, Piatã, Zip code: 41650-010, Salvador-Bahia-Brazil; phone: (55 71) 3879-5501; or sent by e-mail: jbth@fieb.org.br / jbth.cimatec@gmail.com.

Permissions

Postmaster

Send address changes to JBTH, Avenida Orlando Gomes, 1845, Piatã, Zip Code: 41650-010, Salvador-Bahia-Brazil.

Information by JBTH-SENAI CIMATEC University
Address: Avenida Orlando Gomes, 1845, Piatã, Zip Code: 41650-010, Salvador-Bahia-Brazil
Home-page: www.jbth.com.br
E-mail: jbth@fieb.org.br / jbth.cimatec@gmail.com
Phone: (55 71) 3879-5501 / 3879-5500 / 3879-9500

DOI:10.34178

ISSN: 2764-5886 / e-ISSN 2764-622X

COVER: Figure 1. Sample collection points in the municipality of Itabuna – BA. Urban Air Quality: Occurrence, Emission Sources and Risk Assessment of Polycyclic Aromatic Hydrocarbons (PAHs) in Airborne Fine Particles by Aldenor Gomes Santos et al. J Bioeng. Tech. Health 2026;9(3):232.

Energy Potential of Biomethane from Municipal Solid Waste in Brazilian Cities Using an Adjusted LandGEM Approach

Luciano Sergio Hocevar[1]*, Paulo Roberto dos Reis Santana[2], Luzia Aparecida Tofaneli[2], Carine Tondo Alves[1], Alex Álisson Bandeira Santos[2]

[1]UFRB Federal University of Reconcavo da Bahia; Feira de Santana, Bahia;
[2]SENAI CIMATEC University; Salvador, Bahia, Brazil

Sanitary landfills for municipal solid waste (MSW) represent a significant and still underutilized source of renewable energy, especially in developing countries where disposal in dumpsites and landfills remains the primary form of final waste disposition. Brazil presents favorable conditions for the utilization of landfill biomethane due to the high organic matter content of its MSW and its tropical climate, which intensifies anaerobic degradation rates. This study evaluates methane generation and the energy recovery potential associated with MSW disposal in two Brazilian municipalities — Salvador and Feira de Santana — using a first-order decay model based on the LandGEM methodology from the United States Environmental Protection Agency (USEPA). Model parameters were adjusted to Brazilian conditions, adopting a methane generation potential (L_0) of 170 m^3 CH_4/Mg MSW and a decay constant (k) of 0.05 yr^{-1} for both Feira de Santana (tropical climate) and Salvador (tropical super-humid climate), both classified as non-arid according to the LandGEM criterion. Historical waste collection data and future projections, assuming an annual growth rate of 5%, were used to estimate methane generation until 2062 for Salvador and until 2075 for Feira de Santana, adopting the 80-year operational lifetime established by LandGEM. The results indicate a peak methane generation of 2.5×10^8 m^3 CH_4/year and a total of 5.9×10^9 m^3 CH_4 for the analyzed period, corresponding to electricity generation potentials of 49 MW. This demonstrates that landfill biomethane utilization can significantly contribute to Brazil's renewable energy matrix, substituting natural gas, and highlights the importance of integrating waste-to-energy solutions into national energy policies.
Keywords: Landfill Gas. Municipal Solid Waste. Biomethane. Renewable Energy. Greenhouse Gases. Brazil.

Municipal solid waste (MSW) management remains one of the main environmental and socioeconomic challenges on a global scale, particularly in rapidly urbanizing regions of developing countries. Despite advances in recycling and material recovery, disposal in sanitary landfills continues to be the primary form of final waste disposition in many countries.

One of the main environmental concerns associated with landfills is the generation of methane (CH_4), considered a potent greenhouse gas (GHG) with a global warming potential 25 times greater than that of carbon dioxide (CO_2) over a 100-year period [1].

Received on 21 December 2025; revised 22 February 2026.
Address for correspondence: Luciano Sergio Hocevar. UFRB – Federal University of Reconcavo da Bahia. Av. Centenário, 697 - SIM. Zipcode:44085-132. Feira de Santana, Bahia. Brazil. E-mail: lucianohocevar@ufrb.edu.br.

J Bioeng. Tech. Health 2026;9(3):185-193

However, the utilization of methane for energy generation presents beneficial environmental and economic effects. The combustion of methane (CH_4) produces heat, water, and CO_2. From an environmental perspective, burning methane to generate energy reduces GHG emissions due to methane's global warming potential being higher than that of CO_2 [2]. The combustion of methane in the energy generation process is sustainable from a GHG standpoint, as it substantially reduces CO_2-equivalent emissions into the atmosphere. From an economic viewpoint, biomethane produced in sanitary landfills is a fuel that can substitute natural gas (NG), with the advantage of being renewable (Renewable Natural Gas - RNG) and produced from residual raw material (MSW).

Methane emissions from landfills result from the anaerobic decomposition of the biodegradable organic fraction present in MSW. According to the Intergovernmental Panel on Climate Change (IPCC), landfills account for a relevant portion of global anthropogenic methane emissions, making them a

strategic target for mitigation actions. At the same time, landfill biomethane constitutes a valuable energy resource that can be recovered and converted into electricity, heat, or purified to biomethane for injection into natural gas networks or use as vehicle fuel [2,3].

Brazil presents a particularly favorable context for landfill biomethane utilization. The country's municipal solid waste is characterized by a high organic matter content, typically between 45% and 55% [2,4], combined with climatic conditions of high temperature and humidity. These factors accelerate biodegradation processes and increase methane generation rates compared to temperate climate regions. Despite this potential, landfill biomethane energy recovery projects in Brazil are still few and concentrated mainly in large metropolitan regions.

Quantifying the energy and greenhouse gas (GHG) mitigation potential of sanitary landfills is essential to support investment decisions, public policy formulation, and the integration of waste-to-energy solutions into national energy planning. Although several studies have applied first-order decay models to estimate methane generation in landfills, there is still a lack of analyses that explicitly adjust model parameters to Brazilian conditions and compare the potential between cities of different sizes.

In this context, the present study evaluates methane generation, energy recovery, and carbon mitigation potential associated with MSW disposal in the two most populous municipalities in the state of Bahia, in northeastern Brazil, located about 100 km apart: Salvador, the state capital and one of the country's largest metropolises, and Feira de Santana, a medium-sized rapidly growing city and the second most populous in the state. Applying an approach based on the Landfill Gas Emissions Model - LandGEM [5] provides relevant technical insights into the role of landfill biomethane utilization in both large urban centers and medium-sized cities.

Biomethane

Biomethane is derived from the purification of biogas, the raw gas obtained from the biological decomposition of organic waste, according to Resolution 886/2022 of the National Agency of Petroleum, Natural Gas and Biofuels - ANP (Agência Nacional de Petróleo) [6]. Biomethane, therefore, has a high methane content in its composition and possesses properties that make it a substitute for natural gas in all its applications. Being renewable in origin, it is a substitute for fossil-derived Natural Gas (NG), hence also called Renewable Natural Gas (RNG).

The production of methane for energy purposes is mainly carried out from residual biomass from sanitary and agricultural landfills, which allow for continuous and sustainable production, contributing to clean energy generation and GHG emission mitigation [7].

A sanitary landfill is generally conceptualized as a giant biochemical reactor, where waste and water are the main inputs, while gas ("biogas") and leachate are the main outputs [8].

Methane production aimed at substituting NG requires biogas purification, a process that reduces concentrations of moisture, CO_2, and other substances, resulting in a methane-rich gas whose physical and chemical properties are like those of NG.

Biomethane can be marketed as compressed natural gas (CNG) or liquefied natural gas (LNG), and can be widely used in domestic, industrial, and vehicular sectors. The commercialization of biomethane is permitted for different actors, including state piped NG concessionaires and authorized distributors. This flexibility of use and commercialization, combined with its environmental advantages, makes biomethane a strategic fuel in the transition towards a more sustainable energy matrix and in strengthening the circular economy in Brazil [9].

Biomethane is a renewable fuel that contributes to GHG emission mitigation. Its production from organic waste prevents the release into the atmosphere of methane (CH_4), a gas with a global warming potential 28 times greater than that of carbon dioxide (CO_2) [10].

Energy Properties of Biomethane

In energy terms, 1 Nm³ of biomethane is equivalent to 1 liter of diesel [11], with the advantage of being produced domestically from residual biomass and not being subject to the international price volatility of petroleum-derived fossil fuels traded in foreign currencies, such as diesel.

The Higher Heating Value (HHV) of biomethane is equivalent to the HHV of Natural Gas, ranging from [9.5 to 11.9\] kWh/m³, according to ANP Resolution 866/2022 [6].

Considering that 1 ton of oil equivalent (toe) equals 11,630 kWh, the HHV of biomethane ranges from [0.0008 to 0.001] toe/m³.

Mathematical Models for Estimating Methane Generation

The use of mathematical models allows for the assessment of the landfill's biomethane generation potential, the necessary adequate infrastructure, and the project's energy yield capacity. Modeling is an estimate where some parameters may be presumed and, in these cases, a simple mathematical model is preferable, one that uses few parameters concerning specific site conditions that can be reliable and easily obtained [12].

According to Gallego and colleagues [2] and Barros [13], several software tools exist for predicting biogas generation in a sanitary landfill, including:

- Biogas, Generation and Energy Use Landfills, version 1.0 [14].
- E-PLUS - Landfill Gas, version 1.0 (USEPA).
- IPCC - National Greenhouse Gas Inventories Programme (IPCC).
- LandGEM®, version 3.1 (USEPA).
- Scholl Canyon Model (World Bank).

Mathematical models have been developed to estimate landfill biomethane emissions based on waste disposal data, waste composition, moisture content, landfill cover material, and biogas collection [15]. A significant number of models have been developed and attracted the attention of many researchers in the field, including, but not limited to, the IPCC default model, the modified triangular method (MTM), the Dutch multiphase first-order model, AMPM, GASSFILL, the Scholl Canyon first-order model, the Rettenberger first-order model, the E-PLUS model, the German EPER zero-order model, the IPCC first-order model, the US EPA Landfill Biomethane Emissions Model (LandGEM). Among these, LandGEM is widely used to assess biomethane and other air pollutants from the decomposition of waste in sanitary landfills. The model was initially developed in 2005 by the US EPA based on a first-order decay (FOD) rate [16].

In the present work, we use the LandGEM landfill biogas emissions model to estimate the CH_4 generation potential.

Materials and Methods

Methane Generation Model

Methane generation from MSW disposal was estimated using a first-order decay (FOD) model consistent with LandGEM, developed by the United States Environmental Protection Agency – USEPA [17]. LandGEM is a Microsoft Excel spreadsheet (.xlsm) with enabled macros that utilizes Visual Basic for Applications (VBA) processes to function. The model assumes that methane generation follows an exponential first-order decay function, reflecting the progressive degradation of organic matter over time.

The annual methane generation rate is calculated by summing the contributions of waste deposited in previous years [5], according to Equation 1:

$$Q_{CH_4} = \sum_{i=1}^{n} \sum_{j=0.1}^{1} kL_0 \left(\frac{M_i}{10}\right) e^{-kt_{i,j}} \quad (1)$$

Where:

Q_{CH4} is the annual methane generation rate in the calculation year (m³/year).

i is the 1-year time increment.

n is (year of calculation) - (initial year of waste acceptance).
j is the 0.1-year time increment.
k is the methane generation rate constant (yr^{-1}).
L_0 is the methane generation potential (m^3 CH_4/ Mg MSW).
M_i is the mass of waste accepted in the i-th year (Mg).
t_{ij} is the age of the ***j-th*** section of waste mass M_i accepted in the ***i-th*** year (decimal years, e.g., 3.2 years).

Parameter Adjustment to Brazilian Conditions

The default LandGEM parameters are predominantly based on waste composition and climatic conditions typical of the United States. To better represent Brazilian conditions, the model parameters were adjusted based on IPCC guidelines [18] and national waste composition data.

Methane Generation Rate Constant (*k*)

The Methane Generation Rate constant, *k*, determines the waste decomposition rate and the associated methane generation from the landfill. The value *k*, as used in the first-order decay rate equation, is in units of inverse years (i.e., 1/year or yr^{-1}). The higher the value of *k*, the faster methane generation occurs and the more quickly it will dissipate [19,20]. The rate constant can be translated into a half-life, as shown in Equation 2. In this case, the half-life represents the amount of time required for the remaining degradable carbon to decrease by 50% (i.e., step 1 = 50% of original carbon degraded, step 2 = 75%, step 3 = 87.5%, and so on).

$$t_{1/2} = \frac{\ln 2}{k} \quad (2)$$

Where:
$t_{1/2}$ is the half-life of biodegradable carbon and *ln 2* is the natural logarithm of 2 (approximately 0.693).

The observed rate of decomposition has been linked to several factors, such as waste composition, moisture content of the waste mass, nutrient availability for microorganisms decomposing the waste, and temperature of the waste mass [21-23].

In LandGEM, *k* is linked to landfill moisture, considering both local precipitation and operational practices such as leachate recirculation or addition and solidification of wastewater liquids. Generally, areas receiving more precipitation are found to have higher methane generation rates [19,20,24].

Methane Generation Potential (L_0)

The Methane Generation Potential (L_0) depends solely on the composition of the waste deposited in the landfill. Anaerobically biodegradable components of waste, such as cellulose, hemicellulose, fats/ lipids, and proteins, are broken down by microbes in a sequence that ultimately produces methane (CH_4) and carbon dioxide (CO_2) gases [5]. The higher the content of these components within the bulk waste mass, the higher the L_0 value. In the LandGEM first-order decay rate equation, L_0 is measured in metric units of cubic meters per megagram of waste [25].

Based on the LandGEM Manual, a decay constant $\boldsymbol{k = 0.05\ yr^{-1}}$ was adopted for Feira de Santana and Salvador (Table 1).

The climate of Feira de Santana is tropical (As) and that of Salvador is tropical super-humid (Af), according to the Köppen-Geiger climate classification [26]. Both cities are classified as "non-arid" according to the LandGEM criterion.

The methane generation potential was set at $\boldsymbol{L_0 = 170\ m^3\ CH_4/Mg\ MSW}$, a value compatible with the high organic matter content of Brazilian MSW, as reported by the Brazilian Association of Public Cleaning and Waste Companies - ABRELPE [27].

Table 1. Parameters and values for the NSPS applicability model.

Parameters	Unity	Non-Arid
k	$year^{-1}$	0.05
L_0	m^3 CH_4·/ Mg MSW	170
Methane Content	% biogas	50

Source: LandGEM Manual, Table 3 (p. 20).

In this context, "Arid" means geographical areas with 30-year average annual precipitation less than 25 inches, as measured at the nearest representative official meteorological site [25], which is not the case for either municipality studied.

Study Areas and Waste Data

In this study, we chose the two most populous cities in the state of Bahia, in the northeast region of the country, equipped with sanitary landfills and with biomethane utilization projects for energy purposes either implemented or under implementation: Salvador, the state capital and one of the most populous metropolises in the country, and Feira de Santana, a medium-sized rapidly growing city and the second most populous in the state.

For Salvador, whose project is already implemented and operating for thermoelectric generation from biogas and under implementation for direct biomethane utilization for energy purposes as renewable natural gas (RNG), MSW collection data were used for a 28-year period, with an average annual collection of 1 million Mg of waste. Despite having detailed data, an annual uniform distribution of collections was assumed to protect the source. Future projections of waste generation were made for the period from 2026 to 2062.

For Feira de Santana, whose project is under implementation for thermoelectric generation, the MSW collection data used was based on an approximate average of 310,000 Mg. Projections were made for the period from 2025 to 2075.

An annual growth rate of 5% for MSW deposition was assumed for both landfills, consistent with population growth, urban expansion, improvement in the population's purchasing power, and the increase in per capita waste generation observed in Brazilian cities.

In both cases, data were obtained from local waste collection service providers and are truthful, but we chose to protect the sources and details of the data that could identify them.

Estimation of Energy and Carbon Mitigation Potential

According to studies by Bueno and colleagues [30], the energy potential of the generated methane was estimated considering a lower heating value of 9.97 kWh/m³ CH_4 and an electrical conversion efficiency of 35%, representative of internal combustion engines widely used in landfill biogas energy utilization plants.

In general terms, the combustion of municipal waste produces fewer greenhouse gas emissions than other technologies, according to information collected by the United States Environmental Protection Agency - EPA (Table 2).

Table 2. Atmospheric emissions from different fuel sources in terms of carbon dioxide equivalent.

Fuel	CO_2 (kg/MWh)*
MSW	460.8
Coal	1,020.1
Oil	758.4
Natural Gas	514.8

* Emissions in kg of CO_2 equivalent per MWh of electricity produced. Source: EPA [28].

Results and Discussion

Methane Generation Profiles

The results indicate distinct methane generation profiles for the two municipalities, driven mainly by differences in the historical stock of disposed waste and future growth trajectories.

Salvador, the state capital and most populous city in Bahia, has approximately 2,500,000 inhabitants, while Feira de Santana, the second most populous city in the state, has about 660,000.00 inhabitants [29].

In Salvador, the large volume of accumulated waste results in sustained methane generation growth over the analyzed period, reaching maximum values above 1.7×10^8 m³ CH_4/year in 2062 and a total of 1.2×10^9 m³ CH_4 for the

period 2013-2062. In Feira de Santana, methane generation grows more gradually due to the smaller population and corresponding lower initial MSW volume. However, the adopted growth rate leads to significant values in the long term, with peaks close to 2.5×10^8 m³ CH_4/year in 2075 and a total of 5.9×10^9 m³ CH_4 for the period 2013-2075.

These results highlight the cumulative effect of continuous waste generation growth in medium-sized cities and the potential to be harnessed for energy purposes.

Energy Recovery Potential

The estimate of maximum power generated at the sanitary landfill was calculated using Equation 3 [13,14,31]:

$$P = \eta \frac{PCI}{860,000} \varepsilon_C Q \quad (MW) \qquad (3)$$

Where:
P is the available power (MW).
Q is the methane flow rate (Nm³/h).
ε_C is the methane capture efficiency (50%).
η is the engine efficiency (35%).
Conversion factor: 1 kcal/h = (1/860,000) MW.
LHV = 8,500 kcal/Nm³ CH_4.

Figure 1 presents the estimated annual methane generation rate for the Salvador (BA) Sanitary Landfill during its useful life, based on the expected MSW deposition over the years and using the LandGEM model with the kinetic parameters presented in Table 3. The methane generation peak occurs in 2062 with 1.7×10^8 m³ CH_4/year, generating a Power of 33 MW (by Equation 3).

Figure 2 presents the estimated annual methane generation rate for the Feira de Santana (BA) Sanitary Landfill during its useful life, based on the expected MSW deposition over the years and using the LandGEM model with the kinetic parameters presented in Table 3. The methane generation peak occurs in 2075 with 2.5×10^8 m³ CH_4/year, generating a Power of 49 MW (by Equation 3).

The estimated methane generation corresponds to a high energy recovery potential in both municipalities. In Salvador, the maximum methane flows result in an available electricity generation potential exceeding 40 MW, sufficient to supply 10,000 households with an average consumption of 150 kWh/month. In Feira de Santana, similar power levels are reached in the long term, demonstrating that medium-sized cities can also economically viabilize landfill biogas energy utilization projects.

The results are consistent with international studies reporting electrical potentials of up to 70 MW for landfills in developing countries [32]. The high organic matter content of Brazilian MSW contributes to higher methane yields, partially compensating for the lower waste volumes in intermediate-sized cities.

The results demonstrate that landfill biogas utilization can and should be considered a central component of integrated waste management and energy planning strategies. In the Brazilian context, the implementation of biogas recovery systems can simultaneously reduce GHG emissions and generate renewable energy.

Conclusions

This study applied an adjusted LandGEM-based approach to evaluate methane generation and the energy recovery potential associated with municipal solid waste (MSW) disposal in the two most populous municipalities in the state of Bahia, in northeastern Brazil, located about 100 km apart: Salvador and Feira de Santana. The results demonstrate that both Salvador, the capital and most populous city in the state of Bahia, and Feira de Santana, the second most populous city in the state, exhibit high potential for the utilization of bioenergy from sanitary landfills. In Salvador, opportunities are immediate and large-scale for bioenergy generation, due to the significant historical waste stock, with a methane generation peak in 2062 of 1.7×10^8 m³ CH_4/year, generating a Power of 33 MW, with energy utilization via a thermoelectric plant already operating since 2011

Figure 1. Estimate of the methane generation rate at the Salvador (BA) Sanitary Landfill.

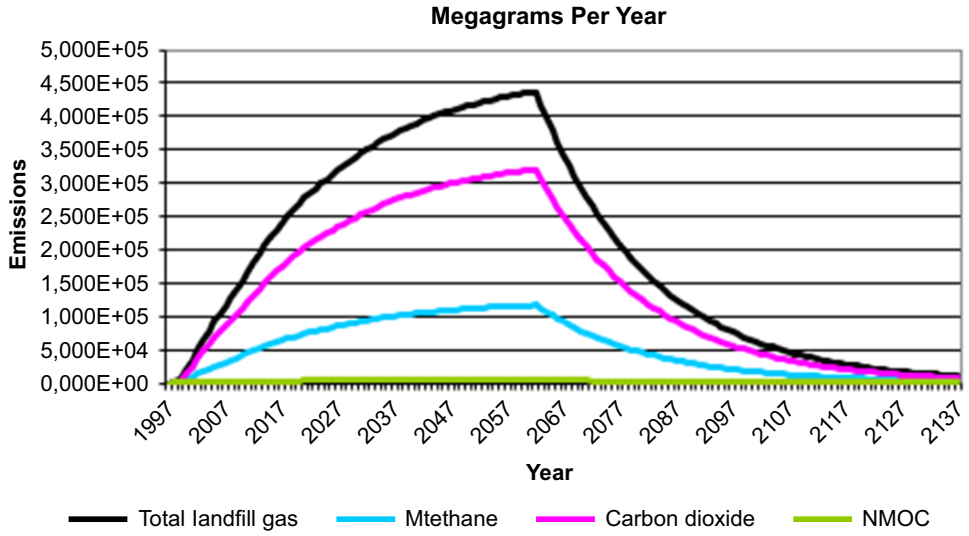

Source: Prepared by the authors based on data entered into LandGEM.

Table 3. Input Data - LandGEM.

Input Review		
LANDFILL CHARACTERISTICS	**Salvador**	**Feira de Santana**
Landfill Open Year	1997	2012
Landfill Closure Year (with 80-year limit)	2062	2075
Actual Closure Year (without limit)	2062	2075
Have Model Calculate Closure Year?	Yes	Yes
Waste Design Capacity [megagrams]		
MODEL PARAMETERS		
Methane Generation Rate, ***k*** [year^{-1}]	0.050	
Potential Methane Generation Capacity, ***Lo*** [m^3/Mg]	170	
NMOC Concentration [ppmv as hexane]	4,000	
Methane Content [% by volume]	50	
GASES / POLLUTANTS SELECTED		
Gas / Pollutant #1	Total landfill gas	
Gas / Pollutant #2	Methane	
Gas / Pollutant #3	Carbon dioxide	
Gas / Pollutant #4	NMOC	

Source: Prepared by the authors based on data entered into LandGEM.

Figure 2. Estimate of the methane generation rate at the Feira de Santana (BA) Sanitary Landfill.

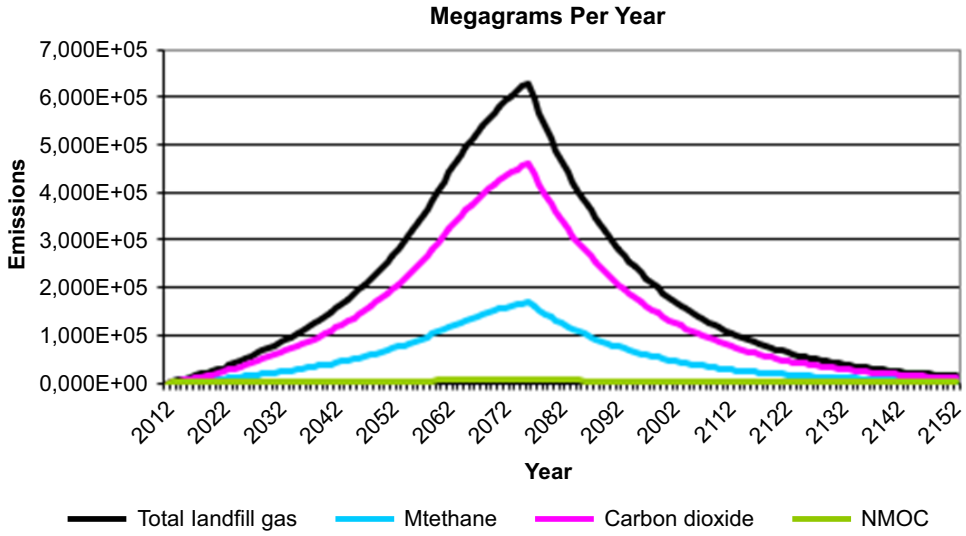

Source: Prepared by the authors based on data entered into LandGEM.

and a biomethane utilization project as RNG in the implementation phase. In Feira de Santana, whose energy utilization project via a thermoelectric plant is still under implementation, the estimated potential reaches comparable levels of biogas generation in the long term due to the continuous growth of waste generation. The methane generation peak occurs in 2075 with 2.5×10^8 m³ CH_4/year, generating a Power of 49 MW. Combined, the generation of the two units totals 82 MW, half the capacity of the Pedra do Cavalo HPP, located in the Feira de Santana region, with significantly lower installation and management costs, in addition to using waste as raw material, contributing to the circular economy, elimination of environmental liabilities, and GHG emissions. The results reinforce the relevance of integrating waste-to-energy into Brazilian energy transition strategies.

Acknowledgment

The authors would like to express their sincere gratitude to SENAI CIMATEC, CNPq and UFRB for its support and provision of researcher resources that greatly contributed to the success of this project.

References

1. Kammann C, Grünhage L, Jäger H, Wachinger G. Methane fluxes from differentially managed grassland study plots: the important role of CH_4 oxidation in grassland with a high potential for CH_4 production. Environ Pollut. 2001. doi:10.1016/S0269-7491(01)00103-8.
2. Gallego AG, et al. Energia do lixo: tecnologias de recuperação energética dos resíduos sólidos urbanos [recurso eletrônico]. Santo André: Universidade Federal do ABC; 2024. 464 p.
3. Konrad O, et al. Atlas das biomassas do Rio Grande do Sul para produção de biogás e biometano. Lajeado: Univates; 2016. 226 p.
4. Coelho ST, Garcilasso VP, Santos MM, Escobar JF, Perecin D, Souza DB. Atlas de bioenergia do Estado de São Paulo [recurso eletrônico]. São Paulo: IEE-USP; 2020. 250 p.
5. Krause M, Thorneloe S. Landfill gas emissions model (LandGEM) version 3.1 user manual and tool. Washington (DC): U.S. EPA; 2024.
6. Agência Nacional do Petróleo, Gás Natural e Biocombustíveis (ANP). Resolução nº 886, de 29 de setembro de 2022. Brasília (DF); 2022. Available at: https://atosoficiais.com.br/anp/resolucao-n-886-2022
7. Hocevar LS, D'Aquino CA, Alves CT, Santos AÁB. Energy use of biomethane: potential, challenges and opportunities in Brazil. Rev Gest Soc Ambient. 2025;19(6):e012707. doi:10.24857/rgsa.v19n6-092.

8. Machado SL, Carvalho MF, Gourc JP, Vilar OM, Nascimento CF. Methane generation in tropical landfills: simplified methods and field results. Waste Manag. 2009;29(1):153–61. doi:10.1016/j.wasman.2008.02.017.
9. Associação Brasileira de Resíduos e Meio Ambiente (ABREMA). Panorama dos resíduos sólidos no Brasil 2024. Available at: https://www.abrema.org.br
10. Lemos GL, Cardoso MFO, Costa HKM. Biogas and biomethane in Brazil: overview and perspectives. Desenvolv Meio Ambient.
11. Empresa de Pesquisa Energética (EPE). Potencial energético dos resíduos urbanos. Rio de Janeiro; 2019.
12. World Bank. Handbook for the preparation of landfill gas to energy projects in Latin America and the Caribbean. Ontario; 2004.
13. Barros RM. Tratado sobre resíduos sólidos: gestão, uso e sustentabilidade. Rio de Janeiro: Interciência; 2012.
14. CETESB. Biogás: projetos e pesquisas no Brasil. São Paulo; 2006.
15. Amini HR, Reinhart DR, Mackie KR. Determination of first-order landfill gas modeling parameters and uncertainties. Waste Manag. 2012;32(2):305–16.
16. Alexander A, Burklin C, Singleton A. Landfill gas emissions model (LandGEM) version 3.02 user's guide. Washington (DC): U.S. EPA; 2005.
17. United States Environmental Protection Agency (USEPA). Air emissions from municipal solid waste landfills. Washington (DC); 1991.
18. IPCC. Guidelines for national greenhouse gas inventories. 2006.
19. Jain P, Wally J, Townsend TG, Krause M, Tolaymat T. Greenhouse gas reporting data improves understanding of regional climate impact on landfill methane production and collection. PLoS One. 2021;16(2):e0246334.
20. Tolaymat TM, Green RB, Hater GR, Barlaz MA, Black P, Bronson D, et al. Evaluation of landfill gas decay constant for municipal solid waste landfills operated as bioreactors. J Air Waste Manag Assoc. 2010;60(1):91–7.
21. De la Cruz FB, Green RB, Hater GR, Chanton JP, Thoma ED, Harvey TA, et al. Comparison of field measurements to methane emissions models at a new landfill. Environ Sci Technol. 2016;50(17):9432–41.
22. Karimi S, Bareither CA. The influence of moisture enhancement on solid waste biodegradation. Waste Manag. 2021;123:131–41.
23. Vu HL, Ng KTW, Richter A. Optimization of first-order decay gas generation model parameters for landfills located in cold semi-arid climates. Waste Manag. 2017;69:315–24.
24. Wang X, Nagpure AS, DeCarolis JF, Barlaz MA. Using observed data to improve estimated methane collection from select US landfills. Environ Sci Technol. 2013;47(7):3251–7.
25. Code of Federal Regulations. 40 CFR 60 subpart XXX: standards of performance for municipal solid waste landfills. 2016.
26. NOAA. JetStream Max: Köppen-Geiger climate subdivisions. Available at: https://www.noaa.gov
27. ABRELPE. Panorama dos resíduos sólidos no Brasil. 2023.
28. Environmental Protection Agency (EPA). Air emissions from MSW combustion facilities. 2014.
29. Instituto Brasileiro de Geografia e Estatística (IBGE). Estimativas de população. Available at: https://www.ibge.gov.br
30. Bueno FS, Araújo GP, Moura EO, Leal PLS. Avaliação da produção de biogás e do potencial energético dos resíduos orgânicos provenientes do restaurante universitário da EACH-USP. São Paulo; 2016.
31. Barros RM. Tratado sobre resíduos sólidos: gestão, uso e sustentabilidade. Rio de Janeiro: Interciência; 2013.
32. Inova HZ. Turkish delight: Europe's largest waste-to-energy plant to be built in Istanbul. 2017. Available at: https://www.hz-inova.com

Gamification and Professional Development: An Assessment for Capacity Building Among Construction Workers

Marina Leite Vieira Lima[1]*, Regina Maria Cunha Leite[2], Ingrid Winkler[3], Fábio Ferreira[4]
[1]Federal University of Bahia; Business School; [2]Federal Institute of Education, Science and Technology of Bahia, Construction Department; [3]Institute for Science, Innovation and Technology in Industry 4.0- INCITE INDUSTRIA 4.0, SENAI CIMATEC University; [4]Federal University of Bahia; Business School; Salvador, Bahia, Brazil

The objective of this study is to examine how gamification and teaching-learning techniques might help construction professionals improve professionally. This was a qualitative study, including case studies as a tool. We chose a medium-sized construction business based in Salvador, Bahia to conduct field investigation. The study identified the construction worker profile; the gamification elements best suited to worker training, development, and education based on the player styles of the Explorer and Socializer archetypes; and the teaching-learning strategies best suited to workers who preferred the Accommodation learning style. This article argues that gamification-based training and development programs may benefit workers, construction sites, and professional training in the construction industry. The study brings the conceptual-theoretical advancement of training and development in the construction industry much closer to the reality of construction sites, as well as introducing an innovative technique such as gamification to facilitate laborer learning and aid in the adaptation of training to the specific needs of this audience. The number of construction sites analyzed, and the sample size are both limitations.
Keywords: Gamification. Construction. Training and Development. Corporate Training.

The construction sector is navigating a wave of transformation, pushing companies to find new ways to stay aligned with shifting market demands—while reducing production setbacks. Amid these challenges, gamification—the integration of game elements into non-game settings—has emerged as a powerful tool to foster deeper engagement and learning. By simulating immersive, game-like experiences, it promotes experimentation, enhances intrinsic motivation, and supports meaningful skill development.

Research by Leite and colleagues [1] and Oke and colleagues [2] underscores gamification's ability to strengthen communication between tactical and operational teams, improve information retention, and boost workplace morale. These benefits are especially relevant in construction, where repetitive tasks, limited feedback, and a heavy reliance on manual labor can dampen motivation.

Training is the key to both personal growth and professional competence. Yet for many construction workers, skills are gained through hands-on experience rather than formal education—creating a disconnect between practical know-how and academic advancements. With few incentives for workers to pursue structured training and the industry's lack of emphasis on workforce development, this gap continues to grow.

To address this, the article investigates gamified training strategies tailored to the needs of on-site workers. By applying an empathy map to understand worker demographics, roles, and motivations, the study identifies which gamification mechanics and educational techniques most effectively build essential capabilities.

Training, Development, and Learning Styles in Corporate Education

Corporate training and development leverage instructional technology to enhance professionals' knowledge, skills, and attitudes (KSA), aiming to

Received on 15 December 2025; revised 18 February 2025.
Address for correspondence: Marina Leite Vieira Lima. Federal University of Bahia; Business School. Reitor Miguel Calmon Avenue, Vale do Canela. Salvador, Bahia, Brazil. E-mail: marina.vieiralima@hotmail.com.

J Bioeng. Tech. Health 2026;9(3):194-200

close performance gaps and prepare individuals for future roles [3]. These efforts foster competencies, which are synergistic combinations of knowledge, abilities, and motivation:

- Knowledge involves understanding gained through education and experience.
- Skills reflect how that knowledge is applied in practice.
- Attitudes reveal a person's drive to effectively use their expertise on the job [4].

To design effective training, it's crucial to understand how people learn. This study adopts Kolb's experiential learning theory, which defines learning as "the process of creating knowledge through the transformation of experience" [5]

Kolb's model integrates four learning processes:

- Concrete Experience (CE): direct engagement with new situations.
- Reflective Observation (RO): thoughtful analysis of experiences.
- Abstract Conceptualization (AC): forming ideas and theories.
- Active Experimentation (AE): applying new concepts in problem-solving.

Learning results from how individuals perceive and transform experiences, forming a continuous knowledge cycle.

Kolb also identified four learning styles—divergent, assimilative, convergent, and accommodating—based on how learners combine these modes. To assess these styles, he developed the Learning Style Inventory (LSI), a tool that promotes self-awareness and supports educational research rooted in experiential learning.

Knowles and colleagues [6] provide a practical basis for adult education. This research examines the learning processes of construction workers, enabling the development of training programs that are specifically tailored to their requirements for improved outcomes.

Gamification and Player Profiles in Training

Gamification is a training strategy that applies game design elements—like mechanics, dynamics, and components—in non-game environments to inspire engagement, motivate behavior, support learning, and solve challenges [7,8]. While these applications include game-like features, they are not considered actual games [8]. Researchers frequently explore gamification as a means to positively influence motivation and behavior [9].

Its growing popularity is attributed to its link with intrinsic motivation, explained through self-determination theory (SDT), which distinguishes between desires to stand out or remain unseen [10]. Gamification can be implemented in both digital and analog formats, offering flexibility in reaching diverse audiences [11].

According to Burke [12], gamification and learning are closely connected, as gamified environments create emotional engagement and encourage progress. They involve structured cycles of instructions, challenges, and feedback that sustain learner interest.

To maximize impact, it's vital to understand player profiles. Alves [11] recommends the Empathy Map—a strategic tool for capturing users' emotional and behavioral patterns. It goes beyond demographics by analyzing six quadrants: what users see, hear, say/do, think/feel, and their frustrations. This holistic view supports the creation of personas for targeted gamification.

In this study, the Empathy Map was used to analyze construction workers' profiles. Bartle's [13] player types were then applied: (1) Predators: competitive, focused on defeating others. (2) Conquerors: driven by achievement and recognition. (3) Explorers: motivated by mastery and experience. (4) Socializers: seek connection and collaboration.

Understanding these styles supports personalized gamified training, improving engagement and outcomes for workers with varied motivations and learning preferences.

Materials and Methods

This research employed a case study design to investigate a contemporary phenomenon within

its real-world context, facilitating the exploration of the interface between theory and practice [14].

The selected case was Company X, a construction firm headquartered in Salvador, Bahia, boasting 33 years of experience in managing public-sector projects across infrastructure, historical restoration, and industrial construction.

A qualitative approach was adopted [15], focusing on in-situ data collection at the construction site to gather descriptive insights into workers' competencies and professional profiles. A total of 37 semi-structured interviews were conducted, eliciting participant reflections on demographic characteristics, lifestyle habits, personal aspirations, sources of frustration, perceptions of success, and challenges in the workplace. Data were analyzed using the Empathy Map framework [16], enabling the development of detailed personas that represent different worker archetypes.

Theoretical saturation guided the sampling process, with data collection continuing until no new themes or perspectives emerged. To assess gamification elements relevant to training engagement, participants completed surveys aligned with Bartle's player archetypes [13].

Additionally, the study explored learning preferences by administering modified versions of Kolb's Learning Style Inventory (1993) to a subgroup of 10 workers. The GCIS research group (IFBA) facilitated the survey distribution through structured phone outreach, using a pre-defined contact spreadsheet. The survey process also adhered to the principle of theoretical saturation.

Results and Discussion

Target Audience Assesment

The first round of interviews revealed that all interviewees were male, with 47% having incomplete primary education and 26% having complete primary education. This low level of education aligns with the sector's low educational attainment, as highlighted by [17-19]. Additionally, 52% of the interviewees held professional positions, 37% were helpers, and 11% were servants. The second block of the interview aimed to get to know the worker using the empathy map, as shown in Figure 1, which depicts the most common themes in each quadrant.

The map analysis indicated that professional development through education is identified as important in the "what they think and feel" quadrant, reflecting career commitment.

All four quadrants of the map represented work and study, indicating a high interest in training among employees. Indeed, a lack of study opportunities is a source of frustration for interviewees, and it may be remedied by investing in professional development. Workers desire advancement and recognition based on merit, as seen by their admiration for those in positions of authority. Recognition occurred in two quadrants of the map (needs and what you hear), emphasizing a key component of gamified training. The fondness for games, football (the most often reported modality), and sports suggests potential themes for gamified training. The "what you hear" and "what you see" quadrants revealed that construction workers rely on their peers for inspiration and advice, emphasizing the importance of interpersonal relationships.

Game Preferences and the Most Common Player Styles

We discovered that workers are familiar with games, potentially indicating a positive attitude towards gamification. Sports-related games emerged as the most frequently suggested themes, a fitting theme for gamified training that aligns with the findings of the empathy map. Team activities are popular among workers, particularly on construction sites where group labor is common. This conclusion supports the empathy map findings, which revealed positive interpersonal interactions among coworkers. This gives crucial information for developing the player engagement model [12] which outlines how employees will interact with gamified training.

Figure 1. Empathy map.

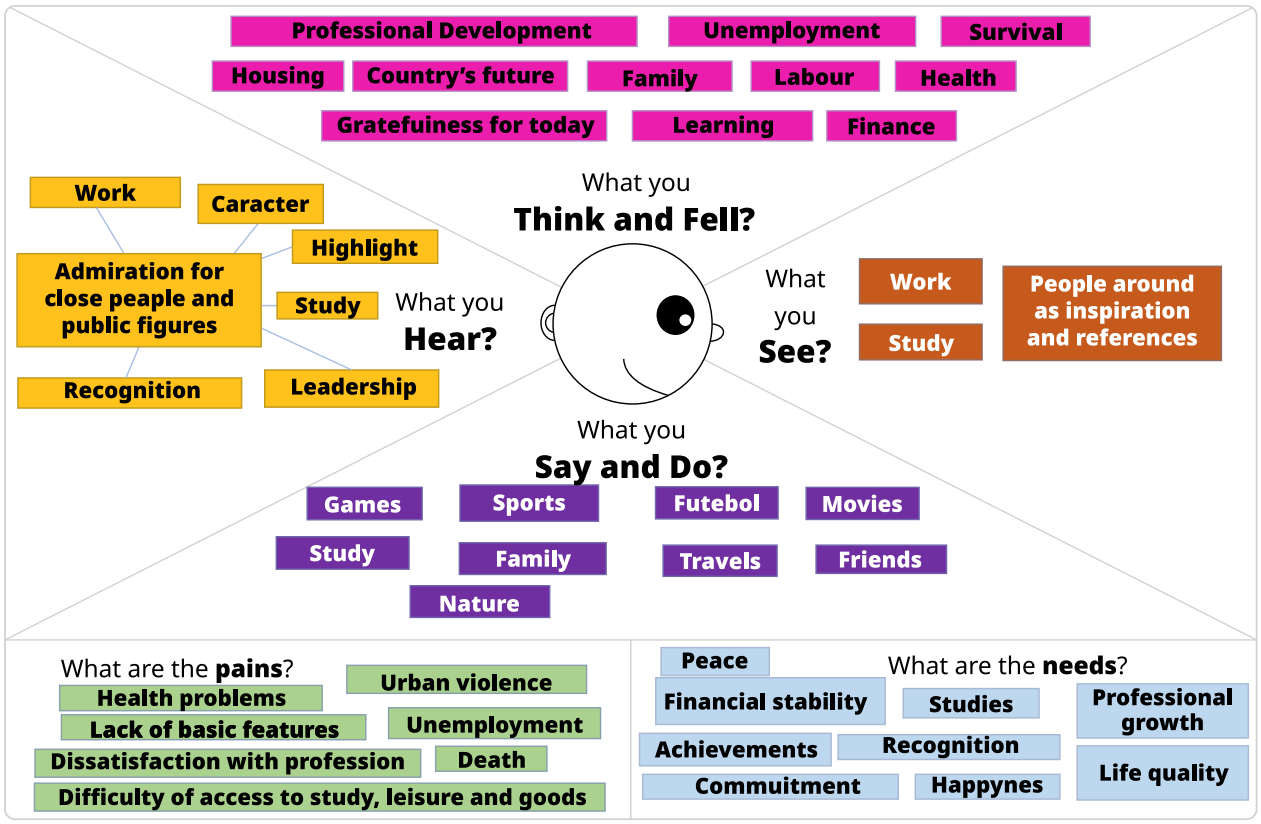

Source: Lima [20].

In this case, respect for team play may signal a willingness to explore more collaborative ways, and any rivalry should take place between work teams rather than individual employees. Workers preferred physical games to online games. This study might suggest that, while workers enjoy games in general, they have a specific allergy to electronic games. When designing gamified training for employees, note that gamification works in both analogue and digital forms and does not require technology for delivery [11]. It is vital to take a more analogue approach, particularly when it comes to workers' daily tasks and the physical surroundings of the construction site, but this does not exclude the use of digital technologies to enhance gamified training, such as screens that display game-specific information.

According to Bartle's Archetypes [13], the most prevalent player styles identified in the employee sample were Socializer (66.6%) and Explorer (33.3%), and this finding, together with the replies concerning gaming preferences, was statistically significant. Based on these findings, we may emphasize game components that enable players to interact with the game (explorer archetype) and with other players (socializer archetype), both of whom value connection. Furthermore, player involvement in the gaming environment is important because Explorers value the opportunity to learn how the game works; thus, they prefer the trip and experience over victory. That is why feedback, which shows the user's progress, and challenges, which motivate the player to succeed, are essential. Regardless of the player typology, feedback and challenges are vital in gamified training since they may rectify mistakes while also acknowledging accomplishments, allowing the player to alter their behaviors and grow closer to the defined objectives.

To Pink [19], including these factors may help raise players' intrinsic motivation through

mastery, which is the drive to improve in a certain area. These two game elements can also positively impact the construction site by addressing a lack of feedback from the tactical team to the workers. This issue has been identified by Leite and colleagues [1,21] and Lima and colleagues [18] as a recurring problem that negatively impacts the worker's motivation and professional development, hindering their ability to acquire new knowledge, skills, and attitudes. Furthermore, it may be necessary to include game components that serve as evolution markers so that the Explorer understands how the game works, such as levels, which are numerical representations of the player's evolution; achievements, which are rewards for completing activities; and badges and medals, which are visual representations of game achievements. To encourage player interaction, which is what socializers desire, game components such as the social graph, which allows you to see friends who are also playing the game; a private channel (chat) for player interaction; and gifts or donations, which allow you to distribute items or virtual currency to other players, are recommended.

According to Burke [12], it is recommended to use game mechanics that promote cooperation and competition in a balanced manner because a highly competitive structure, in addition to not stimulating the two dominant archetypes in this sample, is unsuitable for gamified training, which aims to train the greatest number of workers. The Empathy Map provided useful insights into how three game dynamics used to depict player-game mechanics interactions: narratives, emotions, and relationships. As previously said, it discovered that construction workers were highly interested in sports, particularly football, which provided a chance to craft a story around this subject that may elicit emotions and foster good ties among workers. Football may be used to create a tale that fosters collaboration by separating employees into teams while also providing a good dose of competitiveness to motivate them to meet the goals of gamified training.

According to Werbach and colleagues [22], collaboration is a valuable resource that may be strengthened by structuring groups of people to work toward a shared objective. To make the story connect with and make sense to the workers, football must be linked to the building site backdrop. Stories are also an essential component of gamification apps because they may alter the meaning of real-world activities by providing a narrative "overlay" [24]. Another important aspect of stimulating players' intrinsic motivation through purpose is linking the narrative to the achievement of meaningful goals larger than the players themselves, as well as using gamification to motivate people not only to achieve the organization's goals but also their own [1,12,21,23].

Given the qualities of the Explorer and Socializer archetypes, giving status and access incentives [7], might be an attractive technique. Status incentives include points, badges, levels, and ranks, which give the player prominence and acknowledgement.

In the case of the workers in this study, the empathy map revealed that people like notable personalities who achieve in their industries and are acknowledged for their contributions, implying that status rewards may be warmly received. Furthermore, because it has been discovered that workers value professional development and see a lack of study or qualification in the area as a barrier, it is proposed that a certificate be made available at the end of the course not only to demonstrate participation but also to recognize those who performed best in the gamified training. Medals can be awarded on paper or online to players who are currently standing out, such as for completing a task or moving up. Other possibilities include a conspicuous portrait of the team leading the round at the cafeteria door, as well as applause from colleagues at important moments of recognition and a celebration at the end.

Badges are visual representations of achievements that may gained in a gamified setting [23]. It advised that rankings done by team rather than by employee to avoid shame for

failing employees or causing future dismissals. If it is necessary to provide individualized feedback to employees during gamified training, it advised that this be done in a way that protects the subjects' identities. Access incentives provide the player with access to a previously unavailable area, person, or environment [7]. The exploited and socialized characters place excellent value on this form of compensation, while the other archetypes find it appealing. A one-time session of expert guidance with a senior member of the construction site or the people management department is one example of a reward for access that may benefit the workers.

As shown in the empathy map, the workers express a desire for professional development and access to new learning opportunities that will allow them to advance in this industry; so, the advice may be appropriate in this context if all parties agree. Material and power incentives [7] which include expenses (just material ones) and necessitate institutional approval, may vary depending on the environment in which the firm receives gamified training. The physical prizes might be related to the topic of gamified training, in this example, football, or to the participants' other interests, as shown by the empathy map.

The design of gamified training should focus on voluntary participation to foster autonomy and intrinsic motivation. By adapting game elements to workers' interests and goals, the experience becomes meaningful and relevant. Additionally, it is essential to identify the most suitable teaching and learning methodologies for this audience.

Learning Styles are Common Among Construction Workers

The predominant learning style among construction workers is the accommodator, characterized by valuing concrete experience and active experimentation, according to Kolb's learning cycle. This means that these professionals learn through hands-on practice at the worksite and by exchanging experiences with more seasoned colleagues [24,25]. Therefore, it recommended that gamification strategies aligned with real worksite activities, reinforcing learning through experience [6]. If it is not possible to offer gamified training on the job, it is suggested that the practical component of courses be adapted to simulate real services, thus facilitating the transfer of knowledge to the work context. A collaborative approach is especially important, since accommodators tend to prefer learning in teams and benefit from mutual support. Finally, gamification proves effective in motivating, stimulating creativity, and fostering worker engagement by integrating playful aspects and challenges into the professional development process.

Conclusion

The lack of professional training for workers has a significant negative impact on the construction industry, emphasizing the importance of investing in training this labor force. We must tailor professional training to the individual needs of workers, utilizing teaching-learning methodologies and gamification. Investigating gamification and teaching-learning strategies revealed that gamified training for construction workers should provide practical challenges, encourage innovation, and emphasize teamwork and collaboration, with game elements that favor the Explorer and Socializer archetypes, as well as the Accommodator learning style. Finally, this article discussed the ability of workers, the building site environment, and professional training in the construction industry to engage in Training and development activities through gamification. The sample size and number of construction sites analyzed are two of the article's shortcomings. Future work may entail studying alternative building companies.

References

1. Leite RMC, Winkler I, Alves LRG. Visual management and gamification: an innovation for disseminating information about production to construction professionals. Appl Sci. 2022;12(11):5682.

2. Oke AE, Aliu J, Mwanaumo EMUM, Abayomi T, Kahanji C. Leveraging gamification to enhance productivity and employee engagement in the Nigerian construction industry. Built Environ Proj Asset Manag. 2023;13(6):813-829.
3. Abbad G, Meneses P, Zerbini T. Manual de treinamento organizacional. Porto Alegre: Artmed; 2010.
4. Abbad GDS, Loiola E, Zerbini T, Borges-Andrade JE. Aprendizagem em organizações e no trabalho. In: O trabalho e as organizações: atuações a partir da psicologia. Porto Alegre: Artmed; 2013. p. 467-527.
5. Madruga R. Treinamento e desenvolvimento com foco em educação corporativa. São Paulo: Saraiva Educação; 2018.
6. Kolb DA. Experience as the source of learning and development. Upper Saddle River: Prentice Hall; 1984.
7. Knowles MS, Holton EF III, Swanson RA. Aprendizagem de resultados: uma abordagem prática para aumentar a efetividade da educação corporativa. São Paulo: Pearson; 2009.
8. Zichermann G, Cunningham C. Gamification by design. Canada: O'Reilly Media; 2011.
9. Deterding S, Sicart M, Nacke L, O'Hara K, Dixon D. Gamification: using game-design elements in non-gaming contexts. In: CHI'11 extended abstracts on human factors in computing systems. 2011. p. 2425-2428.
10. Hamari J, Koivisto J, Sarsa H. Does gamification work? A literature review of empirical studies on gamification. In: 47th Hawaii international conference on system sciences. IEEE; 2014. p. 3025-3034.
11. Xi N, Hamari J. Does gamification satisfy needs? A study on the relationship between gamification features and intrinsic need satisfaction. Int J Inf Manag. 2019;46:210-221.
12. Alves F. Gamification: como criar experiências de aprendizagem engajadoras. São Paulo: DVS Editora; 2014.
13. Burke B. Gamificar: como a gamificação motiva as pessoas a fazerem coisas extraordinárias. São Paulo: DVS Editora; 2015.
14. Bartle R. Hearts, clubs, diamonds, spades: players who suit MUDs. J MUD Res. 1996;1(1):19.
15. Bogdan R, Biklen SK. Qualitative research for education. Boston: Allyn & Bacon; 1997.
16. Osterwalder A, Pigneur Y. Business model generation: inovação em modelos de negócios. Rio de Janeiro: Alta Books; 2020.
17. Fontanella BJB, Ricas J, Turato ER. Amostragem por saturação em pesquisas qualitativas em saúde: contribuições teóricas. Cad Saude Publica. 2008;24:17-27.
18. da Silva Nunes J, Alvarenga MCS. Avaliação da qualidade de mão de obra, projetos e fiscalização em obras de construção civil. Construindo. 2018;10(1):28-49.
19. Lima MLV, Benevides TM, Leite RMC. Desenvolvimento corporativo: uma análise da gamificação como ferramenta de desenvolvimento humano no segmento da construção civil. 2020. doi:10.22533/at.ed.7561913034.
20. Pink DH. Drive: the surprising truth about what motivates us. Amazon.com; 2009.
21. Lima MLV. Gamificação e desenvolvimento de competências profissionais dos operários da construção civil [dissertação]. Universidade Federal da Bahia; 2020.
22. Leite RMC, Bastos Costa D, Meijon Morêda Neto H, Araújo Durão F. Gamification technique for supporting transparency on construction sites: a case study. Eng Constr Archit Manag. 2016;23(6):801-822.
23. Werbach K, Hunter D, Dixon W. For the win: how game thinking can revolutionize your business. Philadelphia: Wharton Digital Press; 2012.
24. Sailer M, Hense J, Mandl H, Klevers M. Fostering development of work competencies and motivation via gamification. In: Competence-based vocational and professional education. 2017. p. 795–818.
25. Kolb AY, Kolb DA. Experiential learning theory: a dynamic, holistic approach to management learning, education and development. In: SAGE handbook of management learning, education and development. 2009.
26. Kolb DA, Boyatzis RE, Mainemelis C. Experiential learning theory: previous research and new directions. Perspect Think Learn Cogn Styles. 2001;1(8):227–247.

Education, Technology, Infrastructure: Comparative Analysis between the Indicators in Company A's Results Report and the Competitive Brazil Movement

Évelyn dos Santos Jardim Esteves[1]*, Ednildo Andrade Torres[1], Felipe Andrade Torres[1,3], Carlos César Ribeiro Santos[2], Guilherme Sobral Santos[2], Vaner Jose do Prado[2]

[1]Federal University of Bahia, PEI; [2]SENAI CIMATEC University, Management, Logistics, and Productivity; [3]Federal University of Recôncavo da Bahia; Center for Exact and Technological Sciences; Cruz das Almas, Bahia, Brazil

This article aimed to conduct a comparative analysis between the operational indicators extracted from the performance report of Company A — a state-owned company responsible for the distribution logistics of objects in Brazil — with an emphasis on the Object Distribution Center, located in Salvador, state of Bahia, and the strategic pillars of the Competitive Brazil Movement. The methodology applied was based on exploratory analysis of documents and the use of descriptive and visual techniques for interpretation, focusing on the pillars of education, technology, and infrastructure. The results allowed us to identify patterns, correlations, and gaps between Company A's internal performance and the standards of excellence desired by Competitive Brazil for the period of 2015 to 2024. It was noted that, while data from Competitive Brazil showed an average increase of 12% in national indices related to education, 18% in technology, and 9% in infrastructure, Company A's internal indicators for the same period recorded significantly lower variations— 5%, 7%, and 3%, respectively. These results reinforce the magnitude of the strategic gaps and highlight flaws in professional training policies, digital transformation processes, and the modernization of logistics infrastructure. This article proposes practical guidelines for requalifying Company A, anchored in a systemic and sustainable vision of public management. The proposal seeks to contribute to the debate on the need for convergence between strategic planning, digitization, and public policies geared toward logistical efficiency.
Keywords: Comparative Analysis. Competitiveness. Logistics. Education. Technology. Infrastructure.

The competitiveness of an organization or country is directly linked to its ability to strategically invest in three key areas: education, technology, and infrastructure. These elements form the basis for sustainable economic growth, institutional innovation, operational efficiency, and productive integration into an increasingly dynamic, digital, and data-driven global market. In this context, logistics — in both public and private companies — plays a central role, as the efficiency of services directly impacts the population, the productive sector, and national integration.

Company A, a public institution responsible for the logistics of distributing objects in Brazil, has undergone profound changes in its operating model. Advances in technology, the exponential growth of e-commerce, and pressure for more agile and responsive services reinforce the need to align its practices with standards of excellence in competitiveness. This implies continuous investment in professional training, technological innovation, and modernization of physical and digital infrastructure — dimensions that reflect the organization's commitment to improving performance and modernizing the state.

The Competitive Brazil Movement (CBM) [1], articulated by entities such as the National Confederation of Industry (NCI) and the World Economic Forum, offers a comprehensive set of indicators that measure Brazil's position relative to other global economies, covering, among other areas, education, technology, and logistics infrastructure. The comparison between these parameters and Company A's internal indicators made it possible to assess the convergence between institutional actions and national objectives to increase productivity and the country's competitive insertion.

Received on 15 December 2025; revised 21 February 2026.
Address for correspondence: Évelyn dos Santos Jardim Esteves. Polytechnic School of the Federal University of Bahia. Prof. Aristides Novis nº 02 - Federação. Salvador, Bahia, Brazil Zipcode: 40210-630. E-mail: evelynsjardim@gmail.com.

J Bioeng. Tech. Health 2026;9(3):201-208

This study analyzed data from Company A's Results Report (CARR) [1], with an emphasis on the Object Distribution Center (ODC), located in Salvador/BA, comparing them with CBM indicators between 2015 and 2024. The three pillars selected — education, technology, and infrastructure — reflect critical areas for strengthening state logistics in Brazil and were defined by their strategic relevance in the current scenario.

By proposing an integrated methodology to compare institutional operational data with international benchmarks, this article provides a replicable model for institutional analysis against national competitiveness indicators. This framework made it possible to identify gaps and misalignments, guide institutional requalification actions, and provide input for public policies and business strategies aimed at digital transformation, professional training, and modernization of logistics infrastructure.

Theoretical Framework

Education, Technology, and Infrastructure as Pillars of Competitiveness

The integration of education, technology, and infrastructure is widely recognized as a necessary condition for strengthening a nation's competitiveness. According to Porter [3], the ability to innovate and adapt quickly to market changes depends on an environment supported by efficient institutions, modern infrastructure, qualified education, and technological capacity.

In the field of education, authors such as Hanushek and Woessmann [4] argue that skilled human capital are crucial for long-term growth. In the logistics sector, the technical and operational training of workers has a significant influence on productivity and service quality. In Brazil, the lack of specialized technical training is still an obstacle to the modernization of public companies such as Company A [5].

In terms of technology, digital transformation has been identified as a key driver of logistical efficiency and increased organizational competitiveness. According to Schwab [6], the Fourth Industrial Revolution requires the digitization of processes and the integration of technologies such as the Internet of Things (IoT), big data, and artificial intelligence. In the public sector, the adoption of these technologies is essential to make services more agile, responsive, and data-driven [7].

With regard to infrastructure, recent studies show that the structure, availability, and quality of the logistics network have a direct impact on transportation costs, delivery times, and consumer confidence [8]. In Brazil, the historical deficit in urban and transport infrastructure represents a significant barrier to competitiveness [9]. In this context, the modernization of distribution centers, such as Company A's ODC, should consider the integration of physical (layout, equipment) and digital (intelligent routing, traceability) solutions.

The articulation between these three pillars — education, technology, and infrastructure — enhances systemic and sustainable gains. Research indicates that countries with solid educational systems, a high degree of digitization, and modern infrastructure have better competitiveness and development indices [10,11]. In the case of Company A, aligning these elements is essential to increase the efficiency, sustainability, and reliability of the services provided to the population.

Materials and Methods

The research adopted a qualitative and quantitative approach, with an exploratory-descriptive character, aiming to analyze the adherence between the institutional indicators of Company A's Results Report (CARR) and the national strategic parameters established by the Competitive Brazil Movement (CBM), focusing on the pillars of education, technology, and infrastructure, from 2015 to 2024.

The data was selected based on availability, institutional reliability, and relevance to the three

pillars analyzed. Focusing on information that was published annually and was methodologically consistent, direct comparisons with the CBM indices for the same time period were allowed.

The analysis was conducted using interactive panels created in Microsoft Power BI®, structured in dashboards that enabled visual comparison of variables, periods, and scenarios. According to Torfing and colleagues, and Costa and Andrade, respectively [12,13], this approach meets the demand for visual, agile, and data-driven analysis methods in the context of public management.

Descriptive statistical techniques and correlation analysis between internal and national indicators were applied to identify performance patterns and the magnitude of differences. The results were presented in thematic graphs (columns and rows), facilitating the interpretation and communication of the findings.

The study complied with the principles of the General Data Protection Law (LGPD – Law 13.709/2018), using only institutional data that is public or has been previously authorized for academic purposes, without any use of sensitive individualized information.

Results and Discussion

The data allowed for a deeper understanding of Company A's internal performance and its relationship with the strategic pillars of national competitiveness. The results presented below are organized by correlated themes and aligned with the axes of education, technology, and infrastructure.

Education and Professional Training: Correlation between CARR and CBM Ranking

In the Education axis, there was a direct correlation between the variation in investments in professional training by Company A and Brazil's position in the CBM ranking. Between 2015 and 2024, the country fell from 9th to 18th place, following significant fluctuations in Company A's internal metrics.

In 2020, the best performance of the period was observed, with 10.47 million hours of training and an annual average of 130.4 hours per employee — an increase of 349% compared to 2019. This result was driven by remote learning during the COVID-19 pandemic, which expanded the use of online learning platforms. However, there was a decline in subsequent years: in 2023, the total number of hours fell by 52.5% compared to 2020, reaching 4.97 million hours, while the average per employee fell by 54.7%, reaching 59.4 hours. Figures 1 and 2 graphically illustrate this trend.

As for the number of trained employees, there was a 23.6% reduction between the peak of 102,449 in 2018 and the lowest figure for the period, 78,798 in 2024 (Figure 3). Despite a slight recovery in 2022 and 2023, this evolution did not prevent Brazil from falling in the ranking, showing that the quality and consistency of training are as important as the volume offered.

This trajectory reinforces the urgency of institutional policies focused on continuous corporate education, prioritizing the development of technical and digital skills compatible with current logistical challenges. It is necessary to avoid the trap of measuring performance solely by hours/class, ensuring that the investment translates into effective gains in productivity and competitiveness.

Innovation and Technology: Mismatch between National Strategy and Organizational Practice

The analysis of the Innovation and Technology pillar confirms that competitiveness requires not only structural investments, but also their continuity and strategic alignment. As shown in Figure 4, between 2015 and 2024, Brazil fell from 8th to 15th place in the CBM ranking, representing a relative loss of 87.5% in its initial position. The sharpest decline occurred between 2022 and 2024, when the country fell from 9th to 15th place, reflecting a weakening of public

Figure 1. Evolution of training hours at Company A (annual) and Brazil's position in the CBM Education pillar.

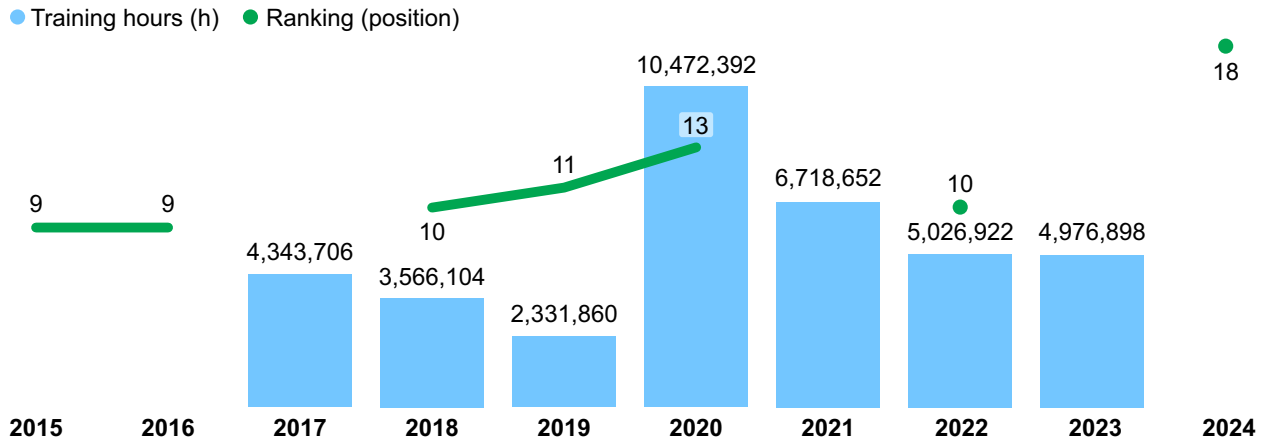

Figure 2. Evolution of average training hours per employee at Company A (annual) and Brazil's position in the CBM Education pillar.

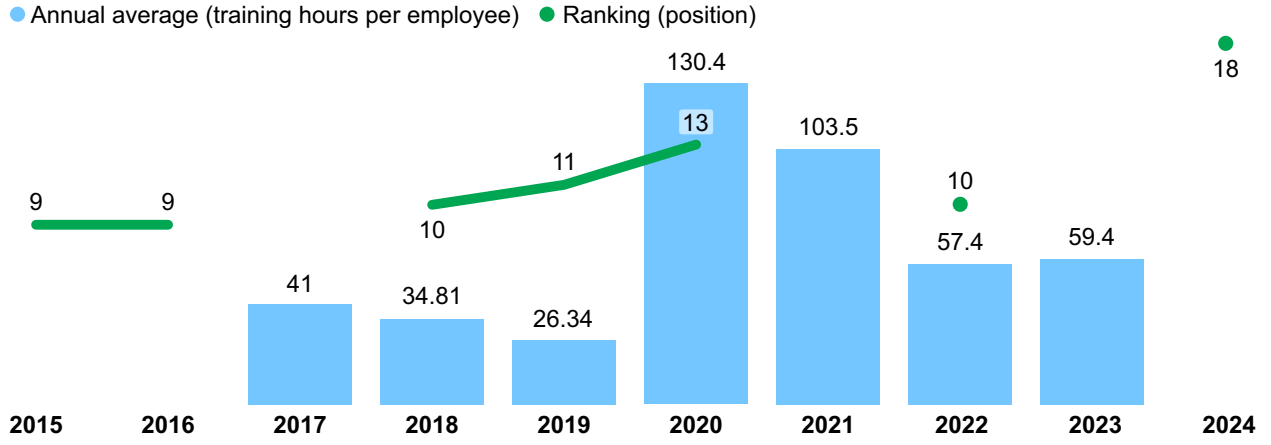

Figure 3. Evolution of the number of trained employees at Company A (annual) and Brazil's position in the CBM Education pillar.

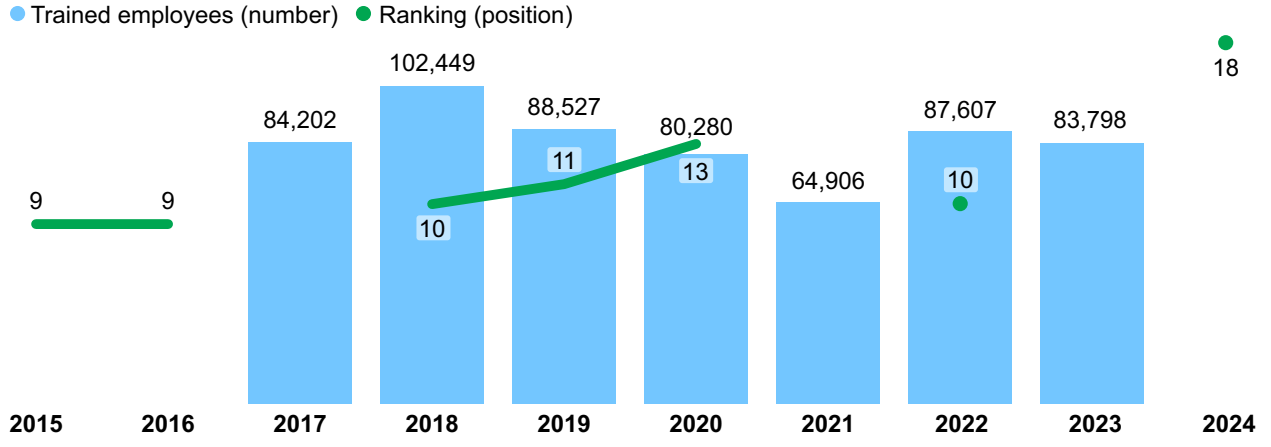

Figure 4. Evolution of Brazil's position in the Innovation and Technology pillar of the CBM.

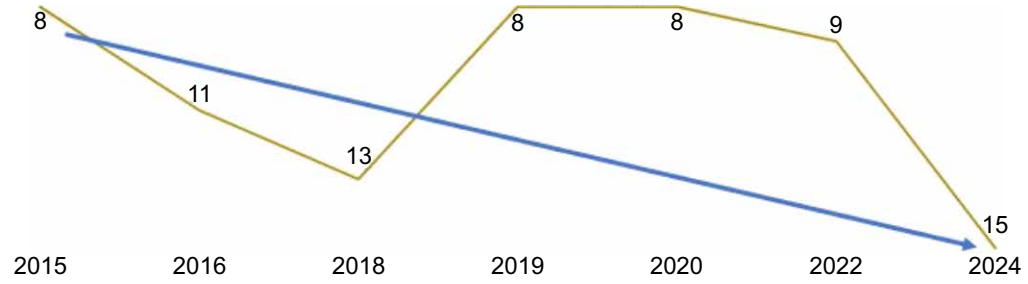

policies to encourage science, technology, and innovation.

In the case of Company A, a gap was identified between specific advances in digital transformation and the consolidation of an innovation-oriented organizational culture. Despite the adoption of initiatives such as routing systems, logistics simulations, and interactive dashboards developed in Microsoft Power BI®, such actions have not yet resulted in significant gains in performance indicators due to the lack of integration with a long-term strategic plan.

This disconnect stems from factors such as the lack of a consistent corporate strategy, high turnover in strategic positions, and insufficient digital training for the workforce. The reduction in investments in technological training, as evidenced in the Education section, reinforces this stagnation.

In addition, the lack of mechanisms to encourage open innovation, partnerships with research centers, and integration with startups widens the gap between the company and practices adopted by public logistics organizations in more competitive countries [5,10].

According to Tidd and Bessant [14], innovation is not limited to the adoption of emerging technologies, but includes process management, new operating models, and the ability to learn from the external environment. Without institutional structures to support this dynamic, results tend to be sporadic and unsustainable.

The performance of Brazil and Company A in this pillar reveals that local organizational decisions can amplify national weaknesses, limiting the company's potential contribution to sectoral and national competitiveness.

Logistics Infrastructure and Operational Efficiency: Intersections between CARR and the Competitiveness Ranking

According to the CBM, infrastructure is one of the key factors in boosting competitiveness, especially in countries with large territories such as Brazil. In the logistics sector, it encompasses not only physical coverage and installed capacity, but also technological integration, operational flow, and efficient use of resources.

Company A has extensive operational reach, with 945 Distribution Centers (ODC) and approximately 6,000 branches, serving 99.75% of Brazilian municipalities. This reach reinforces its role as a vector of national integration. However, when compared to the CBM ranking, it can be seen that between 2020 and 2024, Brazil remained in 15th place in the Logistics Infrastructure factor, with no relative gains — which shows that mere physical availability has not translated into effective performance improvements (Figure 5).

Despite the robustness of the network, the analysis indicates that the lack of continuous modernization and digital integration in the units prevents the potential from translating into a competitive advantage. Between 2022 and 2023, there was a decrease from 45 to 43 units in the Integrated Logistics Center (-4.4%) and an increase from 51 to 54 in the Object Treatment Center (+5.9%), but these variations did not have a positive impact on the ranking.

Figure 5. Evolution of Company A's operational network and Brazil's position in the Logistics Infrastructure pillar of the CBM.

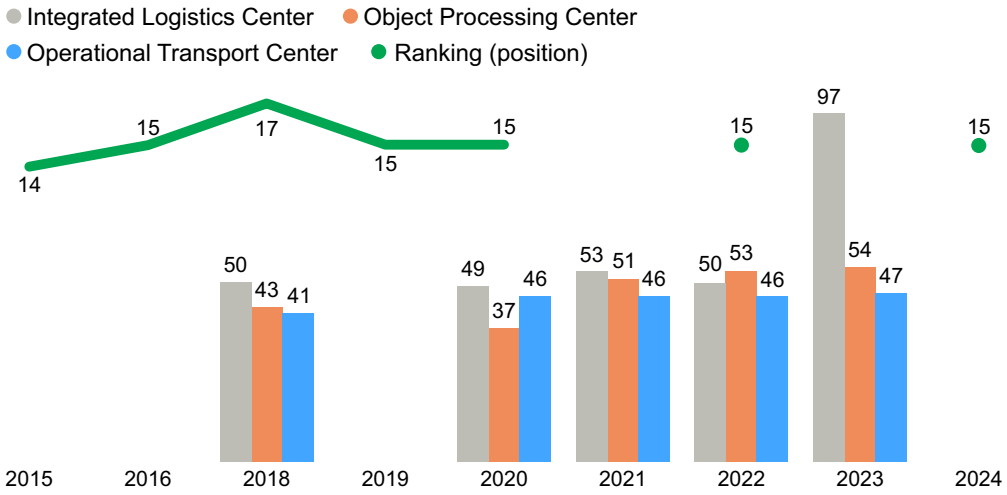

For Schawb [6] and IPEA - Institute of Applied Economic Research [9], Brazil's logistics deficit, characterized by bottlenecks in urban networks, highways, and distribution centers, compromises both private and public companies. The integration of physical infrastructure with digital solutions — such as intelligent routing, automated delivery management, and computer simulation — is strategic for increasing operational efficiency.

The use of tools such as Microsoft Power BI® and digitization of plans in AutoCAD has allowed greater visibility into indicators and space usage, resulting in gains at the tactical management level. However, these advances are sporadic and require support through permanent institutional policies for structural requalification.

The analysis of average activity execution times revealed that units with optimized layout and ergonomic standardization showed an increase in delivery time and a decrease in internal work time, confirming the direct relationship between infrastructure and operational efficiency [15].

The results indicate that, although there are isolated initiatives for modernization and digitization, the absence of a national and integrated plan for continuous investment limits the sustainability of improvements. A retraining program that combines physical redesign, operator training, and management based on indicators aligned with the national competitiveness strategy is essential to transform Company A's logistics infrastructure into a high-impact strategic asset.

Taken together, the analyses of the Education, Innovation and Technology, and Logistics Infrastructure axes show that Company A's performance, although showing occasional advances, still lacks strategic alignment and consistency in institutional policies for its potential to translate into sustainable gains in competitiveness. By identifying gaps and proposing practical guidelines, it offers a replicable analysis model that can guide public and private organizations in increasing their efficiency and effectively contributing to national competitiveness.

Conclusion

A comparative analysis between data from Company A's Results Report (CARR) and indicators from the Competitive Brazil Movement (CBM) revealed a strategic misalignment between the organization's operational performance and the national pillars of competitiveness—education, technology, and infrastructure. Although specific advances have been identified in training, use of

digital tools, and localized physical improvements, these actions remain fragmented, without consistent integration or alignment with national development goals.

In the education pillar, there was a strong correlation between investment in training and Brazil's position in the CBM ranking. The peak recorded in 2020, driven by the pandemic and the adoption of distance learning, led to a significant increase in training hours. However, the subsequent decline, both in total hours and in the average per employee, exposed the absence of a continuous and structured human development program. It is recommended that a permanent corporate education policy be institutionalized, focused on technical, digital, and managerial skills, aligned with the demands of contemporary logistics.

As for technology, progress was limited to isolated initiatives, such as the use of Microsoft Power BI® and layout modeling in AutoCAD, without any systemic digital transformation. Brazil's drop to 15th place in the innovation and technology ranking highlights the need to expand digitization and incorporate solutions such as automation, artificial intelligence applied to routing, and real-time monitoring of key indicators. To this end, it is essential to consolidate an integrated logistics platform that strategically connects operations, data, and management.

In terms of infrastructure, the analysis identified an extensive physical network with broad territorial coverage, but with structural and operational bottlenecks that reduce efficiency. Significant differences in average execution times between locations indicate problems with sizing, planning, and technological integration. The modernization of logistics assets should be guided by industrial engineering criteria, sustainability, and intelligent use of space, accompanied by continuous investments and productivity indicators.

The results reinforce that the competitiveness of an institution such as Company A—which is nationally significant—cannot be sustained by isolated actions, but rather by coordinated long-term policies that combine continuous corporate education, digitization, and infrastructure modernization.

This study contributes to advancing discussions on the modernization of essential public services by proposing an analysis model that can be replicated by other state organizations. By highlighting the relationship between internal indicators and strategic pillars of competitiveness, it reinforces the importance of public management guided by results, innovation, and social responsibility, capable of transforming institutional potential into a competitive advantage for the country.

References

1. Competitive Brazil Movement. National competitiveness indicators 2015–2023. Brasília: CBM; 2023.
2. Carr Company Results Report A. Indicators 2017–2023. 2023.
3. Porter ME. The competitive advantage of nations. New York: Free Press; 1990.
4. Hanushek EA, Woessmann L. The knowledge capital of nations: education and the economics of growth. Cambridge (MA): MIT Press; 2015.
5. Organisation for Economic Co-operation and Development (OECD). Education at a glance 2022: OECD indicators. Brasília: OECD; 2022. Available from: https://www.oecd.org
6. Schwab K. The fourth industrial revolution. Geneva: World Economic Forum; 2016.
7. Morrar R, Arman H, Mousa S. The fourth industrial revolution (Industry 4.0): a social innovation perspective. Technol Innov Manag Rev. 2017;7(11):12–20. doi:10.22215/timreview/1117.
8. World Economic Forum. The global competitiveness report 2023. Geneva: WEF; 2023. Available from: https://www.weforum.org
9. Institute of Applied Economic Research (IPEA). Transportation infrastructure in Brazil: diagnosis and challenges. Brasília: IPEA; 2022. Available from: https://www.ipea.gov.br
10. International Institute for Management Development (IMD). World competitiveness ranking 2023. Lausanne: IMD; 2023. Available from: https://www.imd.org/wcc
11. World Bank. World development report 2021: data for better lives. Washington: World Bank; 2021. Available from: https://www.worldbank.org
12. Torfing J, Andersen LB, Greve C, Klausen KK. Public governance as co-creation: a strategy for revitalizing the

public sector and rejuvenating democracy. Cambridge: Cambridge University Press; 2022.
13. Costa LF, Andrade RM. Interactive dashboards and data-driven public management: trends and challenges in contemporary administration. Rev Bras Adm Pública. 2023;57(2):233–252.
14. Tidd J, Bessant J. Managing innovation: integrating technological, market and organizational change. 5th ed. Chichester: John Wiley & Sons; 2015.
15. Rodrigues CA, Silva MB. Public management and innovation: challenges of competitiveness in the logistics sector. São Paulo: Atlas; 2020.

Evaluation of Mechanical and Physicochemical Properties of Materials for 3D Printing

Carlos H. B. M. Filho[1]*, Marcos F. M. Ferreira[1], Uilian S. Silva[2], Fabio O. C. Feirreira[2], Marcus V. M. Gomes[2], Pollyana S. Melo[2], Lilian L. N. Guarieiro[2], Daniela S. Anunciação[1]

[1]Chemistry and Biotechnology Institute of Federal University of Alagoas; Alagoas, Maceió, Brazil; [2]SENAI CIMATEC University; Salvador, Bahia, Brazil

The study evaluated mercury adsorption and the mechanical properties of polymer filaments (ABS, PLA, and Tritan) after exposure to contaminated environments. Using methodologies such as atomic absorption spectrometry and tensile testing, it was found that Tritan showed high adsorption (69.3%), while ABS and PLA showed lower affinity for mercury (<2%), making them more suitable for applications in critical environments. Significant structural changes were observed in all materials, indicating the need for further research on chemical stability under different environmental conditions.

Keywords: 3DP. Water Quality. Mechanical and Physical-Chemical Parameters. Mercury. DMA-80.

Additive manufacturing is characterized by a variety of printing techniques, including stereolithography (SLA—stereolithography), in which liquid resin is used; model fabrication through the process of fused deposition modeling (FDM—fused deposition modeling); and selective laser sintering (SLS—selective laser sintering), in which materials are selectively fused by a laser.

These processes are collectively referred to as three-dimensional (3DP) printing. Notwithstanding the absence of indicators that would facilitate the evaluation of the repercussions of the proliferation of 3DP utilization, as well as the replacement of production methodologies for materials that are presently obtainable through homemade means, it is nevertheless possible to discern the considerable potential in domains such as dentistry, particularly in the fabrication of aligners, the production of molds, and suction devices for pediatric dentistry, among others [1].

In the field of construction, the practice of printing models of architectural designs, pre-fabricated structures, and prototypes in miniature, along with the use of FreeFAB Wax in concrete molds, has become increasingly prevalent [2,3]. The development and implementation of 3DP have had significant ramifications, particularly in the context of environmental protection and the pursuit of a more sustainable manufacturing process (CP).

This approach aligns with the principles of Green Chemistry and addresses the imperative to mitigate the impact of climate change, as outlined in ODS 9, 11, 12, 13, and 17.

According to Santana (2018) [4], the numerous FDM filaments available on the market, PLA (polylactic acid) [5]; ABS (acrylonitrile butadiene styrene) [6]; PETG (polyethylene terephthalate glycol); Tritan (Copolyester) [7], in addition to various types of liquid resins, have well-established mechanical properties that are made available by manufacturers. However, there is a lack of qualitative and quantitative information about the chemical composition and behavior of printed materials in the environment. As a result, they can be sources of contamination that pose an imminent risk to the environment, compromising the use of these materials and the advancement of 3DP technologies for commercial purposes. Therefore, it is necessary to apply methods to acquire information regarding material stability. The purpose of the stability test is to provide evidence of how the quality of a product varies over time under the influence of environmental factors such as temperature, humidity, solar incidence, salinity, acidity, and chemical species with high toxicological potential.

Received on 12 December 2025; revised 27 February 2026.
Address for correspondence: correspondence: Carlos H. B. M. Filho; Daniela S. Anunciação. Rua Manuel dos Santos Correa – Pitangueiras, Lauro de Freitas, Bahia, Brazil. Zipcode: 42701-320. E-mail: carlos.filho@iqb.ufal.br; daniela.anunciacao@iqb.ufal.br.

J Bioeng. Tech. Health 2026;9(3):209-213

This information can also provide data to determine the shelf life of printed products, in addition to recommending appropriate conditions for use, storage, and disposal [8].

In cases of environments contaminated with ions with high toxic potential, such as in the Mundaú-Maguaba Estuarine Lagoon Complex (CELMM) in Alagoas, mercury levels above the limit established by Brazilian law have already been found [9]. As this is a high-risk element to health, and due to the significant socioeconomic and environmental importance of the CELMM, products intended for use in this region must meet physical and chemical stability criteria in the natural environment in order to be viable for use.

Based on the high adsorption capacity of a functionalized resin for retaining mercury species, both in their inorganic and organic forms, the Portable Floating Device for Removing Hg Species in Aqueous Media was developed and registered with the National Institute of Industrial Property (INPI) under registration number BR 10 2024 024566 0 [10,11].

This technology is an innovative solution for the treatment of water bodies contaminated by mercury, with direct application in natural aquatic environments and effluent systems. The device was designed with a focus on low-cost floating structure, ease of handling in the field, and compatibility with 3D-printed materials, ensuring that there is no interference in the adsorption process by structural components. This approach prevents cross-contamination and maximizes the selectivity and efficiency of the contaminant removal system

Considering the need to advance the TRL and evaluate the characteristics and quality parameters of the 3D-printed material, the present study aimed to characterize the mechanical properties through printed samples inserted in different extreme environments containing mercury and then obtain the chemical properties. It also sought to draw an analogy between pure samples and samples after insertion in critical environments, providing a more accurate comparative study between chemical stabilities. This ensures the possibility of manufacturing products following the principles of environmentally friendly manufacturing and the development of cleaner production.

Materials and Methods

Glassware cleaning and solution preparation were performed with ultrapure water (electrical conductivity < 0.1 μS cm-1) with a resistivity equivalent to 18.2 MΩ.cm-1, using a Milli-Q Reference reverse osmosis purifier (Merck, HE, Germany).

Materials Decontamination

All glassware used in the analyses underwent a decontamination process, beginning with washing in running water and Extran neutral detergent (Merck, HE, Germany) to remove macroscopic residues, followed by rinsing with ultrapure water. The glassware was immersed in a 10% (v/v) nitric acid (HNO_3) solution for a minimum of 12 hours to ensure the removal of contaminants. Subsequently, a new rinse with ultrapure water was performed to eliminate residues. Drying was conducted in a manner that differentiated between volumetric glassware, non-volumetric glassware, and 1.5 mL quartz cuvettes. Volumetric glassware was kept at room temperature to preserve calibration, while non-volumetric glassware was dried in an oven (Soldatel, MG, Brazil) at 50°C for 1 hour to eliminate moisture without compromising the integrity of the material. The quartz cuvettes were dried and any residues were evaporated in a muffle furnace for 1 hour at a temperature of 200°C.

Reagents and Solution Preparation

All reagents used in the experiments were of analytical purity. The solutions were prepared using ultrapure water obtained through a Milli-Q Reference purification system (Merck). Among the materials used, the following polymer filaments stand out: ABS (acrylonitrile butadiene styrene) (GTMax3D, SP, Brazil), PLA (polylactic acid)

(Stratasys, MN, USA) and Tritan, as well as the mercury standard (1000 mg/L) acidified with 5% HNO_3 (Agilent Technologies, California, USA).

Separation Techniques

It began with the dilution of the 1000 ppm (mg/L) mercury standard to a stock solution of 1 ppm, followed by dilutions to 20 ppb (µg/L). The 20 ppb dilutions were transferred to shotts bottles containing 3D printed test specimens (ISO 527 – 5A) with ABS, PLA, and Tritan filaments. All bottles were then transferred to the TE-421 shaker (TECNAL, Piracicaba, São Paulo) and exposed to agitation at 150 RPM for 1 hour, thus beginning the adsorption kinetics test (Figure 1).

At the end of the adsorption stage, all samples were transferred for mercury determination. The total mercury in the samples was determined using a DMA-80 analyzer (Milestone, BR, Denmark), a device based on thermal decomposition coupled with atomic absorption spectrometry. Aliquots of 500 µL were taken from the samples in order to standardize the mercury mass to 10 ng and deposited in quartz cuvettes. The samples, deposited in quartz cuvettes, were inserted directly into the system and subjected to a temperature ramp reaching >600°C, promoting the release of mercury in the form of vapor. This vapor is then concentrated in gold wires, forming amalgams ($AuHg_2$, Au_2Hg, and/or AuHg). Subsequently, a second heating releases the monoatomic mercury, which is quantified by atomic absorption at 253.7 nm. The main advantage of this technique lies in the elimination of pretreatment steps, allowing direct analysis of liquid and solid matrices without the need for conversion to an aqueous medium, unlike conventional atomic absorption methods.

Finally, the test specimens were subjected to a tensile test using EMIC (São José dos Pinhais, Paraná) DL 200 equipment, with a displacement rate of 5 mm/min. The aim was to obtain data such as: modulus of elasticity (MPa), yield stress (MPa), yield strain (%), tensile strength (MPa), and elongation at break (%).

The equipment used is operationally versatile, allowing for multiple types of tensile, compression, and flexural tests to be performed, in addition to covering a wide range of materials such as metals, plastics, composites, and insulators, as a result of

Figure 1. Filament adsorption Kinetics test.

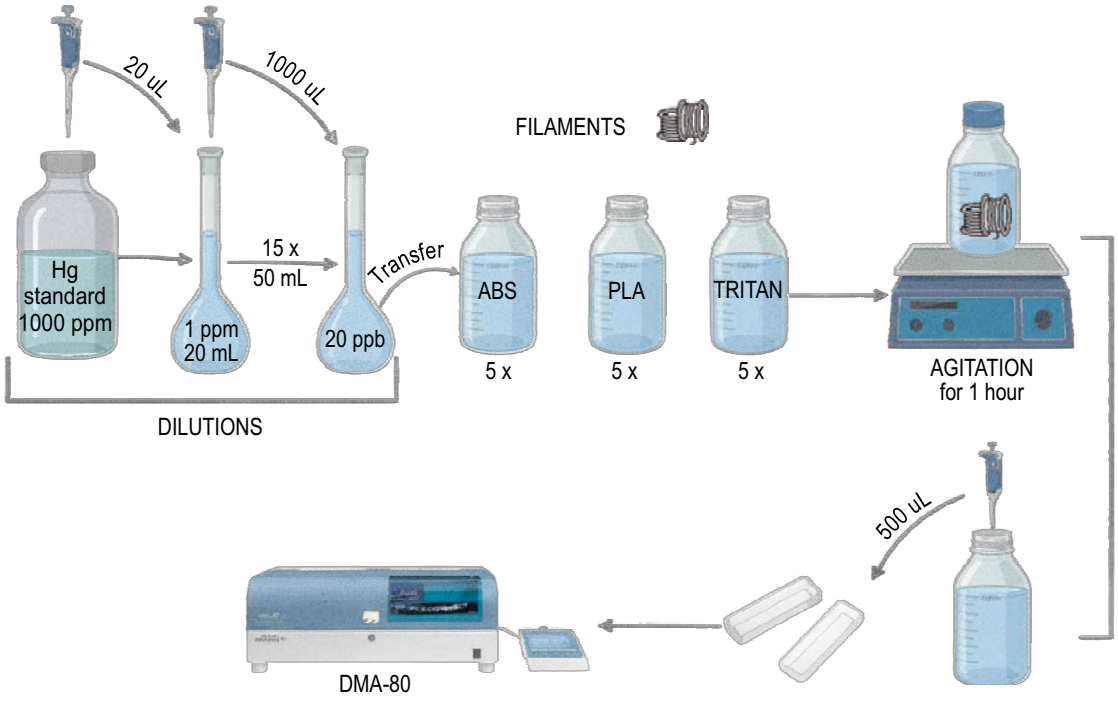

the robust structure of the machinery, variable speed in the range of 0.01 to 500 mm/min, and maximum load of 20kN.

Results and Discussion

Adsorption Test

The adsorption test made it possible to obtain the adsorption efficiency of each polymer filament used. The Figure 2 represents the adsorption capacity of each filament.

The ABS, PLA, and TRITAN filaments resulted in adsorption percentages of 0.12%, 1.83%, and 69.30%, respectively. TRITAN showed high adsorption, which makes it unsuitable for use in products that may be in contaminated environments, despite being the filament with the best physical characteristics compared to the other filaments. Furthermore, ABS and PLA resulted in adsorption efficiencies of 0.12% and 1.83%, respectively, thus, they demonstrated greater feasibility for printing the device structure without material interference and, at the same time, without a memory effect in the event of reuse of the device or filament.

Figure 2. Adsorption efficiency of tritan, ABS, and PLA.

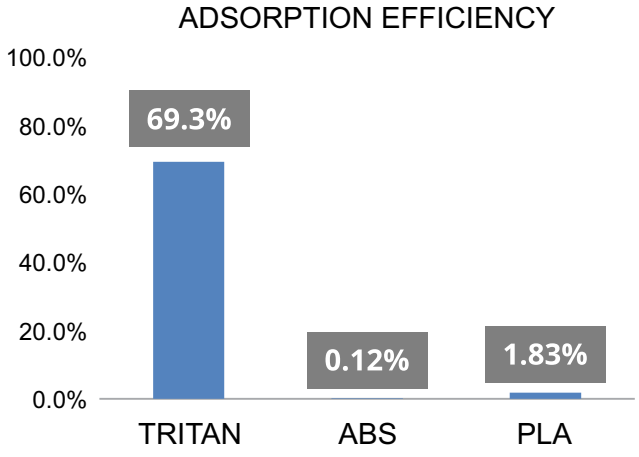

Tensile Test

The results obtained from the tensile analyses of all filaments were compiled in the Table 1 to facilitate the evaluation of these data.

Comparing the physical and mechanical properties listed in the datasheets for each filament, it is possible to determine that there were major structural changes in all filaments due to exposure to water or contact with mercury.

Conclusion

The study showed significant results in a new physical-chemical and mechanical evaluation of the filaments. ABS and PLA showed adsorbent activity of less than 2%, compared to TRITAN's adsorption of 69.3%, emphasizing that both are the most viable options for manufacturing products in contaminated environments, following environmental protection guidelines and the development of cleaner production.

However, all these filaments showed significant structural changes in a critical aquatic environment

Table 1. Results of the tensile test of filaments after adsorption with mercury.

Tensile Test							
Test piece	Stress with Max Force (MPa)	Specific Def with Max Strength (%)	Specific Breakage Def (%)	Breaking Strength (MPa)	Yield stress (MPa)	Def Specific of Flow (%)	Modulus Elasticity (MPa)
Tritan	23.87	7.770	11.88	14.03	13.28	2.669	546.8
ABS	19.77	3.183	7.942	13.81	15.80	2.195	827.2
PLA	27.14	2.877	3.493	22.80	22.28	1.937	1329

with the presence of mercury. This indicates the need for new medium- and long- term chemical stability tests, in addition to the addition of new variables such as other inorganic ions, changes in pH of the medium, and salinity. Thus, increasing the range of data related to the filaments.

References

1. Pinho AC. Análise ambiental, financeira e social da construção por impressão 3D: uma revisão da literatura [dissertação]. Universidade do Porto; 2024.
2. Carvalho JGA. Processos de fabricação aditiva: oportunidades emergentes em arquitetura [dissertação]. Universidade do Porto; 2018.
3. Aguiar LCD. Um processo para utilizar a tecnologia de impressão 3D na construção de instrumentos didáticos para o ensino de ciências [dissertação]. Universidade Estadual Paulista (UNESP); 2016.
4. Santana L, Alves JL, Sabino Netto AC, Merlini C. Estudo comparativo entre PETG e PLA para impressão 3D através de caracterização térmica, química e mecânica. Rev Matéria. 2018;23(4).
5. Stratasys Latin America. PLA filament technical datasheet. 2018
6. Creality. Hyper-ABS filament technical datasheet. 2024.
7. 3DLAB. Ficha técnica tritan. 2024.
8. Agência Nacional de Vigilância Sanitária (ANVISA). Guia de estudos de estabilidade: medicamentos. Guia nº 28, versão 1. Brasília (DF); 2019.
9. Queiroz MIC. A exposição crônica in vivo ao mercúrio inorgânico piora a hipercolesterolemia, o estresse oxidativo e a aterosclerose em camundongos knockout para o receptor de LDL. Ecotoxicol Environ Saf. 2024;275:116254.
10. Associação Brasileira de Normas Técnicas (ABNT). Dispositivo portátil flutuante para remoção de espécies de Hg em meio aquoso. BR 10 2024 024566 0; 2024.
11. Sheremetieff A, Gonçalves AAG. Uma introdução às tecnologias de manufatura aditiva em acordo com a ABNT NBR ISO/ASTM 52900:2018. REUCP. 2020;14(2):81-91.

Development of a Hair Tonic from the Plant Extract of Jaborandi (*Pilocarpus jaborandi*) and Copaiba (*Copaifera langsdorffii*) to Aid in the Treatment of Seborrheic Dermatitis

Débora de Souza Acácio[1]*, Tayná Arcanjo da Costa[1], Thais Alves Rodrigues[1], Natália Leite Ferreira[1], Tatiana Oliveira do Vale[1], Erica Patrícia Lima Pereira[1]

[1]SENAI, CIMATEC University; Salvador, Bahia, Brazil

Seborrheic dermatitis is a chronic inflammatory dermatosis characterized by scaling, sores and other symptoms that negatively impact the patient's quality of life. The aim of this study is to develop a herbal tonic from jaborandi extract (*Pilocarpus jaborandi*) and copaiba oil (*Copaifera langsdorffii*) that can help treat this condition, analyzing the effectiveness of each substance. The research has a qualitativequantitative approach, experimental methodology and descriptive objective. For the microbiological tests, specific analyses were carried out to assess the tonic's potential to promote the growth of microorganisms. The results indicated positive properties of the compounds, revealing, in direct application, the absence of mold and staphylococcus growth in the treated samples. This finding suggests that the extracts potentially have effective antifungal and antimicrobial properties, since they are not capable of enabling the development of microorganisms under the experimental conditions tested. In addition, the organoleptic tests and the flavonoid detection assay also pointed to the efficiency of the compound. Therefore, based on these results, it can be concluded that the herbal tonic made from jaborandi and copaiba extracts is potentially effective in the treatment of dermatitis. In this way, it provides an effective product at a lower cost, making it more accessible to a large part of the population.

Keywords: Tonic. Herbal Medicine. Seborrheic Dermatitis. Jaborandi. Copaiba.

Seborrheic dermatitis is a very common skin disease that causes scaling, redness, itching, sores, alopecia and general discomfort on the skin. It mainly affects the scalp and areas of the head that may include the face, but it is also present in other oily areas of the body, such as the chest and back [1,2].

Therefore, as it is a condition that requires constant and intensive treatment, most products for treating dermatitis are expensive and not very accessible to a large part of the group affected by this disease [1,2].

In this context, and in order to mitigate this obstacle, the project aims to develop a more cost-effective and accessible herbal hair tonic that meets the demands and effectively aids in the treatment of seborrheic dermatitis. This product will be developed from the oils of *Pilocarpus jaborandi* and *Copaifera langsdorffii*, popularly known as jaborandi and copaiba, respectively, because these plants are chemically composed of substances that have antioxidant, antibacterial, anti-inflammatory and other properties, which are capable of alleviating the symptoms of seborrheic dermatitis and strengthening the hair. In addition, this study also aims to explore and prove the efficacy of the plants, as well as the potential and behavior of their respective properties [3,4]. It is worth mentioning that microbiological tests will be carried out and the components will be observed in triplicate, precisely in order to highlight the susceptibility of the herbal hair tonic [4].

Theorethical Background

In this topic, the research associated with the use of *Copaifera Iangsdorffii* oil and *Pilocarpus jaborandi* extract as an auxiliary product in hair treatment will be analyzed. Information will then be presented that underpins the project and scientifically proves the efficacy of the oils, as well as their respective properties [3].

It is stated that jaborandi extract contains a large amount of alkaloids, coumarins, flavonoids

Received on 27 December 2025; revised 23 February 2026.
Address for correspondence: Débora de Souza Acácio. Av. Orlando Gomes, 1845, Piatã, Salvador, Bahia, Brazil. Zipcode: 41650-010. E-mail: debb09souza@gmail.com.

J Bioeng. Tech. Health 2026;9(3):214-220

and terpenes that can be used to treat scalp ailments. Copaiba oil also contains the substances cariophylene and bisabolene, which can help the healing process and act as an anti-inflammatory. Therefore, these data reiterate the susceptibility of the hypothesis under analysis [4]. Therefore, the aim is that the combination of jaborandi extract and copaiba oil can help in the treatment of seborrheic dermatitis.

Seborrheic dermatitis

Seborrheic dermatitis (SD) is a conventional, non-contagious, chronic inflammation that affects around 1 to 3% of the immunocompetent population [1,2]. It has various causes, including: allergies, stress, use of some medications, the presence of a fungus (*Malassezia furfur*) and there may be a genetic predisposition, the diagnosis must be clinical and it is a disease that has no cure, only mitigating treatment. However, treatment is not very accessible, due to the high cost of products that have to be used continuously.

SD is characterized by the appearance of disfigured reddish patches and scaling, which often cause enormous social discomfort. The most affected areas are those with an abundance of sebaceous glands [2]. There is therefore an urgent need for an alternative, more accessible herbal product to help treat the disease.

Jaborandi Extract (*Pilocarpus jaborandi*)

Jaborandi is widely used in the cosmetics industry, as its antioxidant properties are capable of treating various hair problems, as they act on cell renewal, stimulate hair growth, have a moisturizing action and combat dandruff.

The jaborandi plant is rich in pilocarpine, its main chemical component, which is an alkaloid soluble in water, alcohol and chloroform; its melting point is 34°C and its boiling point is 260 °C [4]. This substance is able to promote normalization of the follicle cycle, as it acts directly on the scalp, thus prolonging hair growth.

Based on studies that have already been completed and proven, the influence of the action of flavonoids has been determined. These stand out among the group of natural phenolic products due to their use to treat hair loss, seborrhea and other scalp conditions [5]. Flavonoids have anti-inflammatory, antimicrobial, antioxidant and enzyme-inhibiting properties and can even be used to prevent scalp diseases.

Copaiba Oil (*Copaifera langsdorffii*)

Copaiba is a plant that has various therapeutic properties, which are still being explored by researchers. The main ones are: antiinflammatory, healing, antiseptic, antibacterial, germicidal, antitumor and analgesic. It's worth noting that the prevalence of each substance depends on the species of copaiba [3,6].

The oil is rich in sesquiterpenes and diterpenes, which are the active substances responsible for its properties. Studies have proven the efficacy of copaiba's chemical compounds in medicinal treatment, the main and most analyzed of which are cariophylene and bisabolene, which have antifungal, anti-inflammatory, anti-oedemic and antibacterial activity.

Panthenol

Panthenol, or pro-vitamin B5, is a vitamin synthesized by the body. It is responsible for maintaining the natural hydration of the skin and hair. This vitamin is already widely used in cosmetics due to its moisturizing and healing properties. Furthermore, studies have shown that the higher the concentration and frequency of use of panthenol, the greater the use of its moisturizing properties [7]. Panthenol is therefore a viable ally for the treatment of SD.

Materials and Methods

The article consists of a qualitative approach, as the aim of the research is to jointly evaluate

the efficacy of the antifungal properties present in jaborandi and copaiba plants. Using an exploratory method, we aimed to produce a herbal hair tonic to help treat seborrhea and strengthen hair.

Pilocarpus microphyllus and *Copaifera langsdorffii* were collected from local businesses in Salvador, Bahia. Both plants were collected from the same place, however, the copaiba oil was purchased ready-made, while the jaborandi oil was extracted by the team in the biotechnology laboratory at Senai Cimatec.

Extraction

To extract pilocarpine from jaborandi, a methodology was adopted in which its use was proven and analyzed in the literature. Initially, it is necessary to prepare the tincture, which will be obtained by macerating the dried leaves of *Pilocarpus microphyllus* and using ethyl alcohol as the extracting liquid. After obtaining the tincture, 50mL of the tincture should be evaporated and the residue treated with 10mL of water and five drops of hydrochloric acid. The sample should be filtered and then washed with ethyl ether, ammonium hydroxide will be used to make the medium basic, and it should be stirred twice with 5mL of chloroform. To separate the phases, the chloroform fractions with the nitric acid should be stirred and then mixed with the acid solution. After combining the substances, the chloroform phase will acquire a blue color, showing the presence of an imidazole or glyoxyl nucleus. Finally, the plate will dry for a while in the oven and come into contact with other solvents to determine the zones of each solution.

Tests

Organoleptic Tests

The organoleptic testing stage is crucial in the production of a herbal medicine, since it will be examined and characterized by the organs of sense in the following parameters: sensation to touch, smell and color. For this study, the test carried out by comparing it to a standard reference sample with controlled environmental factors.

Hydrogen Potential Test - pH

To carry out the hydrogenic potential (pH) test, a sample of the product will be used, following the protocol of ANVISA RDC No. 67 (2007) [8] for the pH hydrogenic potential test, using the pH electrode device. A sample of the product is added to a beaker and then the pH electrode is immersed directly into the liquid so that the bulb is completely submerged.

Microbiological Tests

Microbiological tests are essential for detecting risks of contamination and microbiological growth in the tonic. Therefore, the test was carried out in accordance with the Guide to the Stability of Cosmetic Products [9]. In addition, solid culture media were prepared and each analysis was carried out in duplicate. Plates made up of Standard Counting Agar (PCA) were used to count mesophiles, after 48 hours of incubation at 37°C. For the analysis of molds and yeasts, Potato Dextrose Agar (BDA) was used, on plates incubated at 22°C for 3 to 5 days. For the analysis of *Staphylococcus aureus*, a sample was incubated on the surface of Mannitol-salt at 35°C for 48 hours. After the incubation times for each sample, the result of each plate was checked to determine whether it met the expected to obtain the planned effect for the product.

Flavonoid Test

The flavonoid determination test is responsible for identifying the presence or absence of flavonoids in the plant extract, exploring their anti-inflammatory and antioxidant properties. The solution is made up of jaborandi extract and a methanolic solution of the extract, with a concentration of 0.05 mg/mL. 5mL of the methanolic solution of the jaborandi extract (0.05 mg/mL) will be added to a test tube and

5mL of the $AICL_3$ solution, at a concentration of 2%, will need to be added. The solution must be stirred for 1 min and reacted for 30 min. Once this step has been completed, 5mL of $AlCL_3$ solution (2% concentration) must be mixed with 5mL of methanol. To carry out the technique, the spectrophotometer needs to be adjusted to the absorbance at 415 nm, a blank solution will also be used to determine the zero of the spectrophotometer, finally, simply measure the absorbance of the prepared sample by operating the spectrophotometer.

Results and Discussion

Formulation (Table 1)

The tonic was satisfactorily produced from a simple mixture of the compounds, 0.6 mL of aqueous extract of *Pilocarpus jaborandi*, 5 mL of panthenol, 0.5 mL of citric acid (preservative) and 6 mL of the hydroalcoholic extract of copaiba. Everything was mixed together and then placed in the chosen container and stored in an airy, dark place.

Relevance of the Study

In order to prove the relevance of the study and the veracity of the problem discussed, a survey was carried out using a form, which indicated the prevalence of data that reaffirms the significance of the study. In the population studied (Table 2), we observed the difficulties, preferences and reliability of the group when obtaining a herbal product. This fact confirms the theory addressed in the study, regarding lack of access and high costs, highlighting the need to create a product that fully serves patients.

Testing Stage

Following the Quality Control Guide for Cosmetic Products [8,9], physical and chemical tests were carried out in order to ascertain and prove the quality and healthiness of the hair tonic. In summary, satisfactory results were obtained, within the standards established by ANVISA [8].

The organoleptic tests were carried out on two different samples of the tonic, which were checked for smell, color and a pleasant sensation to the touch. Table 3 shows the results of each analysis. In addition, the pH test was also carried out on two different samples and there were no variations, even in different media and prepared at different times (Table 4). It is therefore worth noting that the product meets the required standards.

As for the density test, it was carried out using a pycnometer, only once, the sample was measured and after following the entire protocol, the calculation was carried out and the density found was 1,250 g/mL, thus meeting the standard established for cosmetics.

The microbiological tests (Table 5) were carried out in duplicate and the plates analyzed were not contaminated, nor did they allow the growth of moulds and yeasts, except for the analysis of mesophiles, in which one colony grew, as shown in the table. However, it was not possible to carry out the *Staphylococcus aureus* analysis, as the Mannitol-salt plates were contaminated, indicating that there had been some carelessness during the preparation of the media and the plates

Table 1. Tonic formulation.

Compounds	Concentration	Quantity
Aqueous extract of Jaborandi	2%	0.6 mL
Panthenol	2%	5 mL
Preservative (citric acid)	1%	0.5 mL
Hydroalcoholic extract of Copaiba	2%	6 mL (75% cereal alcohol and 25% water)
Destilled water	59.6%	17.9 mL

Table 2. Research relevance of the study.

Categories	Data Collected	Percentage (%)
People who have Seborrheic dermatitis	8	12.1
People who have already used herbal products	28	42.4
People who prefer to use herbal products	31	47
People who find it difficult to use herbal products	46	69.7
People who would use a herbal tonic	55	83.3
People who would treat Seborrheic dermatitis with a herbal tonic	43	89.6

Table 3. Sample analysis.

Characteristics	Sample 1	Sample 2
Color	Medium brown	Neutral
Smell	Ethilic	slightly scemted
Touch sensation	Pastier, slightly sticky	Liquid, light

Table 4. pH and density test.

Characteristics	Sample 1	Sample 2
pH	3 to 4	3 to 4
Density	-	1,250 mL

Table 5. Microbiological tests.

	Plate 1 (mesophiles)	Plate 1 (molds and yeasts)	Plate 2 (molds and yeasts)
Contaminated	x (1UFG/g)		
Not contaminated		x	x

were unusable. So, with regard to these studies that determine the viability of the cosmetic to provide an ideal environment for the development of microorganisms, we have incomplete data, but it still points to the non-contamination of the hair tonic.

Flavonoids

Flavonoids are antioxidant and anti-inflammatory compounds that are extremely important for ensuring the efficacy of hair tonics.

For this reason, a method used was capable of detecting and indicating the presence of flavonoids in the extract, which proved to be positive, as evidenced by the change in the color of the extract to an orange tone, which is equivalent to the presence of flavone, a subtype of flavonoids. The presence of flavonoids in the product is therefore proven, indicating a likelihood of success for the properties explored in this study.

The results obtained from using the tonic to help treat seborrheic dermatitis show a promising alternative for managing the disease. The

composition of jaborandi extract with copaiba oil is potentially effective in helping to treat the symptoms of dermatitis. Compared to conventional treatments, such as antifungal shampoos and topical corticosteroids, the jaborandi and copaiba tonic presents a more natural and less aggressive approach, not only for the individual, but also for nature. However, conventional treatments, although more intensive and with immediate results, are often associated with side effects, such as scalp irritation and microbial resistance, as well as being more expensive on the market.

Therefore, the use of herbal medicine can offer a less aggressive alternative that is more affordable for the patient, as well as generating less waste to dispose of. Furthermore, despite the encouraging results, this study has some limitations, such as the lack of direct tests on the *Malassezia furfur fungus* and the short duration of follow-up.

Future research should involve a larger number of participants and longer observation periods to confirm these findings and better understand the mechanisms of action of the active compounds. Standardizing the concentration of the jaborandi and copaiba extracts is also crucial to ensure the consistency of the results. The hair tonic based on jaborandi and copaiba has therefore emerged as a promising, natural alternative to support the treatment of seborrheic dermatitis, offering and enabling an improvement in patients' quality of life. However, more studies are needed to confirm its long-term efficacy and safety.

Conclusion

Therefore, the components of Pilocarpus jaborandi have vasodilating, antioxidant, anti-inflammatory and antimicrobial actions. In addition to promoting various benefits for the treatment of hair problems, such as cell renewal, stimulation of hair growth, moisturizing and anti-dandruff action. Among the substances present in the leaves of Pilocarpus Jaborandi, pilocarpine, the active ingredient explored in this study, which has a high vasodilating action, enables the normalization of the follicle cycle, acting directly on the scalp. Copaiba, a plant also explored during the study, has various therapeutic properties, such as antiinflammatory, healing, antiseptic, antibacterial, germicidal, antitumor and analgesic action. However, the prevalence of each activity depends on the species. Copaiba oil is full of sesquiterpenes and diterpenes, which are the active ingredients that give the leaves their properties. And studies have already proven the substance's susceptibility. Thus, the use of jaborandi and copaiba is very promising for helping to treat SD, since the tests and bibliographical research point to the efficacy and guarantee of the expected action of the product and the increase in its potential when compiling the elements. Finally, the study achieved the desired result and fulfilled the objective of exploring the behavior of each component in the face of the problem presented, and the tests carried out highlighted the properties and advantages associated with the use of phytotherapics, thus bringing more visibility and corroborating the development of studies that promote the growth of the use of phytotherapic products, since they are more beneficial to human health and the environment.

References

1. Formariz T, Spera L, Concenza MC, Cinto P. Seborrheic dermatitis: causes, diagnosis and treatment. Araraquara (SP); 2005. Available at: https://www.cff.org.br/sistemas/geral/revista/pdf/72/i06-infdermatite.pdf
2. Casagrandi I. Seborrheic dermatitis: a literature review on general aspects. Barra Funda (SP); 2020. Available at: https://bwsjournal.emnuvens.com.br
3. Carvalho LO, Milke LT. Importância terapêutica do óleo-resina de copaíba: enfoque para ação anti-inflamatória e cicatrizante. Rev Eletr Farm. 2014;11(2):12. doi:10.5216/ref.v11i2.27852. Available at: https://revistas.ufg.br/REF/article/view/27852
4. Tinoco EE, Sousa K, Marques MJ, Silva NC. Development of a hair tonic using *Pilocarpus extract* (jaborandi). 2021. Available at: http://www.mastereditora.com.br/bjscr
5. Lima CG, Comarella L. Suggestion for the development of auxiliary soap-shampoo formulations for the treatment of seborrheic dermatitis. 2013. Available at: https://revista.uniandrade.br/index.php/revistauniandrade/article/view/43

6. Santos F, et al. Use of coconut oil (*Attalea speciosa*) as an emollient in a phytocosmetic formulation with moisturizing action. Imperatriz (MA); 2020. Available at:http://ojs.unirg.edu.br/index.php/1/article/download/3227/1708
7. Camargo Junior FB. Development of cosmetic formulations containing panthenol and evaluation of their moisturizing effects on human skin by cutaneous bioengineering [dissertação]. Ribeirão Preto: Universidade de São Paulo; 2006. doi:10.11606/D.60.2006.tde-17012007-143439.
8. Agência Nacional de Vigilância Sanitária (ANVISA). Guia de controle de qualidade de produtos cosméticos. Brasília (DF); 2007.
9. Agência Nacional de Vigilância Sanitária (ANVISA). Resolução RDC nº 14, de 28 de março de 2014. Dispõe sobre registro de produtos cosméticos. Brasília (DF); 2014.

Evaluation of the Protein Production of Fungal Strains in Alternative Media

Lavínia Laís Nepomuceno da Silva[1]*, Carine dos Reis Teixeira[1], Amanda Tanan Pereira[1], Tatiana Oliveira do Vale[2], Letícia de Alencar Pereira Rodrigues[2], Marcelo Andres Umsza Guez[1]

[1]Federal University of Bahia (UFBA); [2]SENAI CIMATEC University; Salvador, Bahia, Brazil

The growing demand for sustainable protein sources in the context of global food security has fueled the development of innovative alternatives to animal meat, and in this research, the use of the fermentation process as a technological solution. In this context, mycoprotein produced by filamentous fungi, such as *Fusarium venenatum*, can be subjected to submerged fermentation to evaluate protein biomass production. Mycoprotein from filamentous fungi stands out as a promising alternative due to its nutritional value, sensory characteristics similar to those of meat, and lower environmental impact. It is necessary to identify the most efficient culture media to optimize biomass production and protein synthesis. Thus, the objective of this study is to evaluate the potential of *Fusarium venenatum* under certain medium compositions and fermentation conditions that can significantly favor mycelial growth and the final protein content of the biomass. Methods were established to evaluate spore growth, demonstrating greater efficacy of the DRBC culture medium. Fermentation tests were performed using liquid SD and FM medium, incorporating winemaking residues. This use of byproducts as an alternative medium contributes to greater mycoprotein sustainability. The parameters for the experiments were 180 rpm and 28°C, with quantification of dry biomass and protein. The results obtained demonstrated that adapted media generated greater biomass, while without adaptation, higher protein levels were observed. Significant growth was observed in the Adapted 2 (3%) medium, with 0.949g of dry biomass. The FM protein results were 35.6% in 24 hours. These findings reinforce the biotechnological potential of this microorganism as a promising source of alternative protein, contributing to technological innovation in the food sector.

Keywords: Mycoprotein. *Fusarium venenatum*. Submerged Fermentation. Alternative Protein.

The rapid growth of the world's population is driving a demand for food, especially protein, requiring an increase of up to 73% in global food production. However, the current food system, based on the high consumption of meat of animal origin, contributes to an increase in greenhouse gas emissions, excessive consumption of water and land, and loss of biodiversity [1,2].

In this scenario, filamentous fungi have emerged as a promising source for protein production due to their rich amino acid composition, natural binding capacity and fibrous texture. It is a valuable source of protein, minerals, vitamins and antioxidants and has a low fat content [2].

Received on 20 December 2025; revised 15 February 2026.
Address for correspondence: Lavínia Laís Nepomuceno da Silva. Av. Orlando Gomes, 1845, Piatã, Salvador, Bahia, Brazil. Zipcode: 41650-010. E-mail: lavinianepomuceno@ufba.br.

J Bioeng. Tech. Health 2026;9(3):221-226

These fungi have been studied in bioprocesses such as submerged fermentation, which allows the production of biomass and metabolites under controlled conditions, with less environmental impact and reduced costs, which generates great interest for industrial applications [1,3].

The sustainability of mycoprotein production can be improved by using agro-industrial waste as cultivation substrate. In the wine industry, byproducts of alcoholic and malolactic fermentations, rich in organic compounds, carbohydrates and nutrients, and a variety of macro- and micronutrients, present potential as alternative sources for filamentous fungi [4,5].

This study aims to prospect and characterize microorganisms with the potential to generate inputs for the alternative protein industry, taking as a starting point the kinetic characterization of microbial growth, including the evaluation of biomass and protein metabolism of *Fusarium venenatum* CML 3311, to offer biotechnological solutions for a more sustainable food system.

Materials and Methods

Submerged Fermentation

The strain used for this work was *Fusarium venenatum* CML 3311, obtained from the Institute of Health Technology (ITS), a laboratory located at SENAI CIMATEC University. Different types of culture media were used: Dichloran Rose Bengal Chloramphenicol Agar (DRBC Agar), Sabouraud Dextrose Broth (SD), GY medium [6], Fermentation medium (FM) [7], and the adaptation of GY and FM media enriched with malolactic and alcoholic fermentation residues from the wine industry.

The process began with the activation of the freeze-dried strain and subsequent testing stages for reactivation, purity and viability analysis. Starting with a fresh pre-culture, it was replenished on DRBC agar medium and incubated at 28°C [8] for a period of more than 10 days, depending on spore growth. Subsequently, the spore solution was prepared by adding 10 mL of sterile distilled water to the entire petri dish, adapted from Tong and colleagues [7], gently scraping the surface with a bacteriological loop, filtering the solution with gauze and the aid of a sterile beaker, removing a 10 uL aliquot and counting the spores in the Neubauer chamber, repeating the process until the macroconidia count is above 2,000 and adjusting the concentration to $5x10^6$ conidia [7]. With the concentration adjusted, the parameters were 28°C, 180 rpm and a maximum time of 72 hours.

Two methodos were applied to quantify the biomass: one with the original media and samples taken every 24 hours, and the other with adapted GY and FM media, using concentrations of 0.7; 2 and 3% of wine fermentation residues, replacing the yeast extract in the original FM formula [7], with samples taken only after 72 hours. The other stages included filtering the biomass using autoclavable systems, a Whatman membrane and a vacuum pump [9], weighing the wet biomass, collecting aliquots for pH measurement, and drying the biomass in a forced-air oven at 40°C for 24 hours [10].

Protein Quantification

To quantify the proteins using the Kjeldahl method, the tests were carried out in the Physical-Chemical Food Laboratory (SENAI CIMATEC University). The procedure was according to Lutz's method [11] with the conversion factor being kept at 6.25 for calculating total biomass proteins. Another methodology was evaluated to quantify the protein content. In the method carried out using the Bradford protocol, reagent and a BSA standard curve prepared at the SENAI CIMATEC Biotechnology Laboratory were used, using a methodological standard prepared at the laboratory and following the methodology of Oliveira [12], which was read on a spectrophotometer at an absorbance of 595nm and with the calculations referring to the standard curve of the laboratory in which the test was carried out.

Results and Discussion

Medium of Culture

To enable the pure and isolated growth of *Fusarium venenatum* CML 3311, the DRBC Agar medium(DichloranRoseBengalChloramphenicol) was determined to be the most viable. With this medium, it was possible to visualize the reproductive structures of macroconidia according to those described by Lazarotto [13].

The design of the liquid media was also determined, with the classic Saboraud Dextrose Broth (SD) medium, the enriched Fermentation medium (FM) medium and, finally, adaptations using malolactic and alcoholic fermentation residues from this culture medium, which had already been validated as viable in previous fermentations.

The first results described the establishment of the ideal culture media for the characteristics that favored the DRBC Agar medium to demonstrate greater efficiency in the sporulation of *F. venenatum* which is attributed to its

formulation, which modulates the fungal metabolism by combining controlled oxidative stress (rose bengal) with the availability of metal cofactors *F. venenatum* sporulation is attributed to its formulation, which modulates fungal metabolism, combining controlled oxidative stress (rose bengal) and the availability of metallic cofactors, inducing the macroconidia required for the concentration adjustment phase of this work, visually compared with Lazarotto's findings [13] to determine the target cells of macroconidia reproductive structures. Taking into account the media that were modified with the adaptation of yeast extract, its rich and complex composition that provides peptides, aminoacids, vitamins and some essential carbohydrates for microbial growth [12], justifying that this approach can meet the demand for cheaper cultivation media and reduce the impacts associated with the disposal of this waste, thus being a relevant alternative [4].

Submerged Fermentation

Based on validation at a temperature of 28°C, carried out in other studies, the ideal speed to stimulate biomass production was determined, with 180 rpm being the best agitation in this temperature range. The fermentation processes were started with four different media, according to the method of Tong and colleagues [14].

Four growth curves were constructed (Figures 1 to 4), with quantification of dry biomass (Tables 1 and 2) and evaluation of post-fermentation pH variation (Tables 3 and 4), within the established submerg parameters and evaluated for a maximum of 72 medium hours.

Both curves in Figures 1 and 2 show exponential growth between 24 and 48 hours and a deceleration phase at 72 hours, according to Table 1.

The curves (Figures 3 and 4) showed higher biomass production with 3% residue. Both showed similar growth to the FM medium with 0.7%, showing that the higher the concentration, the higher the level of biomass generation, as shown in Table 2.

Figure 1. Growth curve of *F. venenatum* in submerged fermentation at 28°C, 180 RPM with FM medium without adaptation.

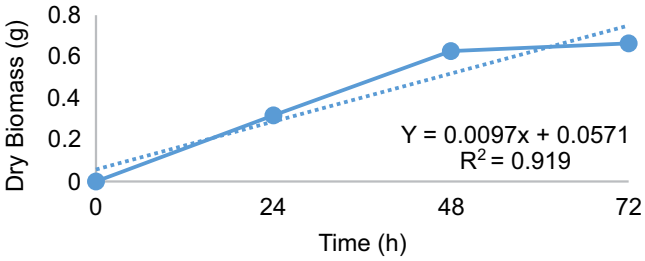

Figure 2. Growth curve of *F. venenatum* in submerged fermentation at 28°C, 180 RPM with SD medium.

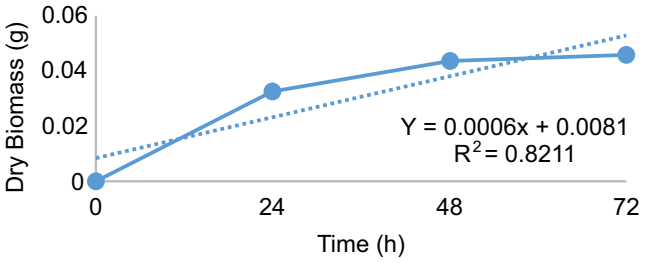

Figure 3. Growth curve of *F. venenatum* in submerged fermentation at 28°C, 180 RPM with FM medium adapted with malolactic residue.

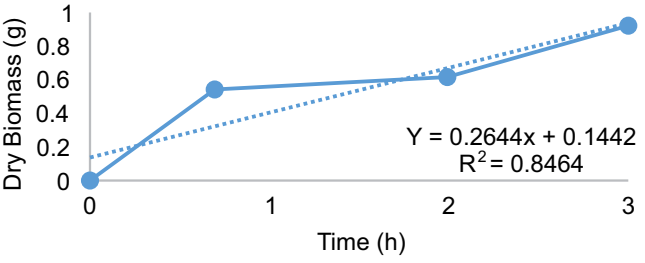

Figure 4. Growth curve of *F. venenatum* in submerged fermentation at 28°C, 180 RPM with FM medium adapted with alcoholic residue.

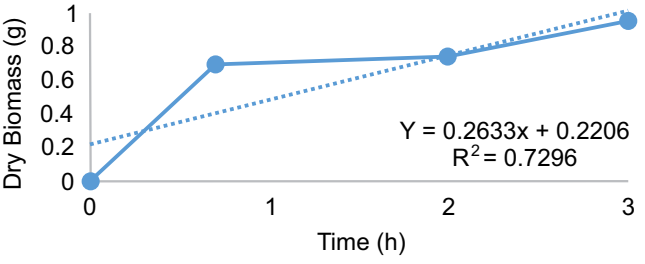

Table 1. Dry biomass (g) of *F. venenatum* under conditions of 180 rpm agitation at 28°C with media without adaptation.

Time	FM	SD
24h	0.319	0.032
48h	0.633	0.043
72h	0.669	0.045

Table 2. Dry biomass (g) of *F. venenatum* under conditions of 180 rpm agitation at 28°C with FM medium adapted.

Residue Concentration	FM malolatic	SD alcoholic
0.7%	0.541	0.697
2%	0.621	0.737
3%	0.923	0.949

In the FM medium (without adaptation), there was a continuous increase in biomass over 72 hours, with exponential growth of 98.43% up to 48 hours and a subsequent slowdown, with an increase of 5.69% (Table 1). As reported by Tong and colleagues [7] using *F. venenatum* strain TB01 grown in a bioreactor with FM medium, 5.80 g/L of biomass was reached after 72 hours and Ahmad and colleagues [5] with *F. venenatum* ATCC 20334, which produced 5.46 g/L of biomass in 72 hours in a complex medium with glucose as a carbon source. When the values from this study are converted into g/L, there is a positive potential, since 72 hours would be 6.69 g/L.

In the SD medium, growth was substantially lower, with 34.3% in 48h and an increase of only 4.65% in 72h, possibly due to the absence of specific mineral salts present in the FM medium, which may have prevented more vigorous mycelial growth. Compared to the literature, Pradeep and colleagues [9] presented a maximum biomass production of 4.47 0.12 g/L for *Fusarium moniliforme* KUMBF1201 in Potato Dextrose Broth (PDB) medium, which is also a less enriched medium, but obtained a significant result. The magnitude of the final biomass obtained by Pradeep and colleagues [9] (which would be 0.447 g in 100 mL) is approximately ten times greater than the 0.045 g/100mL produced in the SD medium, suggesting that the Fusarium strain used requires nutrients not provided by the SD medium.

In FM modified with malolactic residue, there was a 70.6% increase in biomass, and in alcoholic FM, a 36.1% increase between the lowest and highest concentrations (Table 2). The experiment carried out by Tong and colleagues [14] showed a production of 9.53 g/L (0.953 g/100mL) of *F. venenatum* mycoprotein in 72 hours, with the pH dropping from 6 to 4 after 48 hours of fermentation, comparable to the production of 0.923g and 0.949g of biomass at the 3% concentration in this study. When comparing these results, the addition of winemaking waste to FM resulted in higher biomass production, with gains proportional to the increase in concentration.

The variation of pH (Table 3) indicates that an increase in biomass in media with an initial pH 6 causes a reduction in this value, which is typical of fermentative processes, due to carbon consumption and the production of organic acids. With regard to the pH of growth in SD medium (Table 4), the stabilization at around 5.11 to 5.24 contrasts with the sharp drop of 3.03 on average in FM medium, reflecting greater metabolic activity and biomass production. On the other hand, the lower biomass production in the SD medium implies less intense metabolic activity [9].

Protein Quantification

The protein production analysis of the biomass generated provided an estimate of biomass production and the synthesis of metabolites of interest.

The quantification of total proteins was evidenced in the Kjeldahl analysis, for the determination of the total nitrogen content in a sample, which is correlated with the total nitrogen content of protein [10].The other method performed by Bradford, is a colorimetric technique [12]. The time-varying protein analyses show a pattern of protein reduction (Tables 5-7).

Table 3. pH results of fermentation under conditions of 180 rpm agitation at 28°C with media without FM and SD adaptation.

Time	FM	SD
24h	3.33	5.24
48h	2.80	5.17
72h	2.74	5.11

Table 4. pH results of fermentation under conditions of 180 rpm agitation at 28°C with media FM adaptation.

Residue Concentration	FM malolatic	FM alcoholic
0.7%	3.25%	3.06%
2%	3.30%	2.98%
3%	3.07%	2.76%

Table 5. Protein analysis using the Kjeldahl method under conditions of 180 rpm at 28°C with FM medium without adaptation.

Time	Protein
24h	35.6%
48h	30.0%
72h	28.4%

Table 6. Protein analysis using the Kjeldahl method under conditions of 180 rpm at 28°C for 72 hours with adapted FM media.

Residue Concentration	FM malolatic	FM alcoholic
0.7%	15.5%	20.7%
2%	19.7%	21.5%
3%	20.3%	24.0%

Table 7. Protein analysis using Bradford reagent under conditions of 180 rpm at 28°C with SD medium.

Time	Protein
24h	1151µg/mL
48h	1068µg/mL
72h	746µg/mL

The analyses showed a reduction of the protein over time, characteristic associated with fungal metabolism in submerged cultures. The drop in pH and the slowdown in growth indicate the progressive consumption of nutrients and the reaching of a plateau in the experimental conditions, where the lower pH generates stress and reduces the production of protein in the biomass Srivastava and colleagues [3]. On the other hand, increasing the concentration of the residue resulted in a higher protein content.

Increasing the percentage of residue stimulates protein production, with better performance in alcoholic residue. However, the method did not prove to be effective, as at 72 hours the values were below those of the non-adapted medium.

According to a report by Tong and colleagues [14], using a wild strain (WT) of *F. venenatum* TB01, results of 39.4% were found at 48h, which remained stable at 72h, close to that found in this work at 24h for FM (35.6%). This difference in protein percentages may be due to other additional factors in this article, such as the strict control of aeration mentioned above.

Thomas and colleagues [10], on the other hand, obtained 49.99% protein in 48h, with a different carbon source and greater agitation, suggesting that these parameters should be evaluated in the future to optimize the protein percentage, since this result is also higher than the aforementioned article which also evaluated under 28°C and 180 rpm.

The Bradford method is widely recognized for its sensitivity and speed for quantifying proteins in micrograms, based on protein-dye binding. In Oliveira's experiment [12] on lipase production by *Fusarium oxysporum* in submerged fermentation (180 rpm, 28 °C) and protein determination by the Bradford method, the values ranged from 0.11; 0.42 and 9.55 mg/mL, depending on the optimization of the medium. These results were higher than those obtained in this study at 24 hours (1.151 mg/mL) compared to 9.55 mg/mL, and lower than the lowest value found at 72 hours (0.726 mg/mL) compared to 0.11 mg/ml in the

article, showing that quantification depends on the medium used.

Conclusion

The project therefore, has broad biotechnological potential, with relevant results on biomass growth and protein quantification in different media. This work shows the potential for producing proteins from the fungal cultivation of the Fusarium strain, as well as demonstrating the potential for using industrial waste. However, limited time and resources indicate the need to optimize parameters in order to increase production over time, and this study could be part of more comprehensive research of interest to the food industry.

Acknowledgement

We thank to the Laboratory ITS for providing the strain of the fungus, and Senai - CIMATEC whose support was crucial to the success of our research.

References

1. Heidemann MS, Pereira IO, Maske BL, Massaki S, Manzoli MC, Valentini N, et al. Fermentação no Brasil: o potencial para a produção de proteínas alternativas. São Paulo: Tikibooks; The Good Food Institute Brasil; 2025.
2. Gonçalves LGF. Avaliação do perfil de diferentes grupos alimentares em relação ao consumo de micélios de fungos como proteína alternativa [trabalho de conclusão de curso]. 2023.
3. Srivastava S, Pathak N, Srivastava P. Identification of limiting factors for the optimum growth of *Fusarium oxysporum* in liquid medium. 2011. doi:10.4103/0971-6580.84262.
4. Karimi S, Mahboobi SN, Lundh T, Mahboubi A, Kiessling A, Taherzadeh MJ. Evaluation of filamentous fungal biomass cultivated on vinasse as an alternative nutrient source of fish feed: protein, lipid, and mineral composition. Fermentation. 2019. doi:10.3390/fermentation5040099.
5. Ahmad ML, Farooq S, Alhamoud Y, Li C, Zhang H. A review on mycoprotein: history, nutritional composition, production methods, and health benefits. Trends Food Sci Technol. 2022. doi:10.1016/j.tifs.2022.01.027.
6. Tong S, An K, Chen W, Zhau W, Sun Y, Wang Q, Li D. Evasion of Cas9 toxicity to develop an efficient genome editing system and its application to increase ethanol yield in *Fusarium venenatum* TB01. 2022. doi:10.1007/s00253-022-12178-5.
7. Tong S, An K, Zhou W, Chen W, Sun Y, Wang Q, Li D. Establishment of high-efficiency screening system for gene deletion in *Fusarium venenatum* TB01. J Fungi. 2022.
8. Leslie JF, Summerell BA, editors. The Fusarium laboratory manual. 2006.
9. Pradeep FS, Pradeep BV. Optimization of pigment and biomass production from *Fusarium moniliforme* under submerged fermentation conditions. Int J Pharm Pharm Sci. 2013.
10. Thomas AB, Shetane TD, Singha RG, Nanda RK, Poddar SS, Shirsat A. Employing central composite design for evaluation of biomass production by *Fusarium venenatum: in vivo* antioxidant and antihyperlipidemic properties. Appl Biochem Biotechnol. 2017.
11. Instituto Adolfo Lutz. Métodos físico-químicos para análise de alimentos. São Paulo: Instituto Adolfo Lutz; 2008.
12. Oliveira BH. Imobilização e caracterização parcial de lipase produzida por *Fusarium oxysporum* em fermentação submersa [dissertação]. 2012.
13. Lazarotto M. Identificação e caracterização de *Fusarium* spp. e *Pestalotiopsis* spp. associados a Carya illinoinensis no Rio Grande do Sul [tese]. 2013.
14. Tong S, Chen W, Hong R, Chai M, Sun Y, Wang Q, Li D. Efficient mycoprotein production with low CO_2 emissions through metabolic engineering and fermentation optimization of *Fusarium venenatum*. J Agric Food Chem. 2024.

Physicochemical Characterization of Licuri Almond (*Syagrus coronata*) as Raw Material for Biodiesel Production

Helen de Souza Campos[1]*, Marcos Machado da Rocha[1], Alison Borges Vitor[1], Jadiel dos Santos Pereira[2], Luciano Hocevar[2], Carine Tondo Alves[2]

[1]Federal University of Recôncavo da Bahia (UFRB), Center for Science and Technology in Energy and Sustainability; Feira de Santana, Bahia; [2]SENAI CIMATEC University; Salvador, Bahia; Brazil

Licuri (*Syagrus coronata*) is a palm tree native to the Brazilian semiarid region. Its kernels have a high oil content, making them a potential raw material for biodiesel production. This study aims to characterize the kernel through analyses of moisture, ash, volatile matter, and fixed carbon, discussing the feasibility of its use in biodiesel production. The discussion includes a comparison of the viscosity of licuri oil with other vegetable oils before and after transesterification, based on previous studies. The results suggest that licuri has properties compatible with established oilseeds, with advantages associated with oxidative stability and potential for regional use.

Keywords: Licuri. Biodiesel. Oilseeds. Physicochemical Properties.

The search for renewable energy sources has driven studies on the use of native oilseeds in biodiesel production. Licuri (*Syagrus coronata*), abundant in the semiarid Northeast region, stands out for its high oil content and potential to generate positive socioeconomic impacts in the region, according to studies by Santos and colleagues (2011) [1] and Agron Food Academy (2021) [2]. Furthermore, the fatty acid composition of licuri oil, rich in lauric acid and other saturates, gives biodiesel high oxidative stability, according to Silva and colleagues (2018) [3]. The same authors present that licuri oil is rich in saturated fatty acids, namely: lauric acid (42.6% to 44.6%), myristic acid (13.2% to 14.8%), palmitic acid (6.5% to 7.1%), caprylic acid (9.06% to 11.6%) and capric acid (6.03% to 6.7%). On the other hand, unsaturated fatty acids are present in smaller quantities, with emphasis on oleic acid (10.9% to 13.1%) and linoleic acid (1.0% to 2.5%).

Transesterification, according to Santos and colleagues (2011) [1], is the reaction between triglycerides and an alcohol (methanol or ethanol) in the presence of a catalyst, resulting in esters (biodiesel) and glycerol. Methanol has advantages such as greater reactivity, lower cost, and shorter reaction time, but it is a toxic alcohol of fossil origin. Ethanol, on the other hand, is renewable, less toxic, and can be produced locally, although it has disadvantages such as lower reactivity and the need for a greater excess of alcohol, higher temperature, and higher reaction time. It is also hygroscopic, which can lead to emulsion formation and saponification.

Biodiesel performance depends on several characteristics, such as cetane index, oxidative stability, pour point, and viscosity. Oils with a high content of saturated fatty acids, such as licuri, provide greater thermal and oxidative stability, reducing the formation of deposits in the engine, according to Silva and colleagues (2007) [4]. Licuri biodiesel, in turn, has excellent fluidity and efficient combustion, comparable to palm oil.

Material and Methods

The licuri almonds were subjected to laboratory analyses to determine moisture, volatile matter, ash, and fixed carbon. Fixed carbon was calculated by subtracting the percentages of moisture, volatile matter, and ash from 100%.

Received on 15 December 2025; revised 20 February 2026.
Address for correspondence: Helen de Souza Campos. Av. Centenário, 697, SIM. Feira de Santana, Bahia, Brazil. Zipcode: 44.085-132. E-mail: helendesouzacampos@aluno.ufrb.edu.br.

J Bioeng. Tech. Health 2026;9(3):227-230

The following methods, which were utilized in this study, are described below in a step-by-step format for replicability.

Ash Content

The ash content was determined by subjecting a known mass of the sample to combustion in a muffle furnace. The procedure followed was based on a standard gravimetric method:

1. A clean, pre-weighed porcelain crucible was placed in an oven at 105 °C for 30 minutes, then transferred to a desiccator to cool for 30 minutes.
2. The crucible was weighed and the mass (mass of crucible) was recorded.
3. Approximately 1 to 2 grams of the licuri almond sample were placed in the crucible.
4. The crucible with the sample was weighed and the mass (mcrucible+sample) was recorded.
5. The crucible was placed on a hot plate to slowly incinerate the sample until the smoke ceased.
6. The crucible was then transferred to a muffle furnace and heated at 550 °C for 2 hours.
7. After heating, the crucible was cooled in the desiccator for 30 minutes and weighed again.
8. This heating, cooling, and weighing process was repeated until a constant mass (constant mass) was achieved.
9. The ash content was calculated using the formula:

Ashes (%) = (mcrucible + sample − mcrucible) (constant mass − mcrucible)×100

Volatile Matter

The volatile matter was determined based on the mass loss after heating the sample to a high temperature under controlled conditions.

1. A clean, pre-weighed porcelain crucible with a lid was placed in an oven at 105 °C for 30 minutes, then transferred to a desiccator to cool for 30 minutes.
2. The crucible and lid were weighed and the mass (mcrucible+lid) was recorded.
3. Approximately 1 to 2 grams of the licuri almond sample were placed in the crucible.
4. The crucible with the sample and lid was weighed and the mass (mcrucible+lid+sample) was recorded.
5. The crucible was placed in a muffle furnace preheated to 950 °C for exactly 7 minutes.
6. After heating, the crucible was cooled in a desiccator for 30 minutes and weighed again.
7. The volatile matter was calculated using the formula:

Volatile (%)=(mcrucible + lid + sample − mcrucible + lid) [(mcrucible + lid + sample) − (crucible+lid+final sample)]×100

Moisture Content

The moisture content of the sample was determined by thermogravimetric analysis using a BEL moisture analyzer (moisture balance). For the procedure, an initial mass of 5.0771 g of the sample was evenly placed on a weighing pan. The equipment, which uses a halogen lamp for heating, initiated an automatic drying cycle, monitoring the mass loss in real time until a constant weight was reached.

Fixed Carbon

The fixed carbon content was determined by difference, using the following formula:

Fixed Carbon (%) = 100% − (Moisture (%) + Volatile Matter (%) + Ash (%))

Results and Discussion

Table 1 presents the average results obtained for the physical-chemical analyses of licuri almonds.

The results obtained from the physical-chemical analysis of licuri almonds (Table 1) reveal important characteristics for their application in biodiesel production. The ash analysis showed an average value of 1.90%. This

Table 1. Average results obtained for licuri almonds.

Parameter	Average Value
Moisture (%)	3.38
Ash (%)	1.90
Volatile Matter (%)	53.15
Fixed Carbon (%)	41.57

low inorganic residue content is a highly positive aspect, since excessive ash can cause problems in combustion equipment. Volatile matter, in turn, showed an average value of 53.15%, indicating a significant amount of compounds that can be released during combustion and contribute to the biomass's energy potential. Fixed carbon, calculated at 41.57%, represents the almond's calorific potential, the energy that can be extracted through combustion. The low moisture content of 3.38% in the licuri sample is a very positive result for biodiesel production. This is important because excess moisture can impair the process, causing soap formation and consuming the catalyst (KOH), which is essential for the reaction. With low moisture, biodiesel production tends to be more efficient.

Table 2 shows the comparison of the viscosity of licuri oil with other vegetable oils before and after transesterification.

As shown in Table 2, licuri oil has an initial viscosity of 8.5-12.0 mm²/s, which is lower than that of other oils such as soybean and sunflower. However, the viscosity reduction after transesterification is significant, approaching the values required by the National Petroleum Agency (ANP) specifications for biodiesel. This characteristic indicates good conversion and compliance with standards, in addition to confirming licuri's potential as a feedstock.

Conclusion

The results indicate that licuri almonds exhibit characteristics consistent with other oilseeds used in biodiesel production, notably low moisture content and good chemical composition. Comparative viscosity analysis reinforces their technical potential, especially considering the oil's oxidative stability. Future studies should include experimental biodiesel production and its complete characterization. Process optimization, considering appropriate parameters, can make licuri biodiesel a sustainable and economically viable alternative, contributing to the diversification of the energy matrix, especially in regions where the raw material is abundant.

Acknowledgement

We thank the Federal University of Recôncavo da Bahia (UFRB) for its support and invaluable encouragement of this research. The scholarship awarded was crucial to the completion of this work

Table 2. Viscosity of oils before and after transesterification.

Oil	Oil Viscosity (mm²/s at 40°C)	Biodiesel Viscosity (mm²/s at 40 °C)	References
Licuri	8.5-12.0	3.8-4.5	Silva and colleagues, 2018 [3]
Soy	30-35	4.0-4.5	Guimarães, 2019 [5]
Palm	35-40	4.5-5.5	Lima and colleagues, 2012 [6]
Sunflower	30-40	4.0-5.0	Silva and colleagues, 2007 [4]
Canola	30-35	4.1-4.6	Lima and colleagues, 2012 [6]
Corn	32-37	4.2-4.8	Silva and colleagues, 2007 [4]
Cotton	45-55	4.5-5.2	Lima and colleagues, 2012 [6]

and the advancement of analyses, allowing me to dedicate myself fully to research. This support, which goes beyond financial considerations, is crucial to scientific development and reflects the institution's commitment to the production and promotion of knowledge.

References

1. Santos JAR, et al. Avaliação das propriedades físico-químicas, fluidodinâmicas e oxidativas do biodiesel de licuri (*Syagrus coronata*) e das blendas (licuri/soja) [dissertação]. João Pessoa: Universidade Federal da Paraíba; 2011.
2. Agron Food Academy. Autenticidade e qualidade do óleo de licuri (*Syagrus coronata*) [Internet]. [citado 2025 fev 20]. Available at: [insira o URL].
3. Silva FAS, Silva SDA, Silva LHM. Avaliação das características físico-químicas do óleo de licuri [Internet]. [citado 2025 fev 20]. Available at: [insira o URL].
4. Silva CG, et al. Estudo da transesterificação de óleo de algodão e mamona para produção de biodiesel. Quim Nova. 2007;30(3):574-8.
5. Guimarães FS. Craqueamento e hidrocraqueamento catalítico de óleo de soja [tese]. Salvador: Universidade Federal da Bahia; 2019.
6. Lima RC, et al. Propriedades físico-químicas de biodiesel de soja e girassol. Rev Bras Eng Agric Ambient. 2012;16(4):439-45.

Urban Air Quality: Occurrence, Emission Sources and Risk Assessment of Polycyclic Aromatic Hydrocarbons (PAHs) in Airborne Fine Particles

Raiane Silva da Cruz[1], Madson Moreira Nascimento[2], Leila Oliveira Santos[3], Aldenor Gomes Santos[4]*

[1]Federal University of Southern Bahia; Porto Seguro, Bahia; [2]Federal University of Southern Bahia; Ilhéus/Itabuna, Bahia; [3]SENAI CIMATEC University; [4]Federal Institute of Northern Minas Gerais, Salinas, Minas Gerais, Brazil

This study evaluated the occurrence, emission sources, and health risks of polycyclic aromatic hydrocarbons (PAHs) bound to fine particulate matter ($PM_{2.5}$) in the urban atmosphere of Itabuna, Southern Bahia, Brazil. $PM_{2.5}$ samples were collected at three sites with distinct anthropogenic influences: a rural area (UFSB Campus Jorge Amado), a predominantly residential area (15th Military Police Battalion), and a high-traffic commercial area (Jequitibá Shopping Mall). Thirteen of the sixteen priority PAHs were detected in all 21 samples, representing 82% of quantified PAHs. The highest total PAH concentration (3.28 ng m^{-3}) occurred at the UFSB site, influenced by nearby industrial activities, freight transport, and vehicular traffic on a federal highway. Benzo(a)pyrene, an indicator of PAH pollution, was present in all samples, with concentrations below the European Union annual limit (1.0 ng m^{-3}). Molecular diagnostic ratios indicated diesel and gasoline combustion as the main emission sources, with coal combustion also contributing. The incremental lifetime cancer risk (ILCR) was estimated for four population groups (infants, children, adolescents, adults), showing values within the acceptable range suggested by the U.S. EPA (10^{-6}–10^{-4}), but indicating potential long-term health concerns, particularly in high-traffic areas. The relevance of this study lies in the fact that Brazil still lacks regulatory limits for PAHs in ambient air, making local assessments essential to guide environmental management and public health policies. Furthermore, data on air quality in medium-sized Brazilian cities are scarce, despite rapid urbanization and increasing vehicle fleets. These findings emphasize the urgent need for continuous monitoring, improved emission control, and preventive strategies to mitigate risks to human health and environmental quality.

Keywords: PACs. $PM_{2.5}$. Urban Air Pollution. Vehicular Emissions. Cancer Risk.

Atmospheric particulate matter (PM) has attracted more and more attentions due to their threats to human health. Airborne particulate, especially fine particles and bound organic components are associated with health effects like cancer, but also allergic reactions, respiratory and cardiovascular diseases [1,2]. As soon, the knowledge of the composition and the concentration of chemical compounds associated with air particles is essential for risk assessment from contaminants bound on PM [3].

Polycyclic aromatic hydrocarbons (PAHs) are and mutagens human carcinogens, defined by World Health Organization through the exposure-response function for cancer of the lung as a result of PAH exposure [4]. The PAHs are a group of harmful compounds emitted into the environment mainly through anthropogenic pyrolytic sources, such as biomass burning, fuel combustion, traffic-related emissions, industrial activities and petrogenic sources [5,6]. Gasoline and diesel vehicles emissions have been recognized as a significant source of these organic pollutants in airborne particulate matter in the urban atmosphere [7].

This study investigated the occurrence of PAHs associated with fine particulate matter (PM2.5) in the urban atmosphere of Itabuna, Southern Bahia, Brazil, aiming to quantify their concentrations, identify potential emission sources and Risk assessment of PAHs based on incremental lifetime cancer risk.

Received on 18 December 2025; revised 22 February 2026.
Address for correspondence: Aldenor Gomes Santos. Rodovia MG-404, Km 02 - s/n - Zona Rural. Salinas, MG, Brazil. Zipcode: 39560-000. E-mail: aldenor.santos@ifnmg.edu.br.

J Bioeng. Tech. Health 2026;9(3):231-236

Experimental

Study Sites and Particulate Matter Collection

The study was conducted in the municipality of Itabuna, located in the southern region of the state of Bahia, Brazil. The city is situated at the geographical coordinates 14°47'21" S and 39°16'40" W, within the Cachoeira River watershed. Itabuna is the fifth most populous municipality in the state, with an estimated population of 214,123 inhabitants (IBGE, 2021).

Particulate matter sampling was carried out at three distinct sites in Itabuna – BA (Figure 1):
Site 1: Federal University of Southern Bahia, Jorge Amado Campus, located in a rural area with minimal influence from anthropogenic activities.
Sites 2 and 3: located in the central region of the municipality, comprising the 15th Military Police Battalion, in a predominantly residential neighborhood, and the Jequitibá Shopping Mall, an area characterized by heavy motor vehicle traffic and high urban activity.

$PM_{2.5}$ samples were collected using a high-volume (Hi-Vol) sampler equipped with a separator

Figure 1. Sample collection points in the municipality of Itabuna – BA.

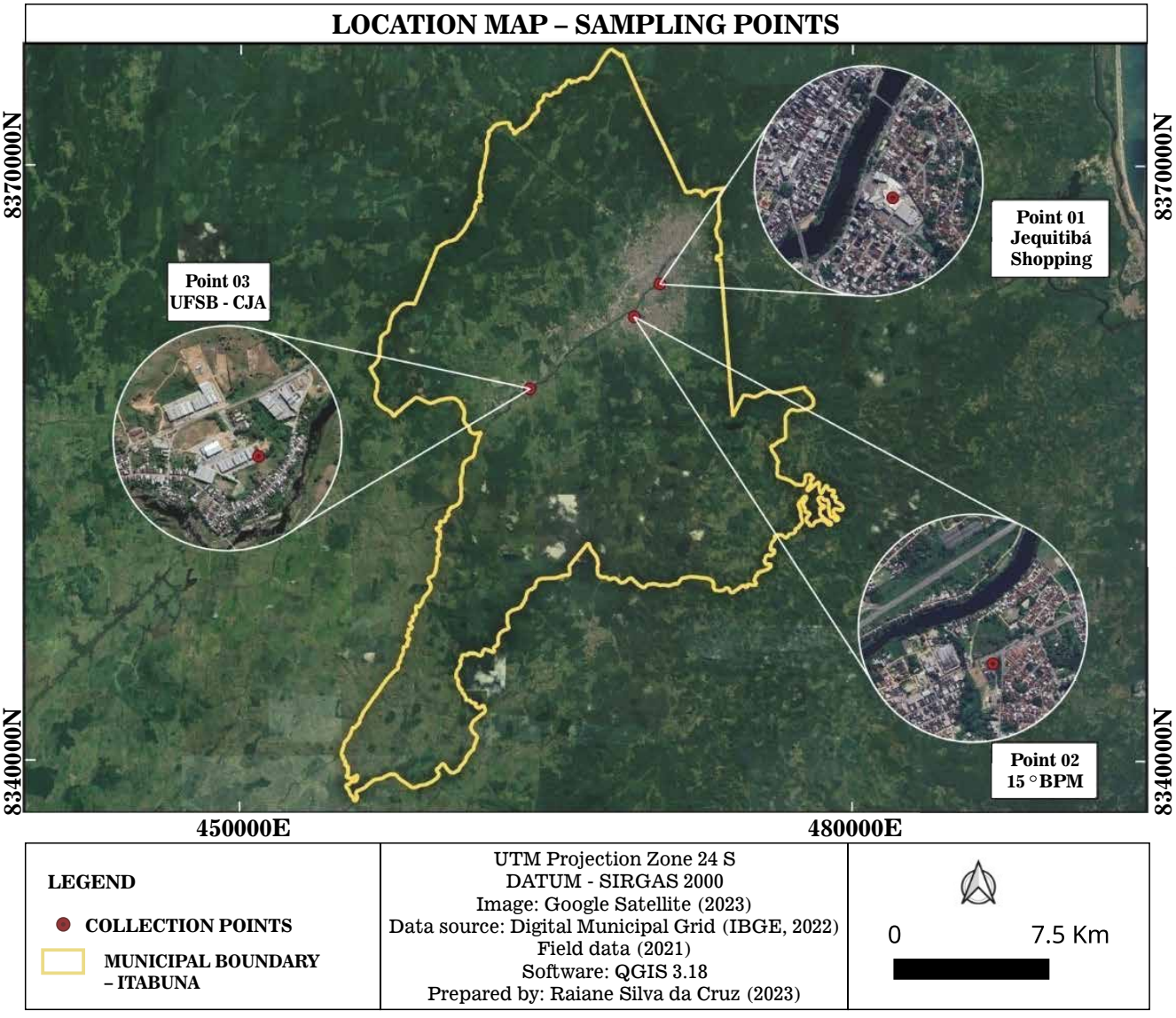

for particles smaller than 2.5 μm aerodynamic diameter. Samples were collected on quartz fiber filters (22.8 cm × 17.7 cm) over 24 h, at 1.13 m^3 min^{-1}. Each $PM_{2.5}$ sample was collected by using at least 271 m^3 of sampled air. After collection, filters were folded in half face to face, placed in a aluminum foil envelope then in a zip lock type plastic bag, transported cool to the laboratory and stored in a freezer (−4 °C) until analysis by GC-MS SIM (Santos et al, 2016).

Instrumentation and Chemical Analysis

The extraction in particulate matter and Chromatographic analyses for determining PAHs were validated by Santos and colleagues (2016) [8] Sample preparation was done using approximately a filter piece of 4.15 cm^2 diameter added to a miniaturized micro-extraction device (Whatman Mini Uniprep Syringelees Filter, Cytiva, USA) with 500 μL of an acetonitrile/dichloromethane (18%:82% v:v) mixture and 23 minutes' sonication.Then, the extract was filtered in the microextraction device and placed for direct injection of a volume of 1.00 μL of the extract in the gas chromatograph coupled to a mass spectrometer GC-MS QP 2010 Ultra (Shimadzu, Japan), equipped with an AOC-20i autosampler and split/splitless injector operating in splitless mode at 310 °C and purge time of 0.80 min was employed for PACs analysis. The injection volume was 1.00 μL. The chromatographic separation was performed using a Rtx-5MS gas capillary column (5 % diphenyl, 95 % dimethylpolysiloxane, 30 m x 0.250 mm ID x 0.25 μm of film thickness) (Restek, Bellefonte, USA). High purity helium (99.9999 %) (White Martins, Brazil) was used as carrier gas under flow rate of 1.00 mL min^{-1}. Oven temperature programing initiated at 70°C (2 min), then rising from 70-200 °C (30 °C min^{-1}, 5 min), and 200-330 °C (5 °C min^{-1}, 0.67 min). Injector temperature was set at 310 °C and transfer line was 280 °C. The MS analysis was performed in electronic impact mode (EI) on positive mode with an energy of 70 eV and in selective ion monitoring mode GC-MS-SIM.

Risk Assessment of PAHs Based on Incremental Lifetime Cancer Risk

To obtain the estimates, it was necessary to convert the concentrations of PAHs into benzo(a) pyrene equivalent concentrations (BaP_{eq}) (ng m^{-3}), calculated using Equation 1, where C_i represents the concentration level of $PM_{2.5}$ for a target compound, and TEF_i corresponds to the toxic equivalency factor of the compound regarding carcinogenicity, determined for the 16 priority PAHs established by the U.S. EPA. For mutagenicity assessment, Equation 1 was applied by replacing the TEF values with the corresponding mutagenic equivalency factors (MEF).

$$BaPeq = \Sigma\, Ci \times TEFi \quad (1)$$

Daily inhalation exposure (EI) levels were calculated using Equation 2, where EI (ng $person^{-1}$ day^{-1}) represents the daily exposure through inhalation, IR (m^3 day^{-1}) is the inhalation rate, and B(a)Peq is the benzo(a)pyrene equivalent concentration (ng m^{-3}).

$$E\,I = BaPeq \times IR \quad (2)$$

Mutagenicity-based EI values were calculated using Equation 2, but replacing the BaPeq values (from Equation 1) obtained with TEF by those obtained with MEF. The incremental lifetime cancer risk (ILCR) was estimated to assess the inhalation risk for the population of Itabuna in the sampling areas defined in the present study, as described in Equation 3. In this equation, SF is the inhalation cancer slope factor for BaP, set at 3.14 (mg kg^{-1} $day^{-1})^{-1}$; ED (years) corresponds to the lifetime exposure duration between the lower and upper bounds of each age range up to 70 years; EF (days $year^{-1}$) is the exposure frequency (365 days $year^{-1}$); AT (days) is the lifetime averaging time for carcinogens over 70 years (70 × 365 = 25,550 days); and BW (kg) is the body weight of an individual in the target population.

$$ILCR=(EI\times SF\times ED\times cf\times EF)/(AT\times BW) \quad (3)$$

Risk assessment was performed considering four distinct target groups within the population: adults (>21 years), adolescents (11–16 years), children (1–11 years), and infants (<1 year) [9]. The inhalation rates (IR) were estimated at 16.4 m^3 day^{-1} for adults, 21.9 m^3 day^{-1} for adolescents, 13.3 m^3 day^{-1} for children, and 6.8 m^3 day^{-1} for infants. The assumed body weights were 80.0 kg for adults, 56.8 kg for adolescents, 26.5 kg for children, and 6.8 kg for infants. The exposure durations (ED) considered were 50, 6, 11, and 1 years for adults, adolescents, children, and infants, respectively.

Results and Discussion

Occurrence of PAHs in the Study Sites

The presence of the sixteen priority PAHs was investigated. A total of thirteen PAHs were detected in all 21 samples. These compounds included fluorene, phenanthrene, fluoranthene, anthracene, benzo[a]anthracene, chrysene, benzo[b]fluoranthene, benzo[k]fluoranthene, benzo[a]pyrene, indeno[1,2,3-cd]pyrene, dibenzo[a,h]anthracene, and benzo[g,h,i] perylene, accounting for 82% of the PAHs quantified in the $PM_{2.5}$ fractions of the collected samples.

The highest total PAH concentration was observed at the UFSB sampling site, with an average of 3.28 ng m^{-3}. Although designated as a rural zone in the master plan of the municipality of Itabuna—where lower pollution levels would be expected due to low population density and reduced anthropogenic activity—this site is actually located in an area subject to high anthropogenic influence, including industrial activities, freight transport companies operating heavy-duty vehicles, and a federal highway with intense traffic, all contributing to increased airborne particulate matter concentrations.

The PAH distribution profiles for each sampling location are shown in Figure 2. The lowest compound concentrations were recorded at the 15th Military Police Battalion site, located in a predominantly residential neighborhood. The compound indeno[1,2,3-cd]pyrene exhibited the highest concentration at the UFSB site,

Figure 2. Average concentration (ng m^{-3}) of PAHs in $PM_{2.5}$ at each sampling location.

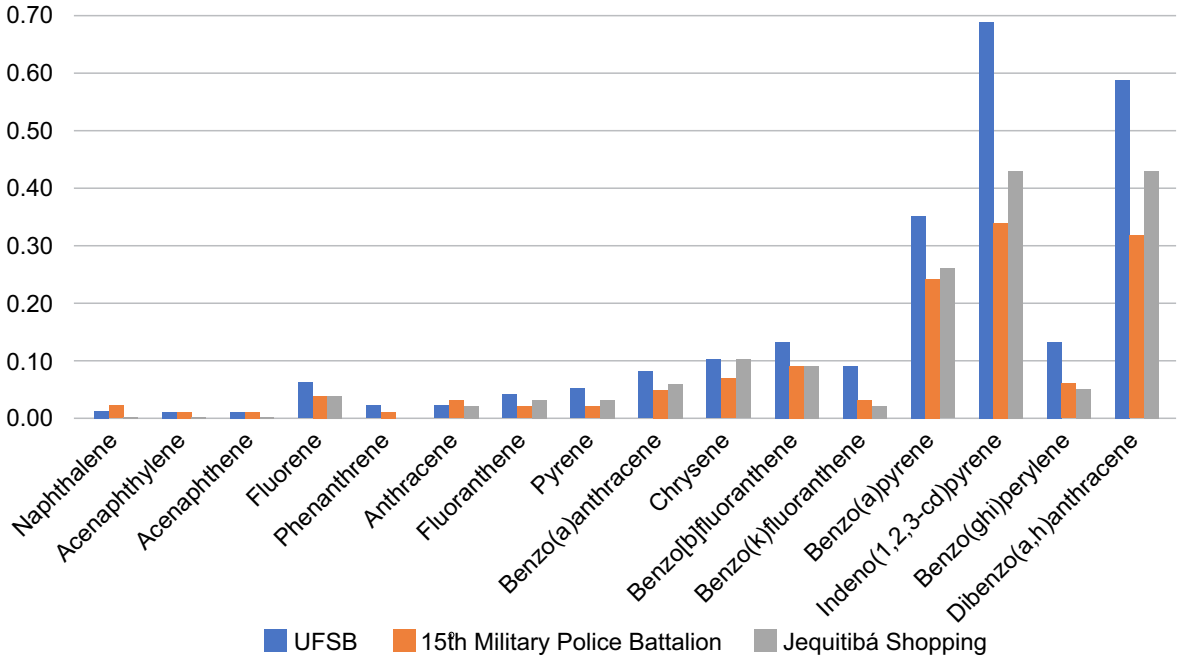

located in the Ferradas neighborhood, with an average of 0.69 ng m^{-3}, followed by elevated levels at the other sites (0.34 ng m^{-3} and 0.43 ng m^{-3}, respectively). This PAH has the potential to exacerbate the severity of allergic pulmonary inflammation [10,11], thereby increasing human health risks, and its presence in particulate matter underscores the contribution of vehicular emissions [12]. In contrast, acenaphthylene showed the lowest recorded concentration, with the average across all sampling sites totaling 0.02 ng m^{-3}.

Benzo(a)pyrene, a key indicator compound representing the PAH class, was detected in 100% of the samples, with mean concentrations of 0.35 ng m^{-3}, 0.24 ng m^{-3}, and 0.26 ng m^{-3}, respectively. These values were below the annual limit established by the European Union for atmospheric concentrations (1.0 ng m^{-3}). In Brazil, no regulatory limits have been established for benzo(a)pyrene in ambient air; therefore, international standards are used as reference.

Molecular Diagnostic Ratios and Identification Sources

Molecular diagnostic ratios among PAHs are commonly used to identify potential sources of atmospheric emissions. The ratios of selected PAHs were obtained following the approaches of Yu and colleagues (2014) and Kamal and colleagues (2015) [13,14]. The BbF/BkF ratios (1.44, 3.0, and 4.5) at the three sampling sites were >0.50, indicating diesel exhaust as the likely source. The BaP/BgP ratios (2.69, 4.0, and 5.20) were >1.25, suggesting coal combustion as a probable source. The BaP/(BaP+CRY) ratio, with a value of 0.73, indicated gasoline combustion as the main source in the Jequitibá Shopping Mall area, a finding further supported for the other sites by the FLT/(FLT+PYR) ratio, which ranged from 0.35 to 0.51.

Overall, the results demonstrate a predominance of emissions originating from the combustion of fuels such as diesel and gasoline, primarily from vehicular sources in the municipality. This aligns with local characteristics, as the sampling sites are located in areas with constant vehicle traffic, contributing to increased PAH emissions into the atmosphere.

Cancer Risk from Inhalation Exposure

The total incremental lifetime cancer risk (ILCR) for the UFSB site was 8.31×10^{-8} (infants), 4.58×10^{-7} (children), 1.92×10^{-7} (adolescents), and 8.51×10^{-7} (adults). These ILCR estimates indicate a probability ranging from approximately 8.31 infants per one hundred million to 8.51 adults per ten million living in the UFSB area developing cancer over their lifetime.

At the 15th Military Police Battalion site, the estimated ILCR values were 4.90×10^{-8} (infants), 2.71×10^{-7} (children), 1.13×10^{-7} (adolescents), and 5.02×10^{-7} (adults). For the Jequitibá Shopping Mall site, the total ILCR values were 5.88×10^{-8} (infants), 3.25×10^{-7} (children), 1.36×10^{-7} (adolescents), and 6.03×10^{-7} (adults).

Across all three sampling locations, the ILCR values fell within the acceptable risk range of 10^{-6} to 10^{-4}, as suggested by the U.S. EPA (2005), in which ILCR values greater than 10^{-4} are considered indicative of high potential health risks.

Conclusion

The results demonstrated the presence of polycyclic aromatic hydrocarbons (PAHs), identified emission sources, and estimated the daily health risk to the population exposed to mutagenic and carcinogenic compounds associated with fine particulate matter ($PM_{2,5}$) in the urban atmosphere of Itabuna, southern Bahia, Brazil. The results highlighted the significant contribution of vehicle emissions to PAH levels in urban air. This study provides the first published data on air quality in Itabuna, highlighting the need for continuous monitoring and mitigation measures to assess the risks to public health and environmental quality in the region.

Acknowledgement

The authors acknowledge the financial support provided by the Federal University of Southern Bahia (UFSB). The authors also express their gratitude to the Interdisciplinary Center for Energy and Environment (CIENAM) of the Federal University of Bahia (UFBA), the 15th Military Police Battalion of Itabuna-BA, and the Jequitibá Shopping Mall of Itabuna-BA for their assistance in sample collection and analysis.

References

1. Kelly FJ, Fussell JC. Size, source and chemical composition as determinants of toxicity attributable to ambient particulate matter. Atmos Environ. 2012;60:504-26. doi:10.1016/j.atmosenv.2012.06.039.
2. World Health Organization. Regional Office for Europe. Air quality guidelines: global update 2005: particulate matter, ozone, nitrogen dioxide and sulfur dioxide [Internet]. Copenhagen: WHO Regional Office for Europe; 2006 [cited 2025 Aug 10]. Available from: https://apps.who.int/iris/handle/10665/107823
3. Mueller A, Ulrich N, Hollmann J, Zapata Sanchez CE, Rolle-Kampczyk UE, von Bergen M. Characterization of a multianalyte GC-MS/MS procedure for detecting and quantifying polycyclic aromatic hydrocarbons (PAHs) and PAH derivatives from air particulate matter for an improved risk assessment. Environ Pollut. 2019;255:112967. doi:10.1016/j.envpol.2019.112967.
4. World Health Organization. Regional Office for Europe. WHO guidelines for indoor air quality: selected pollutants [Internet]. Copenhagen: WHO Regional Office for Europe; 2010 [cited 2025 Aug 10]. Available from: https://apps.who.int/iris/handle/10665/260127
5. Keyte IJ, Albinet A, Harrison RM. On-road traffic emissions of polycyclic aromatic hydrocarbons and their oxy- and nitro-derivative compounds measured in road tunnel environments. Sci Total Environ. 2016;566-567:1131-42. doi:10.1016/j.scitotenv.2016.05.152.
6. Harrison RM, Alam MS, Dang J, Ismail IM, Basahi J, Alghamdi MA, et al. Relationship of polycyclic aromatic hydrocarbons with oxy(quinone) and nitro derivatives during air mass transport. Sci Total Environ. 2016;572:1175-83. doi:10.1016/j.scitotenv.2016.08.030.
7. Zhao T, Yang L, Huang Q, Zhang Y, Bie S, Li J, et al. PM2.5-bound polycyclic aromatic hydrocarbons (PAHs) and their derivatives (nitrated-PAHs and oxygenated-PAHs) in a road tunnel located in Qingdao, China: characteristics, sources and emission factors. Sci Total Environ. 2020;720:137521. doi:10.1016/j.scitotenv.2020.137521.
8. Santos AG, Regis ACD, Rocha GO, Bezerra MDA, Jesus RM, Andrade JB. A simple, comprehensive, and miniaturized solvent extraction method for determination of particulate-phase polycyclic aromatic compounds in air. J Chromatogr A. 2016;1435:6-17. doi:10.1016/j.chroma.2016.01.018.
9. Santos AG, Rocha GO, Andrade JB. Occurrence of the potent mutagens 2-nitrobenzanthrone and 3-nitrobenzanthrone in fine airborne particles. Sci Rep. 2019;9:1-13. doi:10.1038/s41598-018-37186-2.
10. Wong TH, Lee CL, Su HH, Lee CL, Wu CC, Wang CC, et al. A prominent air pollutant indeno[1,2,3-cd]pyrene enhances allergic lung inflammation via aryl hydrocarbon receptor. Sci Rep. 2018;8:1-11. doi:10.1038/s41598-018-23542-9.
11. Liu K, Gao Y, Xiao W, Fu J, Huang S, Han X, et al. Multidimensional analysis of lung lymph nodes in a mouse model of allergic lung inflammation following PM2.5 and indeno[1,2,3-cd]pyrene exposure. Environ Health Perspect. 2023;131:1-14. doi:10.1289/ehp11580.
12. Xing W, Zhang L, Yang L, Zhou Q, Zhang X, Toriba A, et al. Characteristics of PM2.5-bound polycyclic aromatic hydrocarbons and nitropolycyclic aromatic hydrocarbons at a roadside air pollution monitoring station in Kanazawa, Japan. Int J Environ Res Public Health. 2020;17:1-11. doi:10.3390/ijerph17030805.
13. Yu B, Yu W, Zhou Q. Human health risk assessment based on toxicity characteristic leaching procedure and simple bioaccessibility extraction test of toxic metals in urban street dust of Tianjin, China. PLoS One. 2014;9:1-9. doi:10.1371/journal.pone.0092459.
14. Kamal A, Cincinelli A, Martellini T, Malik RN. A review of PAH exposure from the combustion of biomass fuel and their less surveyed effect on blood parameters. Environ Sci Pollut Res. 2015;22:4076-98. doi:10.1007/s11356-014-3748-0.

A Dynamic Simulation Framework for Performance Analysis of a Three-Phase Separator

Michel Cardoso Natividade[1*], Reinaldo Coelho Mirre[2], Igor Oliveira de Freitas Campos[3]
[1]Chemical Engineering, – PRH 27.1 ANP/FINEP – Exploration, Development and Production of Oil, Natural Gas and Biogas; [2]Federal University of Bahia; [3]SENAI CIMATEC University; Salvador,Bahia, Brazil

The present study addresses the mathematical modeling and dynamic simulation of a three-phase gravitational separator. The overall goal was robust construction and modeling to optimize the reduction of water composition in crude oil emulsions. The presence of emulsified water severely impacts primary oil processing, decreasing the final quality of the product (increase in BS&W - Basic Sediment and Water), exponentially increasing operating costs (OPEX). For the construction of the model, the Python language was used, implementing mass balances and equations that describe the dynamics of phase separation. Correlations from the literature were incorporated for the calculation of fluid properties, such as density, and efficiency of the phases as a function of API gravity, and the classification of the oils used in the simulation scenarios themselves was validated. The results obtained show that the model was successful in describing the behavior of the system. Notably, the simulations demonstrated that oils with higher API gravity (lighter, with lower density) have faster and more efficient separation kinetics. This is because the lower viscosity of the oil (continuous phase) offers less resistance to the movement of water droplets, and the greater density difference between the phases intensifies the gravitational force, accelerating decantation. The behavior of the model compared to real scenarios can be correlated with the impact of the chemical composition, and the higher concentration of components such as asphaltenes and resins, natural emulsifiers present in oils, in heavy oils tend to form more rigid interfacial films, stabilizing the emulsion, making it difficult to coalescence. It is concluded that the simulated model obtained satisfactory accuracy, presenting results consistent with the theory and industrial practice in all the proposed scenarios, proving to be a valuable tool for the analysis and optimization of separation processes.
Keywords: Primary Petroleum Processing. Crude Oil. BS&W. Three-phase Separator. Mathematical Modeling.

Hydrocarbon production in fields such as pre-salt involves the extraction of a multiphase mixture of oil, gas, and water. The energy introduced into this flow during lifting, especially due to high pressure drops in valves and shear in pumps, disperses the water in the oil phase, creating emulsions that can be highly stable [1].

Emulsions are phenomena found in the primary processing of petroleum, caused by adverse factors, formed by the intense agitation (shearing) to which the fluids are subjected during the production and transport processes. Thus, some compounds found in crude oil aid in the formation of emulsions, such as asphaltenes and resins.

These emulsions can be formed into oil, water, gas, and solids, and are classified as oil-in-water, water-in-oil, depending on the predominant fluid in the phase. There are several techniques for the treatment of these emulsions, which derive from the emulsion content, cost, and development of the technology [2,3].

Demulsification can be performed using various techniques, the choice of which depends on factors such as emulsion characteristics, investment (CAPEX) and operational (OPEX) costs, the level of technological development, and other related variables. The goal of applying these technologies is to ensure that the treated oil meets the rigorous quality standards required for its commercialization.

In Brazil, oil commercialization is regulated by the National Petroleum Agency (ANP), which establishes specifications to ensure oil quality. Among these, the water and sediment content (BS&W) must be equal to or less than 1.0% by volume. Additionally, the ANP stipulates a limit for salt concentration, which must be a maximum of 285 mg/L [2-5].

Received on 16 December 2025; revised 15 February 2026.
Address for correspondence: Michel Cardoso Natividade. Av. Orlando Gomes, 1845, Piatã, Salvador, Bahia, Brazil. Zipcode: 41650-010. E-mail: michel.cardooso@fbest.org.br.

J Bioeng. Tech. Health 2026;9(3):237-246

With the excessive costs of CAPEX and OPEX in upstream oil industries, new layouts are sought that offer greater techno-economic efficiency. An essential tool for this purpose is process modeling, and consequently process simulation [6,7]. This work develops a dynamic simulation model in Python for a three-phase separator, with the objective of analyzing its operational performance for different API degrees, specifically in separation efficiency, as well as in the stability of interface levels.

Materials and Methods

The method for this work began with a literature review on water-oil separation methods and modeling approaches for BS&W reduction. The mathematical model was developed based on the formulation from Condori (2014) [5] for three-phase separators, representing an evolution of previous work by Natividade and colleagues (2024) [7], in which calculations for phase efficiency and mixture density were enhanced using experimental data and fluid properties supplemented by Filgueiras (2005) [6]. The model was implemented in Python and validated against results from the literature.

Finally, a case study was conducted to analyze the impact of different API gravities on the separator's performance. Figure 1 summarizes the steps of this method.

Figure 1. Method diagram in the applied research.

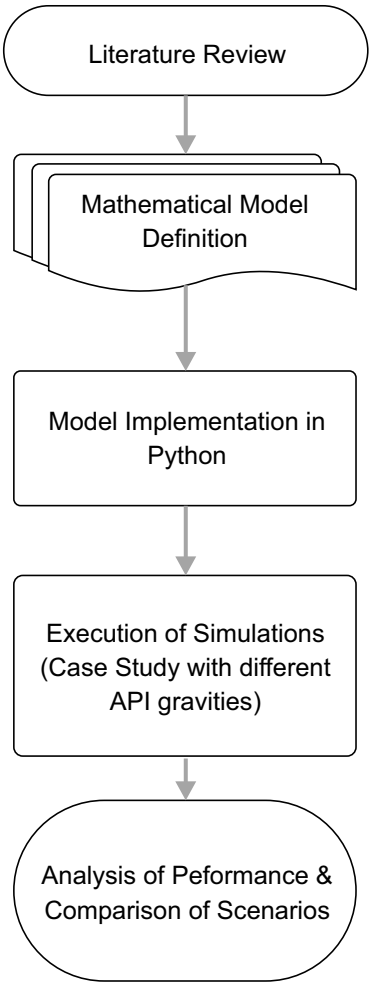

System Modeling

Three-Phase Separator

The three-phase separator is a cylindrical shaped equipment, which has some internal components making it help in the separation of phases, shown in the Figure 2.

The separator is designed to operate at low to medium pressures, such as temperatures above ambient. The vase consists of a few sections:

Separation Chamber

Upon entering the separation chamber, the multiphase flow loses momentum, initiating a separation process governed by gravity and the distinct densities of the fluids. The gas, being the least dense phase, immediately rises to occupy the upper vapor space of the vessel. Simultaneously, the liquid components stratify. Water, being denser, settles to the bottom, while the oil, with an intermediate density, forms a distinct layer on top of the water.

Secondary Separation Section

In this section, gas make up the largest volume of the section. As it has the phenomenon of dragging part of the liquid droplets, it is necessary to use mechanical devices such as mist eliminators.

Figure 2. Graphical diagram of a three-phase separator.

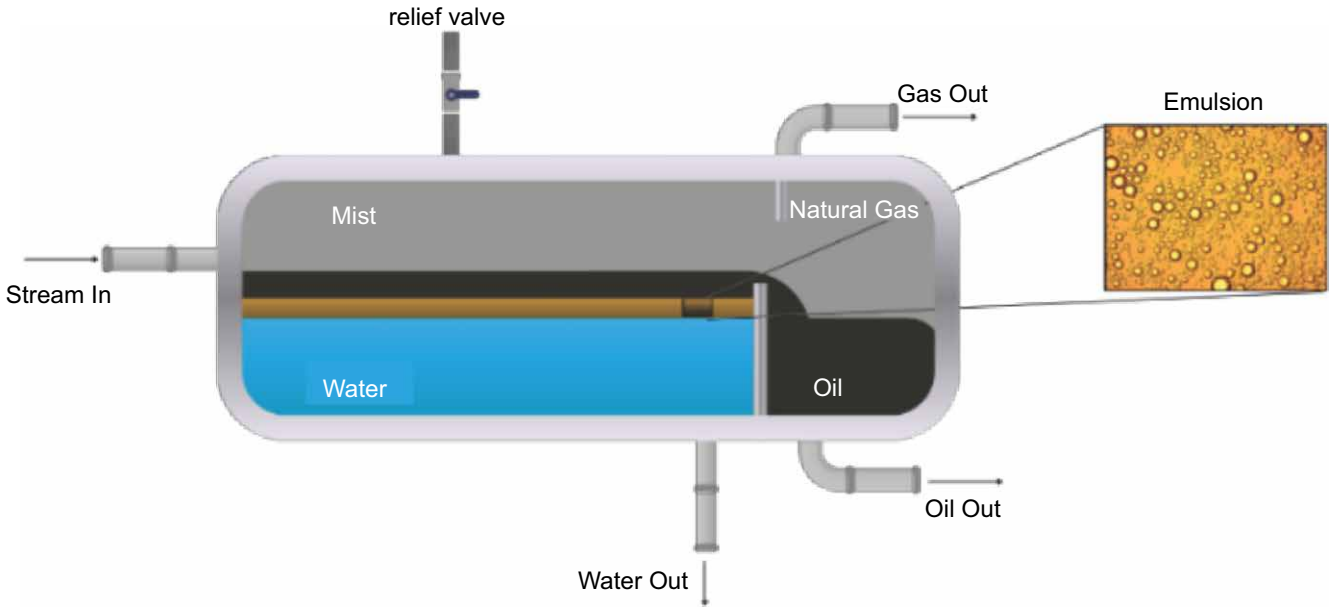

Source: Júnior (2023) adapted [8].

Oil Chamber

Phase separation in the vessel is achieved through gravitational settling, a process enhanced by inertial effects at the baffle plate and droplet coalescence. This separation occurs because of the density difference between the fluids.

As a result, the oil, being lighter, rises and accumulates in the upper part of the separation chamber. From there, it flows over a weir to a collection section located downstream of the baffle plate.

Inertial separation – sudden changes in velocity and flow direction allowing the gas to detach from the liquid phase due to the inertia that this phase has.

Agglutination of the particles – contact of the oil droplets dispersed on a surface, which facilitates its coalescence, agglutination, and consequent decantation [7].

The model developed in this work is based on the thesis by Condori (2014) [5], which proposes a simplified approach. The main simplifications adopted include disregarding interphase drag, treating the gas as ideal, and not modeling the droplet size distribution. This approach diverges from more rigorous methods, the importance of which for the thermodynamic representation of gases had already been highlighted by Nunes (1994) [9] showing that the thermodynamic representation of the phases is important in the study of gases, but has little significant effect on the dynamics of liquid/liquid separation, considering that there is no mass transfer between the thermodynamic phases. For the efficiencies of the aqueous and oily phases, Ribeiro (2016) [10] empirical constants were used, based on the Filgueiras (2005) model [6].

Balance Equations

The mathematical modeling in this work is based on the application of mass balances to three distinct control volumes: the separation chamber, the oil chamber, and the gas space. From these balances, the equations that describe the dynamic behavior of the system are derived, as well as the flow rates and properties of the separator's outlet streams.

Mass Balance in the Separation Chamber

The flow modeling in the separation chamber considers two distinct operational regimes, designated Case 1, and Case 2. The first case occurs when the height of the oil layer is less than the total emulsion height in the chamber, resulting in standard flow behavior. The second case, in turn, represents the condition where the oil height equals the total emulsion height, characterizing an overflow, which directly affects the phase separation efficiency. Each scenario results in a distinct set of equations to describe the flow, as illustrated in Figure 3 and Equations 1 to 7.

Figure 3. Systems generated inside the separator due to the presence of the baffle.

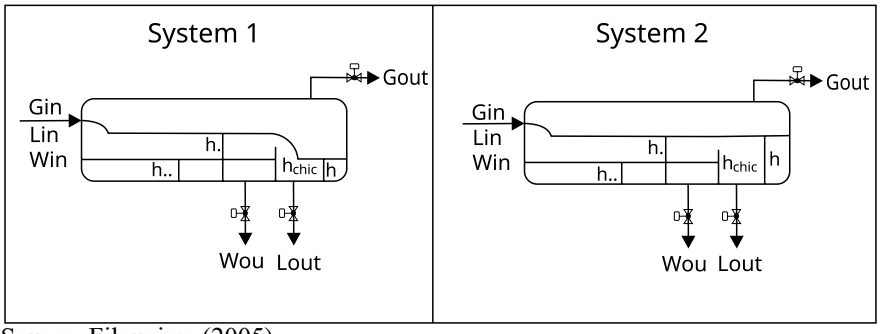

Source: Filgueiras (2005).

$$\frac{dh_{wy(t)}}{dt} = \frac{\{W_{ey} \cdot [1 - TOG_{ey} \cdot ef_{lwy}] + L_{ey} \cdot BSW_{ey} \cdot ef_{wly} - W_{sy}\}}{2 \cdot C_{Csy} \cdot \sqrt{h_{wy}[D_y - h_{wy}]}} \quad (1)$$

Case 1 ($\boldsymbol{h_{ty} < h_{vert}}$)

$$\frac{dh_{ly}(t)}{dt} = \frac{[L_{vy} - L_{Sy}]}{2 \cdot C_{cly}\sqrt{h_{ly} \cdot [D_y - h_{ly}]}} \quad (2)$$

$$\mathrm{L_{vy}} = 0 \quad (3)$$

$$\frac{\mathrm{dh_{ty}}(t)}{\mathrm{dt}} = \frac{1}{\mathrm{C_{csy}} \cdot \sqrt{h_{ty} \cdot (D - h_{ty})}} \cdot (\mathrm{W_e} + \mathrm{L_e} - \mathrm{L_{vy}} - \mathrm{W_{sy}}) \quad (4)$$

Case 2 ($h_{ty} > h_{vert}$)

$$\frac{dh_{ly}(t)}{dt} = \frac{dh_{ty(t)}}{dt} \quad (5)$$

$$\mathrm{L_{vy}} = \frac{\mathrm{k}}{60} \cdot (L_{vert} - 0.2 \cdot (h_{ty} - h_{vert}) \cdot (h_{ty} - h_{vert})^{1.5} \quad (6)$$

$$\frac{dh_{ty}(t)}{dt} = \frac{W_{ey} + L_{ey} - L_{sy} - W_{sy}}{\left(2 \cdot (C_{csy} + C_{cly}) \cdot \sqrt{h_{ty} \cdot (D - h_{ty})}\right)} \quad (7)$$

Output Equations of Separator Currents

$$G_{s(t)} = \frac{CV_{maxgy} \cdot S_{gy}}{\frac{2{,}832 \cdot 60 \cdot P_y \cdot MW_g}{R \cdot T_y}} \cdot \sqrt{\left(P_y + P_{comp_y}\right) \cdot \left(P_y - P_{comp_y}\right) \cdot d_g} \quad (8)$$

$$L_{sy} = \frac{CV_{maxly} \cdot S_{ly}}{0.0693 \cdot 60 \cdot \rho_{fl}} \cdot \sqrt{(P_y - P_{jusy}) \cdot d_l + \gamma_l \cdot h_{ly} \cdot 10^{-4}} \quad (9)$$

$$W_{sy} = \frac{CV_{maxwy} \cdot S_{wy}}{0.0693 \cdot 60 \cdot \rho_{fw}} \cdot \sqrt{(P_y - P_{jusy}) \cdot d_w + \{\gamma_w \cdot h_{wy} + \gamma_l \cdot [h_{ty} - h_{wy}]\} \cdot 10^{-4}} \quad (10)$$

$$\frac{dP_y(t)}{dt} = \frac{\{[W_{ey} + L_{ey} + G_{ey} - W_{sy} - L_{sy} - G_{sy}] \cdot P_y\}}{V_{ty} - V_{csy} - V_{cly}} \quad (11)$$

Results and Discussion

Initially, to perform a sensitivity analysis of how different oil compositions will behave in the separator, it is important to relate the types of oils. Farah [11] classify the main types of oils present, according to their API gravity, as evidenced in Table 1.

Table 1. Oil classification as of API gravity.

°API	Oil Classification
°API< 15	Asphaltic
15 < °API< 19	Extra Heavy
19 < °API< 27	Heavy
27 < °API< 33	Medium
33 < °API< 40	Light
40 < °API< 45	Extra Light

Numerical Solution

For the solution of the system of ordinary differential equations (EDOs) that describe how the three-phase separator behaves, the fourth order Runge-Kutta (RK4) was used. This method is widely used in engineering simulations due to its high accuracy and computational stability [13] The RK4 method makes it possible to bring the solution of an EDO closer to the $\frac{d\omega}{dt} = f(t, \omega)$ from an initial condition known as ωi in time ti. The subsequent value, $\omega i+1$, at a time $ti+1 = ti + h$ where h is the integration step, being calculated by the following Equation 12:

$$\omega_{i+1} = \omega_i + \frac{h}{6} \cdot (k_1 + 2 \cdot k_2 + 2 \cdot k_3 + k_4) \quad (12)$$

The coefficients k1-k4 represent slopes calculated at strategic points of the integration interval:

$$k_1 = hf(t, \omega) \quad (13)$$

$$k_2 = hf\left(t + \frac{h}{2}, \omega + \frac{k_1}{2}\right) \quad (14)$$

$$k_3 = hf\left(t + \frac{h}{2}, \omega + \frac{k_2}{2}\right) \quad (15)$$

$$k_4 = hf(t + h, \omega + k_3) \quad (16)$$

Numerical Simulation Results

Table 2 presents the values used for the initial conditions, input variables, and operational parameters of the model.

To evaluate the separator's performance across multiple scenarios, simulations were carried out using various API gravities (detailed in Table 1).

The dynamic model proved to be robust, as evidenced by the high stability of the operational pressure, which varied minimally (on the order of 0.1-0.2 kgf/cm²). Furthermore, the main performance result, illustrated in Figure 4, is that lighter oils (higher API gravity) achieve greater separation efficiency, leading to a lower BS&W content in the outlet stream.

As demonstrated in Figures 5 and 6, there is a direct correlation between the oil's API gravity and the separation efficiency, such that lighter oils (higher API gravity) result in higher flow rates at the separator's oil outlet.

From the scenarios evaluated, in different classifications of oils, as illustrated in Figure 7,

Table 2. Parameters of the three-phase separator.

$P = \frac{15kg}{cm^2}$	T = 305 K	$W_e = 0.184\frac{m^3}{h}$	$S_l = 0.5$
$M = 28.97g/mol$	$h_{ly} = 2.328m$	$L_e = 6.006e^{-3} \cdot \frac{m^3}{h}$	$S_g = 0.43638$
$\rho_{water} = \frac{965kg}{m^3}$	$h_{wy} = 1.152m$	$G_e = 7.182e^{-2}\frac{m^3}{h}$	$S_w = 0.79$
$\rho_{oil} = \frac{855kg}{m^3}$	$h_{ty} = 2.5171m$	BS&W = 0.02	$h_{vert} = 2.8m$

Figure 4. Pressure variation by BS&W out (%).

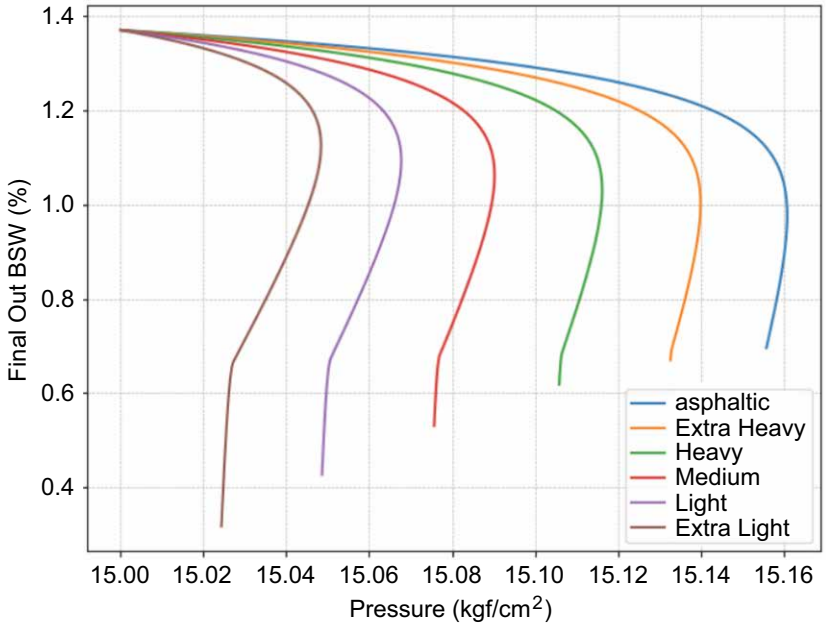

Figure 5. Oil outflow by oil gravity.

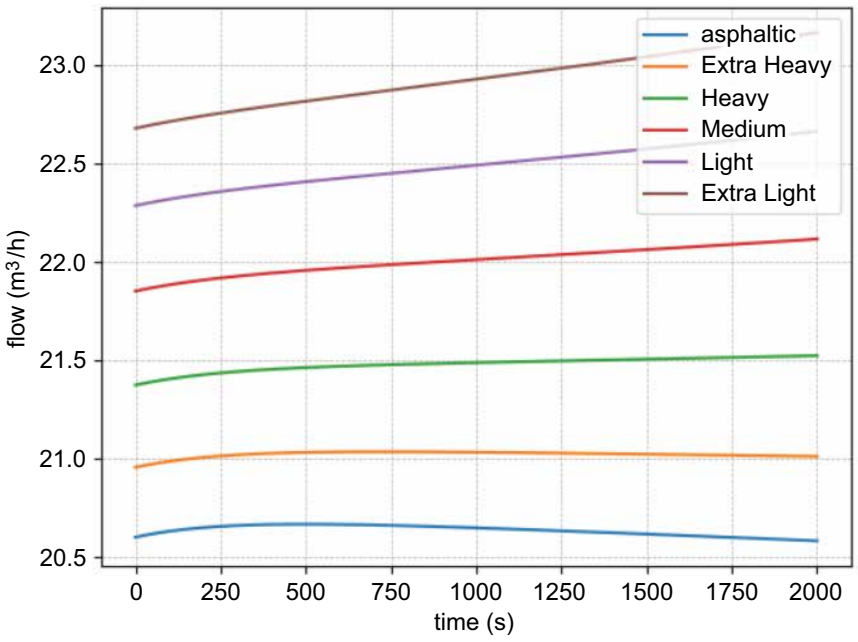

Figure 6. Pressure in separator by oil gravity.

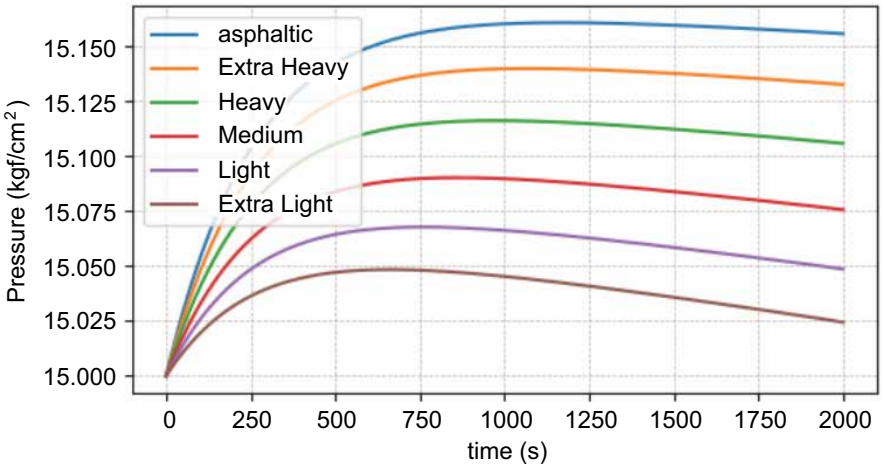

Figure 7. BS&W out oil by oil gravity.

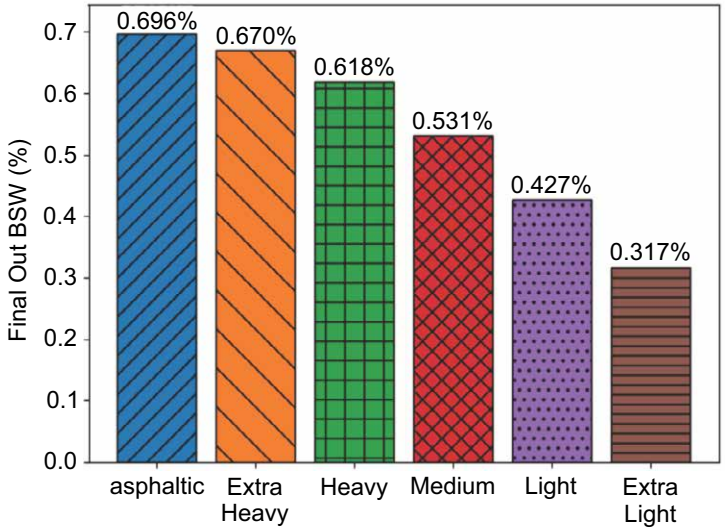

oils with a higher API gravity (lighter) exhibit a lower BS&W content after treatment. This result is a direct consequence of the greater density difference between the oil and water, which facilitates the settling of droplets and results in a more efficient phase separation. Heavier oils have a substantial heavier compound, including naphthenic, asphaltene and paraffinic compound, which help stabilize the emulsions. Thus, the API gravity has an inverse correlation with the BS&W content, and a direct correlation with the separation efficiency. In other words, higher API gravities tend to have better separations.

Conversely, vessel pressure is not significantly affected by variations in oil composition. The model's governing equations ensure a consistent mass balance, where the total liquid outflow is merely partitioned differently between the outlets. For instance, in crudes with a higher BS&W content, a greater volume of entrained water exits with the oil phase, which is offset by a corresponding reduction in flow from the water outlet, as depicted in Figure 8. This redistribution of liquid flow has a negligible impact on the vessel's pressure control loop.

Furthermore, the dynamic response of higher API gravity oils reveals a distinct inflection point

at approximately t = 200 seconds (Figure 8). It is crucial to note that this point represents the peak rate of change during the startup transient, not the onset of stability. Physically, it marks the instant of maximum flow acceleration, after which the system's response begins to dampen as it asymptotically approaches steady-state conditions.

Stabilization of the separator interface levels is preceded by a transient regime, dictated by the primary separation chamber's filling time. Initially, the oil chamber's outflow, without the corresponding supply, generates a negative mass balance, resulting in a decrease in its level. The inflection point occurs when the interface in the primary chamber reaches the 2.8 m mark, corresponding to the spillway, initiating overflow. With the oil chamber's supply restored, the system evolves to a state of equilibrium, in which the interface levels stabilize, as shown in Figures 9-11.

Conclusion

The present work proposed a simulation with different classifications of oils according to the API gravity for the modeling and simulation of a water-oil separation system, which is a three- phase separator. Thus, the current study demonstrated that higher API gravities reduce the BS&W content at the oil outlet, being inversely proportional,

Figure 8. Water outflow by oil gravity.

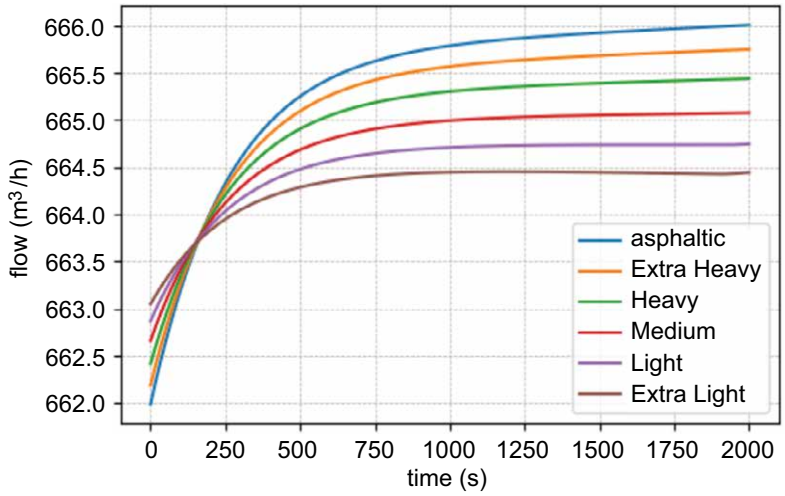

Figure 9. Oil level in separator chamber by oil gravity.

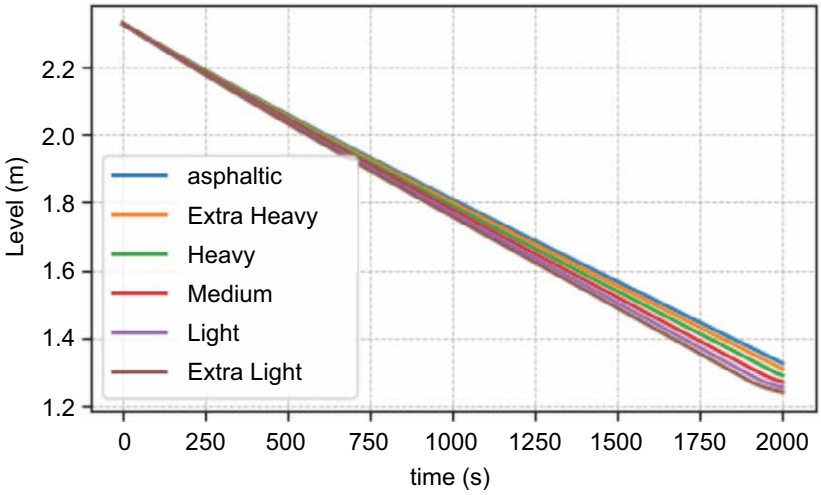

Figure 10. Water level in chamber separator by oil gravity.

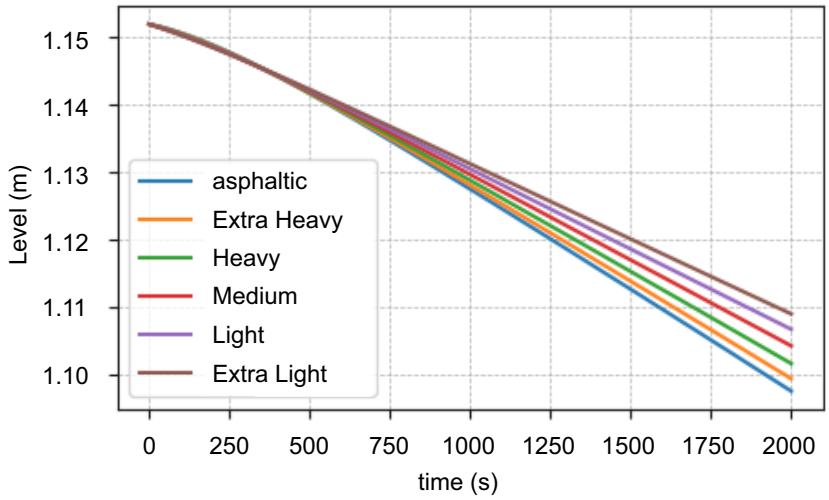

Figure 11. Total Level in chamber separator by oil gravity.

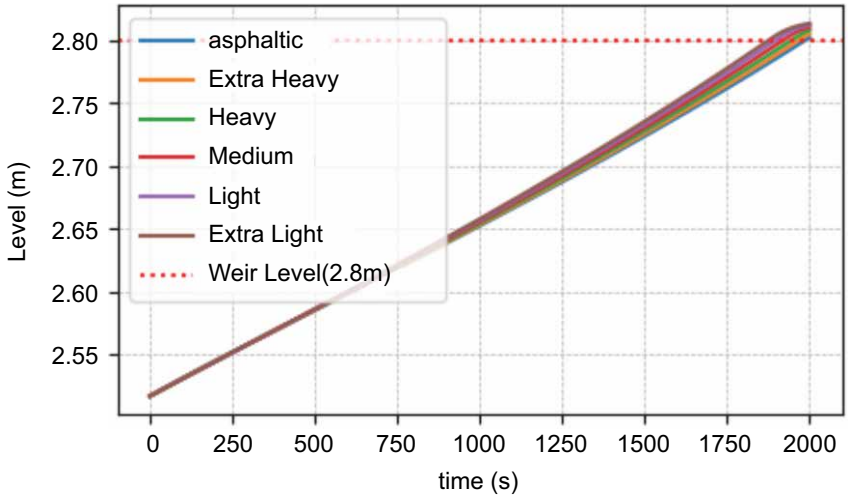

as well as the API gravity does not significantly affect the outlet pressure in the different scenarios, following a trend, as well as the water and total levels in the separation chamber, and oil in the separation chamber.

In summary, the approach to modeling the three- phase separator in Python language presented interesting robustness for applications in different scenarios. For future work, it is recommended to include the implementation of a controller in the percentage of opening of the outlet valves better represents the dynamic system, as well as droplet dynamics, and emulsion thermodynamics, in addition to the experimental validation of the results.

Nomenclature

hwy: Water interface level (m); hly: Oil interface level (m); hty: Total emulsion level (m); hvert: Weir height (m); We, Le,Ge: Inlet water, oil, and gas flow rates (m^3/h); Wsy ,Lsy,Gsy: Outlet water, oil, and gas flow rates (m^3/h); Lvy: Oil flow rate over the weir (m^3/h); Py: Separator pressure (kgf/cm^2); Ty: Temperature (K); Dy: Separator diameter (m); BSWey: Inlet oil BS&W fraction (dimensionless); efwly, eflwy: Separation efficiencies (dimensionless); Sgy,Sly,Swy: Outlet valve openings (%); CVmax: Maximum valve flow coefficient; k: Weir overflow constant

(dimensionless); Ccsy,Ccly: Characteristic length coefficients of the chambers (m); ρfl,ρfw: Density of oil and water (kg/m³).

Acknowledgement

The authors acknowledge the financial support of the Human Resources Program of the National Agency of Petroleum, Natural Gas and Biofuels (PRH/ANP – PRH27.1/SENAI CIMATEC), supported with resources from the investment of oil companies qualified in the RD&I Clause of ANP Resolution No. 50/2015 and the São Paulo Research Foundation (FAPESP), Process No. 2024/12067-7.

References

1. Noik C, Muller S, Karnitz O, et al. subsea separation behavior of a brazilian crude oil. Rio de Janeiro: OTC; 2015. doi:10.4043/26069-MS.
2. Delgado B. síntese de sistemas de regeneração e tratamento final de efluentes [tese]. Rio de Janeiro: Universidade Federal do Rio de Janeiro; 2008. Silvino PFG. análise do grau de agregação do asfalteno e da formação de emulsão água/óleo através de modelo coarse grain [tese]. Fortaleza: Universidade Federal do Ceará; 2018.
3. De Oliveira G. utilização de adsorventes (carvão ativado e argilas organofílicas) no processo de separação de emulsões óleo/água [dissertação]. Campina Grande: Universidade Federal de Campina Grande; 2012.
4. Natividade MC, Campos IOF, Mirre RC. análise comparativa da simulação computacional do processo de separação trifásica de petróleo. In: anais do X SAPCT. Salvador (BA): Doity; 2025.
5. Condori MEG. modelagem matemática e simulação de uma unidade de processamento primário de petróleo no peru [dissertação]. Belo Horizonte: Universidade Federal de Minas Gerais; 2014.
6. Filgueiras NGT. modelagem, análise e controle de um processo de separação óleo/água [dissertação]. Rio de Janeiro: Universidade Federal do Rio de Janeiro; 2005.
7. Natividade M, Campos IOF, Mirre RC. proposta de metodologia para síntese de sistemas de separação de água em óleo visando redução de BSW. In: anais do IX SAPCT. Salvador (BA): Doity; 2024.
8. Junior AMV, Altoé L, Antunes PASBM, et al. principais métodos de tratamento da água produzida em unidades marítimas de produção de petróleo. Lat Am J Energy Res. 2023;10:23-32. doi:10.21712/lajer.2023.v10.n1.p23-32.
9. Nunes GC. modelagem e simulação dinâmica de separador trifásico água-óleo-gás [dissertação]. Rio de Janeiro: Universidade Federal do Rio de Janeiro; 1994.
10. Ribeiro CHP, Miyoshi SC, Secchi AR, et al. model predictive control with quality requirements on petroleum production platforms. J Pet Sci Eng. 2016;137:10-21. doi:10.1016/j.petrol.2015.11.004.
11. Farah MA. petróleo e seus derivados: definição, constituição, aplicação, especificações, características de qualidade. 1ª ed. Rio de Janeiro: LTC; 2012. Burden R, Faires D. numerical analysis. 9th ed. Boston: Richard Stratton; 2010.

Urban Agriculture and Smart Cities: The Integration of Controlled Environment Agriculture, Community Gardens, and Public Health Policies

Evelyn Seilhe Guerreiro[1]*, Márcio Luis Valença Araújo[2], Adilson Oliveira de Almirante[3], Eduardo Oliveira Teles[3], Aloísio Santos Nascimento Filho[4], Hugo Saba Pereira Cardoso[5]

[1]Federal Institute of Education, Science and Technologia of Bahia, Campus Salvador; [2]Federal Institute of Education, Science and Technologia of Bahia, Campus de Lauro de Freitas; Federal Institute of Education, Science and Technologia of Bahia, Campus Camaçari; [4]SENAI CIMATEC University; 5State University of Bahia; Salvador, Bahia, Brazil

Urban agriculture has emerged as a key strategy for building smart cities, fostering synergies between environmental sustainability, technological innovation, social inclusion, and food security. This article aims to analyze the integration of Controlled Environment Agriculture (CEA), community gardens, and public health policies, emphasizing their contributions to urban resilience and sustainability. The study adopts a qualitative methodology, based on literature review, analysis of official documents, and case studies from Brazilian cities such as Salvador, Recife, São Paulo, and Rio de Janeiro. Results indicate that CEA enhances productivity in small spaces with reduced water and input consumption, community gardens strengthen social cohesion, mental health, and local food supply, while public policies link these initiatives to school feeding programs, health promotion, and income generation. Despite significant progress, challenges remain regarding high implementation costs, regulatory gaps, and lack of institutional support. The findings reinforce the need to incorporate urban agriculture into master plans and legal frameworks, promoting research, training, and public-private partnerships. By combining food production, innovation, and policy integration, urban agriculture positions itself as a structural axis for more resilient, sustainable, and equitable cities.

Keywords: Urban Agriculture. Smart Cities. Community Gardens. Public Health. Controlled Environment Agriculture (CEA).

Urban agriculture has been consolidated as a strategic dimension in the context of smart cities, articulating sustainability, and technological innovation. By integrating technologies such as Controlled Environment Agriculture (CEA), sensors, Internet of Things (IoT), and renewable energy solutions, it offers responses to growing urbanization, climate change, and food insecurity. In developing countries, about 30 to 40% of vegetable production is lost during post-harvest, processing, and distribution stages, representing one of the sustainable methods of growing vegetables and small fruits such as strawberries, for example. Conscious consumers value local producers, the consumption of fresher foods, and demand that production be closer to the point of sale to avoid such waste.

Urban Agriculture in Smart Cities

Smart cities are defined by the articulation beween urban infrastructure, digital data, citizen participation, and sustainability. In this context, urban agriculture is understood as essential green infrastructure that offers: I) Reduction of missions and waste by avoiding long food transport distances; II) Resource optimization through intelligent monitoring systems; III) Requalification of underutilized urban spaces; IV) Integration with urban, environmental, and health policies.

The presence of growing spaces within the urban fabric significantly contributes to urban sustainability, by acting on: Ecosystem services: microclimate regulation, rainwater retention, increased urban biodiversity; Urban efficiency: integration with water collection systems, solar energy, organic waste recycling; Digital and social

Received on 10 December 2025; revised 18 February 2026.
Address for correspondence: Evelyn Seilhe Guerreiro. R.uaEmídio dos Santos, s/n - Barbalho, Salvador, Bahia, Brazil. Zipcode: 40301-015. E-mail: evelyn.seilhe@ifba.edu.br.

J Bioeng. Tech. Health 2026;9(3):247-253

inclusion: promoting access to techno-logy, use of open data, formation of collaborati-ve networks; Food resilience infrastructure: de-centralization of production, reduced dependence on long logistics chains, and prioritization of family farming.

Food production in urban areas can be seen as a potential strategy to meet part of the food demands in urban areas [2].

Modern architects envision opportunities for requalifying degraded urban areas and enhacing public and collective spaces through urban agriculture. Productive green roofs and walls, vertical cultivation, CEA in greenhouses, vertical farms, smart agricultural containers, gardens in ecological corridors or abandoned subway stations (as in Paris and London) demonstrate how integration can occur even in dense cities. This type of agriculture not only optimizes underused urban spaces but also functions as green havens, contributing to improved air quality a community well-being. Cultivation in greenhouses and/or controlled environments can ensure year-round production of locally grown and consumed crops regardless of climatic conditions, significantly reducing the use of natural inputs such as water and soil.

Added to this is the possibility of being integrated into urban digital platforms. In this way, urban agriculture can dialogue with real-time data on energy consumption, food production, air quality, and population well-being, becoming part of evidence-based decision systems. Supporting local public policy decision-makers. “The bridge between smart cities and urban agriculture is not just a connection; it is a path to a more sustainable and vibrant future” [3].

Therefore, within the smart city ecosystem, urban agriculture operates as a cross-structuring axis, with positive impacts on housing, transportation, environment, education, and health policies.

In May 2019, the ISO 37122:2019 standard, last revised version: 2024 ("Sustainable cities and communities — Guidance on the use of ISO 37120, ISO 37122, and ISO 37123 standards") on performance measurement in smart cities was published, which specifies and establishes definitions and methodologies for a set of indicators for smart cities (ISO, 2019). The Brazilian version translated by the Brazilian Association of Technical Standards (ABNT), ABNT NBR ISO 37122:2020 Corrected Version: 2021 — Sustainable cities and communities — Indicators for smart cities [4], includes 19 themes: economy, education, energy, environment and climate change, finance, governance, health, housing, population and social conditions, recreation, safety, solid waste, sports and culture, telecommunications, transportation, local/urban agriculture and food security, urban planning, sewage and water.

According to the 2023 Connect Smart Cities Ranking, Salvador became the first Brazilian capital certified by ABNT – Brazilian Association of Technical Standards in international indicators of urban service quality, quality of life, and smart city standards established by ABNT NBR ISO 37120:2021 and NBR ISO 37122:2020.

In the general Connected Smart Cities ranking, the capital of Bahia ranked 9th (Table 1), 1st among cities in the Northeast, and reached 11th place in the Urbanism axis. In 2024, it remained the best-ranked city in the Northeast but dropped to 10th in the general Connected Smart Cities ranking (Table 2), and ranked 7th in technology and innovation.

The Salvador City Hall presents in its 2022 Smart City Technology Master Plan, 50 challeges aligned with the Smart CI’s). This is a framework that adopts the United Nations Sustainable Development Goals (SDGs) as foundations for urban transformation, guided by sustainability purposes that support the adoption of innovation and technology in local public service. In its Objective 32 – Agriculture, aligned with SDGs 2 – Zero hunger, 11 – Sustainable cities and communities, and 12 – Responsible consumption and production, the city’s 2021-2024 strategic plan is cited with the Urban Gardens program, which aims to “Stimulate local food production, reduce costs, and increase the population's access to healthy and affordable food. Among the expected

Table 1. Connected smart cities ranking 2023 edition.

Position	District	Value
1º	Florianópolis - SC	36.762
2º	Curitiba - PR	35.789
3º	São Paulo - SP	35.604
4º	Belo Horizonte - MG	35.540
5º	Niterói- RJ	35.492
6º	Barueri - SP	35.477
7º	Vitória - ES	35.468
8º	Santos - SP	35.429
9º	Salvador - BA	34.308
10º	Rio de Janeiro - RJ	34.307

Source: Connected Smart Cities Ranking. (2023) [5]

Table 2. Connected smart cities ranking edition. 2024

Position	District	Value
1º	Florianópolis - SC	37.525
2º	Vitória - ES	37.513
3º	São Paulo - SP	36.828
4º	Curitiba - PR	36.808
5º	Niterói- RJ	36.765
6º	Balneário Camboriú - SC	36.699
7º	São Caetano do Sul - SP	36.164
8º	Belo Horizonte - MG	35.705
9º	Barueri - SP	35.579
10º	Salvador - BA	35.364

Source: Connected Smart Cities Ranking (2024) [6].

results are the strengthening and expansion of urban agriculture and income generation for vulnerable communities.” [7].

Controlled Environment Agriculture (CEA) and Technological Innovation

Indoor and vertical urban production, supported by CEA, represents a systemic technological approach: sensors, controls, automation, LED, AI/ML, and computer vision form an ecosystem capable of producing food with high resource efficiency. Energy, financial (high initial investment), skills and knowledge gaps, and regulatory challenges still need to be overcome.

According to food security expert Dickson Despommier from Columbia University [8], foods grown in controlled urban environments (such as microgreens) represent an important step toward food resilience in the face of climate change and rapid urbanization. These systems reduce the need for long-distance transportation and minimize waste, while increasing production

efficiency and consistency regardless of regional climate conditions. Controlled environment agriculture (CEA), also referred to as indoor or home growing, involves more advanced techniques than traditional field cultivation, including artificial lighting, automated irrigation, and precise control of temperature and humidity tailored to each crop [9].

A microclimate must be simulated for controlled environment production, consisting of the ideal combination of air temperature, relative humidity, and light, assuming that other factors such as CO_2, soil pH, and nutrients are not limiting [10]. This control aims to provide plants with the ideal conditions for germination and/or growth, mimicking outdoor conditions without the unpredictability of weather and seasonality, bringing harvest predictability. Because the environment is enclosed/controlled, the incidence of pests is greatly reduced.

These characteristics promote higher yields, demonstrating efficiency and excellence produc tion. Cultivation can be done in small spaces using trays and shelves, also known as farming or vertical gardens.

According to Gould and Caplow [11], implementing agriculture within urban centers has great potential to significantly reduc fuel consumption, improve urban ecology, ensure food security, enhance public health, and conserve building energy. Still little known and developed in most countries, vertical farming or urban farms – presents itself as a solution to improve urban populations' access to higher quality food.

“In Brazil, however, the practice of urban agriculture has encountered numerous challenges, such as insufficient financial support, limited technical assistance, lack of legal land owner-ship, and the absence of a legal framework or legislation to promote i strengthening, which leads to the slow development of the activity [13]." Controlled agriculture systems are gaining momentum but lack consolidated statistics and strong government support. According to (Table 3), the global market is already more mature and rapidly growing, with expectations of widespread adoption of AI, automation, and water efficiency.

Community Gardens and Social Cohesion

Community gardens go far beyond food production: they function as social infrastructures, promoting social engagement, strengthening, cohesion, solidarity, mental health, and cultural identity. They create learning and socializing spaces, contribute to food security, and support the democratic use of urban space. Benefits are particularly evident vulnerable neighborhoods, with a direct impact on collective well-being inclusion, and urban resilience.

According to the 2022 Smart City Technology Master Plan, the Salvador City Hall presents in its Objective 32 (Urban Agriculture) the “Urban Gardens” program with the following action lines: a) Mapping non-building areas suitable for urban agriculture; b) Providing training for sustainable urban agriculture aimed at commercialization c) Drafting an Urban Agriculture Law Project; d) Implementing community urban gardens aimed at subsistence and income generation in vulnerable communities; e) Encouraging residential gardens through the Home Garden program.

The Salvador City Hall, through the Secretariat for Sustainability, Resilience, Well Animal Protection (Secis), is implementing agroecological commercial gardens. These examples demonstrate a path for the development of urban agriculture and its contribution to smart cities and public well being.

Integration with Public Health Policies

The articulation between SUS and urban agriculture initiatives can foster the creation of public policies that encourage the production of healthy and sustainable food in cities. Urban agriculture is directly related to health: improving the population’s in preventing chronic diseases (diabetes, hypertension); promoting mental well physical activity; combating food insecurity.

Table 3. Connected Smart Cities Ranking edition. 2024

Aspect	Brazil	World
Development Stage	Emerging: growing number of urban gardens and hydroponic systems	Established: presence of large networks and consolidated indoor farming startups
Market Scale	Country still in the initial phase, no consolidated USD data	Global indoor farming market estimated at ~US 43 billion (2024), projected to reach ~US 88 billion by 2030 (CAGR ~13.5%)
Key Technologies	Hydroponies, CEA, community gardens and local startups	Hydroponies, aquaponics, vertical farms automated with AI and LED lighting
Resouce Use	Up to 90% water savings via hydroponics; energy depends on source	Globally, indoor farms use up to 95% less water, but higher energy consumption
Main Challenges	Higher initial cost: lack of institutional support and regulation	High CAPEX and operational costs (energy, infrastructure), legal frameworks in progress
Growth Prospects	Likely expansion with support for technologies and urban Sustainability (carly stage)	Global market projects continued: indoor farming ~US 88B by 2030, vertical farms worth ~US 35B by 2032

Cities such as Belo Horizonte, Medellín, and Vancouver have established programs integrating gardens with school meals.

Studies conducted by the School of Public Health, University of São Paulo [13], on the effects of Urban and Periurban Agriculture (UPA) practices in Basic Health Units (BHUs) as a health promotion activity, and the extent to which their therapeutic dimension aligns with integrative and complementary practices, in the municipality of Embu das Artes in São Paulo, concluded that community garden cultivation activities serve as health-promoting practices that integrate key elements of integrative and complementary practices (PIC).

Urban Planning and Governance

Data from the 2022 Demographic Census by the Brazilian Institute of Geography and Statistics (IBGE) [14] indicate that 87% of Brazil's population lives in urban are urbanization rate at 84.4% compared to the previous 2010 census. The highest percentages of urban population were observed in the Southeast (94.44%) and Centerregions, followed by the South (88.24%), North (78.47%), and Northeast (77.64%).

Sustainable urban development planning must address challenges that, in addition to ensuring adequate environmental conditions, must consider the population's food and nutritional security.

To ensure urban agriculture is sustainable and integrated, the following are necessary: favorable land use policies; incentives, training, and financial support for vertical cultivation in controlled environments; technical and community support and training for family farmers; and the inclusion of urban agriculture and planning for family farmers; and the inclusion of urban agriculture in master plans and planning instruments.

The National Urban and Periurban Agriculture Program (PNAUP) [15] is a Brazilian govern-ment policy aimed at promoting sustainable agriculture development in urban and periurban areas. The

program seeks to enhance food security, generate income, promote environmental education and agroecological production, and encourage organic waste management. Instituted by Decree No. 11.700/2023, PNAUP focuses on food, medicinal, aromatic and ornamental plants, herbal medicines, and inputs. The program covers all stages, from production to commercialization, including organic waste management.

Challenges and Recommendations

The potential benefits of implementing urban agriculture are still underexplored and overlooked by municipal governments. Given the country's size and vast agricultural potential, Brazil is doing far less than the global standard in this area. International trends, climate emergencies, sustainable water and soil use, and the increasing and aging global population call for stronger and more concrete actions.

Recommendations include incorporating urban agriculture into public health, education, and socio-economic well-being policies; public funding and public-private partnerships; cooperation with universities and research institutes; training community-based multipliers; utilizing idle and underused public spaces; and strengthening family farming.

Conclusion

Increasing urbanization and the challenges related to food security, climate change, and social inequality have driven the search for innovative solutions in cities. In this context, the integration between urban agriculture, technology, and public policies has emerged as a synergistic and essential strategy to promote more sustainable, resilient, and inclusive cities.

Urban agriculture – which includes community gardens, vertical farming, hydroponic systems, and farms in controlled environments – contributes directly to local food supply, income generation, the strengthening of community bonds, and the requalification of idle spaces. Additionally, by reducing the dependence on long logistics chains and minimizing the carbon footprint of food transport, it aligns with the principal urban sustainability.

The use of digital technologies and controlled environment agriculture (CEA) systems further enhances these benefits. Solutions such as IoT sensors, automation, artificial intelligence, and optimized spectrum LED lighting allow maximizing productivity and reducing the consumption of resources such as water and energy. These advances are especially relevant in dense urban areas, where space is scarce, and environmental challenges are more intense.

However, for these practices to be viable on a large and equitable scale, the active role of the public sector is essential. Well-designed public policies are fundamental to ensure access to urban land, technical and financial support, specific land use regulations, and integration with intersectoral agendas such as health, education, and environment. Cities like Belo Horizonte, São Paulo, and Recife already implement local policies that incorporate urban agriculture into their sustainable development strategies, often associated with public health and food security programs.

The synergy between urban agriculture, technology, and public policies not only expands the efficiency and scale of these practices but also strengthens community protagonism, promotes social innovation, and transforms the way cities produce, consume, and organize themselves. By integrating these dimensions, it is possible to build a new urban paradigm based on resilience, socio-environmental justice, and food sovereignty.

References

1. Gustavsson J, Cederberg C, Sonesson U, van Otterdijk R, Meybeck A. global food losses and food waste: extent, causes and prevention. Rome: Food and Agriculture Organization of the United Nations; 2011.
2. Nicholls E, et al. the contribution of small-scale food production in urban areas to the sustainable development goals: a review and case study. Sustain Sci. 2020;15:1585-1599.

3. Simos N. bridging the gap between smart cities and urban agriculture [internet]. 2024 [cited 2025 Jun 27]. Available from: https://www.agritecture.com/blog/bridging-the-gap-between-smart-cities-and-urban-agriculture
4. Associação Brasileira de Normas Técnicas (ABNT). NBR ISO 37122: cidades e comunidades sustentáveis – indicadores para cidades inteligentes. Rio de Janeiro: ABNT; 2021.
5. Connected Smart Cities. connected smart cities ranking 2023 [internet]. [cited 2025 Jun 27]. Available from: https://web.nectainova.com.br/ranking-csc_2023/
6. Connected Smart Cities. connected smart cities ranking 2024 [internet]. [cited 2025 Jun 27]. Available from: https://web.nectainova.com.br/rcsc_ranking-csc_2024/
7. Prefeitura Municipal de Salvador. smart city master plan 2022 [internet]. Salvador: Prefeitura Municipal de Salvador; 2022 [cited 2025 Jun 27]. Available from: https://semit.salvador.ba.gov.br/plano-diretor-de-cidades-inteligentes/
8. Despommier D. the vertical farm: feeding the world in the 21st century. New York: Macmillan; 2010.
9. Saha MK. automated farming using microcontroller and sensors. Int J Sci Res Manag Stud. 2017;2(1):21-30.
10. Niu G, Sun Y, Masabni JG. impact of low and moderate salinity water on plant performance of leafy vegetables in a recirculating NFT system. Horticulturae. 2018;4(6).
11. Gould D, Caplow T. building-integrated agriculture: a new approach to food production. In: metropolitan sustainability. Cambridge: Woodhead Publishing; 2012. p.147-170.
12. Farias A, et al. sustainable cities and communities: contributions from embrapa [internet]. 2018 [cited 2025 Jun 30]. Available from: https://www.researchgate.net/publication/359169993
13. Cunha M, Cardoso R. urban gardens in promoting food and nutrition security and sustainable development in Salvador, Bahia [internet]. 2022 [cited 2025 Jun 30]. Available from: https://www.scielo.br
14. Brazil. Ministry of Health. national policy on integrative and complementary practices in SUS. Brasília: Ministry of Health; 2006.
15. IBGE – Instituto Brasileiro de Geografia e Estatística. censo 2022: 87% da população brasileira vive em áreas urbanas [internet]. 2025 [cited 2025 Jun 30]. Available from: https://agenciadenoticias.ibge.gov.br
16. Brazil. decree no. 11.700, september 12, 2023. establishes the national urban and periurban agriculture program and its working group. Brasília; 2023.

Mathematical Modeling of Photovoltaic Generation Applied to Unmanned Aerial Vehicles

Amanda Andrade Alves Barreto[1]*, Arthur Ribeiro de Cerqueira[1], Aldalice Rodrigues Dias[1], Miguel Oliveira do Amaral[1], Leonardo Ferreira Daltro[1]

[1]SENAI CIMATEC University; National Industrial Learning Service - Integrated Manufacturing and Technology Center, Drone Competence Center, Salvador, Bahia, Brazil

The increasing use of Unmanned Aerial Vehicles (UAVs) in long endurance and range missions has intensified the demand for energy solutions capable of extending operational autonomy. Among the energy sources most employed, electrochemical batteries remain the predominant solution. However, the available energy depends on the energy density of these devices, meaning that extending autonomy requires the installation of additional units or higher-capacity batteries, resulting in a significant increase in aircraft mass. A complementary alternative consists of integrating photovoltaic cells into the UAV structure, operating in conjunction with batteries to partially provide the power demand of on-board systems and contribute to the recharging of the energy storage system during flight. In this context, this work presents a mathematical modeling approach based on the single-diode equivalent circuit to represent the electrical behavior of photovoltaic cells under varying irradiance conditions, enabling the estimation of solar generation potential considering the expected operational profile of the UAV. The results indicated an additional autonomy of 4 hours and 14 minutes in the most favorable irradiance scenario and 2 hours and 51 minutes in the least favorable scenario, corresponding to increments of 70.55% and 47.50%, respectively. The integration of the photovoltaic system added 575 g to the total aircraft mass, equivalent to 1.44%. The trade-off analysis between energy gain and mass impact demonstrated a favorable relationship, reinforcing the potential of on-board solar generation as a complementary strategy for UAV projects still in the early design phase, in which extending autonomy constitutes a design guideline and the feasibility of photovoltaic integration remains under evaluation.

Keywords: UAV. Solar Energy. Autonomy. Photovoltaic Cells. Mathematical Modeling.

Applications of Unmanned Aerial Vehicles (UAVs) have become increasingly popular due to their versatility to operate in different types of missions, such as remote sensing, cargo transportation, search and rescue operations, military and agricultural activities. Among the challenges associated with these operations, one of them would be energy autonomy, which directly influences flight time and mission range [1].

Among the energy sources used to power on-board systems, electrochemical batteries are the most recurring solution [2]. The main limitation of these devices, in the context of UAVs, relates to their energy density, defined as the amount of energy stored per unit of mass or volume, so that extending autonomy requires the installation of additional batteries or batteries with a higher nominal capacity, which significantly increases the mass of the aircraft [3]. This restriction compromises the capacity for continuous energy supply during prolonged missions, imposing periodic interruptions for recharging or replacing the batteries, which negatively impacts logistical and economic efficiency in long-range missions that require greater energy autonomy [1].

Many studies have investigated the use of complementary energy sources as a strategy to reduce exclusive dependence on batteries and, consequently, increase the operational autonomy of UAVs [4]. Among the alternatives analyzed, the integration of photovoltaic systems into the structure of the aircraft has been considered, allowing the energy generated to act as an auxiliary source during flight, with the capacity to partially supply the energy demand of the on-board systems and contribute to the gradual recharging of the storage system [5,6].

Received on 13 December 2025; revised 18 February 2026.
Address for correspondence: Amanda Andrade Alves Barreto. Av. Orlando Gomes, 1845 - Piatã, Salvador – BA – Brazil, Zipcode: 41650-010. E-mail: barretoamandaandrade@gmail.com.

J Bioeng. Tech. Health 2026;9(3):254-261

This work aims to analyze the contribution of on-board photovoltaic generation to partially recharge the storage system during flight, with a view to extending the UAVs autonomy. In addition, it analyzes the trade-off between additional autonomy and the mass impact of photovoltaic integration in UAV projects still in the early stages of development.

Materials and Methods

Mathematical Modeling of a Photovoltaic Cell

The mathematical modeling of photovoltaic devices consists of formulating equations that describe the electrical behavior of the device, based on an equivalent circuit built to represent the main electrical characteristics associated with the conversion of solar energy into electrical electrical energy. This modeling approach has been applied in computer simulations, in the development and evaluation of control strategies, in dynamic analysis of converters and in the study of Maximum Power Point Tracking (MPPT) algorithms [7].

The work by Treter and colleagues presented different photovoltaic models based on equivalent electrical circuits, classified according to the number of parameters that describe the device's characteristics [8]. Among the models, the single diode model stands out because it presents a favorable relationship between the accuracy in the representation of electrical behavior and the computational complexity associated with its implementation.

Figure 1 illustrates equivalent circuit of the single diode model. The circuit consists of a current source, a diode, an equivalent resistance in series (Rs) and an equivalent resistance in parallel (Rp).

Equation 1 relates the model's output current and voltage, which was proposed by Wolf and Rauschenbach, and is described by Rauschenbach [9]:

$$I = I_{pv} - I_0\left[\exp\left(\frac{V + R_s I}{V_t a}\right) - 1\right] - \frac{V + R_s I}{R_p} \quad (1)$$

Where:
Ipv: current generated by the incident light;
I_0: diode's leakage current;
a: diode's ideality constant ($1 \leq a \leq 1.5$);
Vt: thermal voltage.

The modeled expression to determine the current I_0, proposed by Souza, is expressed in Equation 2 [4].

$$I_0 = \frac{I_{sc,n} + K_I \Delta T}{\exp\left(\frac{V_{oc,n} + K_V \Delta T}{a V_t}\right) - 1} \quad (2)$$

Where:
Voc,n: nominal open circuit voltage;
K_V: coefficient of variation of the voltage as a function of temperature.

The current *Ipv* varies linearly with the effective irradiance (*G*) and is influenced by the variation between the operating temperature and the nominal temperature, as seen in Equation 3 [10].

$$I_{pv} = \left(I_{pv,n} + K_I \Delta T\right)\frac{G}{G_n} \quad (3)$$

Figure 1. Equivalent circuit of the single diode model.

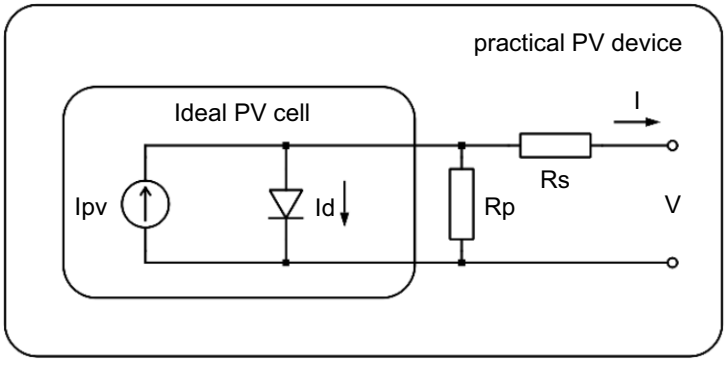

Where:
K_I: coefficient of variation of the current as a function of temperature.

The current generated by the incident light in nominal condition $I_{pv,n}$ is determined by the Equation 4 [10].

$$I_{pv,n} = \frac{R_p + R_s}{R_p} \cdot I_{sc,n} \quad (4)$$

Where:
$I_{sc,n}$: nominal short-circuit current.

The work by Villalva and colleagues proposed an iterative method for estimating the parameters Rs and Rp, assuming the existence of a specific pair capable of ensuring that the maximum power calculated from the model ($P_{max,m}$) equals the maximum experimental power given in the datasheet ($P_{max,e}$) [7]. This equality criterion, applied specifically at the point of maximum power (Vmpp, Impp), guided the adjustment of the parameters to minimize the error in representing the electrical behavior of the photovoltaic device under Standard Test Conditions (STC) [11]. According to this criterion, the maximum power calculated from the model is given by the following expression:

$$P_{max,m} = V_{mp}\left\{ I_{pv} - I_0\left[\exp\left(\frac{q(V_{mp} + R_s I_{mp})}{aN_s kT}\right) - 1\right] - \frac{V_{mp} + R_s I_{mp}}{R_p} \right\} = P_{max,e} \quad (5)$$

The combination of Equations (1) to (5) enables the computational implementation of the photovoltaic model, which represents the electrical behavior of the device under varying irradiance and temperature conditions, and provides a basis for quantitative analyses in simulation, system design, and performance evaluation of photovoltaic systems [12].

Correction of the Area Available for Photovoltaic Cell Installation

Determining the area effectively available for integrating photovoltaic cells into the wing surface requires taking into account geometric constraints that reduce the useful surface in relation to the aerodynamic reference area (*Sref*). To reflect these limitations, specific correction factors are applied: the leading-edge factor (CF_{LE}), the trailing-edge factor (CF_{TE}) and the span factor (CF_W) [5].

The correction factor applied to the leading edge takes into account the sharp curvature of this region, which makes it impossible to install photovoltaic cells properly due to the rigidity of the cells [6]. The correction factor applied to the trailing edge considers the need to preserve the operation of movable surfaces positioned at the rear end of the wing, such as ailerons and flaps, which act directly in controlling the aircraft [5]

Meanwhile the factor applied to the ends of the wingspan seeks to represent the safety zone, due to the susceptibility to structural deformations in flight and the installation of auxiliary components such as navigation lights and antennas [13]. These factors vary according to the geometric and functional characteristics of the aircraft.

Applying the correction factors in Equations (6) and (7) allows the average corrected wing chord (C_{PV}) and corrected wingspan (B_{PV}) to be calculated [5].

$$C_{PV} = \frac{100 - CF_{LE} - CF_{TE}}{100} - c \quad (6)$$

$$B_{PV} = \frac{100 - CF_W}{100} - b \quad (7)$$

Based on these corrected geometric parameters, Equation (8) makes it possible to determine the effective area available for the installation of photovoltaic cells (S_{PV}).

$$S_{PV} = C_{PV} - B_{PV} \quad (8)$$

Case Study

The case study was based on a fixed-wing UAV with a combustion propulsion system. The on- board electronic systems include avionics (navigation, flight control and communication) and payload, powered by batteries. The UAV has

a required autonomy of 6 hours, maintaining a constant energy consumption of 150Wh. To meet this demand, two Tattu Plus 22 Ah/22.2V LiPo batteries were used, with a mass of 5.3kg, as specified in the Gens Ace Tattu datasheet [14]. The main parameters of the UAV used in this study are shown in Table 1.

Table 1. UAV data.

Parameter	Symbology	Value
Maximum take-off weight (N)	W_{TO}	40
Wingspan (m)	b	4,660
Average wing chord (m)	c	0.358
Wing area (m²)	S_{ref}	1,668

In this study, the mathematical modeling of the photovoltaic cell was proposed with a view to estimating energy generation under a given operating profile, considering the application in battery recharging. To determine the model parameters, the iterative method proposed by Villalva and colleagues was implemented in MATLAB, which enabled the resistances *Rs* and *Rp* to be obtained [7].

The photovoltaic cells were installed on the surface of the wing, respecting the geometric limitations of the structure. The wing's reference area was corrected by application of the factors CF_{LE} = 15%, CF_{TE} = 10% and CF_{W} = 18%, resulting in an effective area of 1.03m². For this application, SunPower C60 monocrystalline silicon photovoltaic cells were selected. The main electrical characteristics of the cell are presented in Table 2, according to the specifications provided in the PV cell C60 datasheet [15].

The photovoltaic cell has a KV of -1.8mV/°C and a KI of - 0.32%/°C, with a mass equivalent to 6.5g, as also described in the C60 cell datasheet. A photovoltaic array consisting of 60 cells was defined, distributed in the 30S2P configuration. The connection between the photovoltaic array and the batteries was implemented by means of an MPPT charge controller, model Genasun GVB-8-Li-25.0V, with a reported mass of 185g, according to Genasun's product specifications [16].

Table 2. Photovoltaic cell data.

Pmpp (Wp)	Eff. (%)	Vmpp (V)	Impp (A)	Voc (V)	Isc (A)
3.42	22.5	0.58	5.93	0.68	6.28

The energy generated over time was estimated based on the Direct Normal Irradiance (DNI) for the year 2024, considering the operating site located in the city of Salvador, Bahia. The irradiance data was obtained from the Global Solar Atlas platform [17]. For the analysis, we considered the monthly average of daily irradiance during the period of highest solar incidence, between 10:00 AM and 03:00 PM, as illustrated in Figure 2.

Although as known that the continuous movement of the UAV implies variations in the angle of incidence of solar radiation, irradiance and cell temperature, the profile shown in Figure 2 was adopted as an approximation of the irradiance conditions to which the UAV would be exposed during operation. This approach was compatible with the exploratory nature of the study and could be improved in future work to more faithfully represent dynamic operating conditions.

Results and Discussion

The mathematical modeling strategy implemented resulted in the estimation of the electrical parameters of the photovoltaic cell that allowed the MPP to be reproduced. The result was Rs = 0.003535Ω, RP = 5.407216 Ω and a = 1.

Figure 3 shows the simulated I-V and P-V characteristic curves with the parameters obtained. The maximum power point was reproduced with Vmpp = 0.579V, Impp = 5.962A and Pmpp = 3.452W. These values are close to the data supplied by the manufacturer, as shown in Table 2, with a relative error of less than 1%. This result reinforces that the mathematical modeling of the C60 photovoltaic cell implemented was able to represent the cell's electrical behavior with

Figure 2. Average peak irradiance throughout the year.

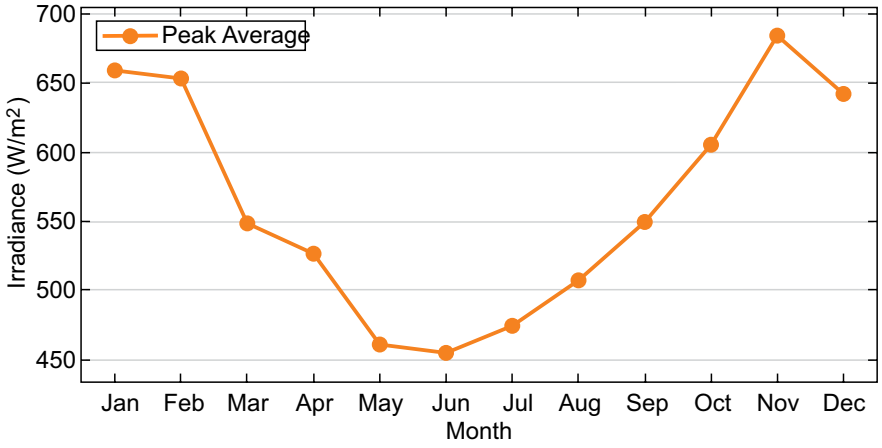

Figure 3. I-V and P-V characteristic curves of the photovoltaic cell.

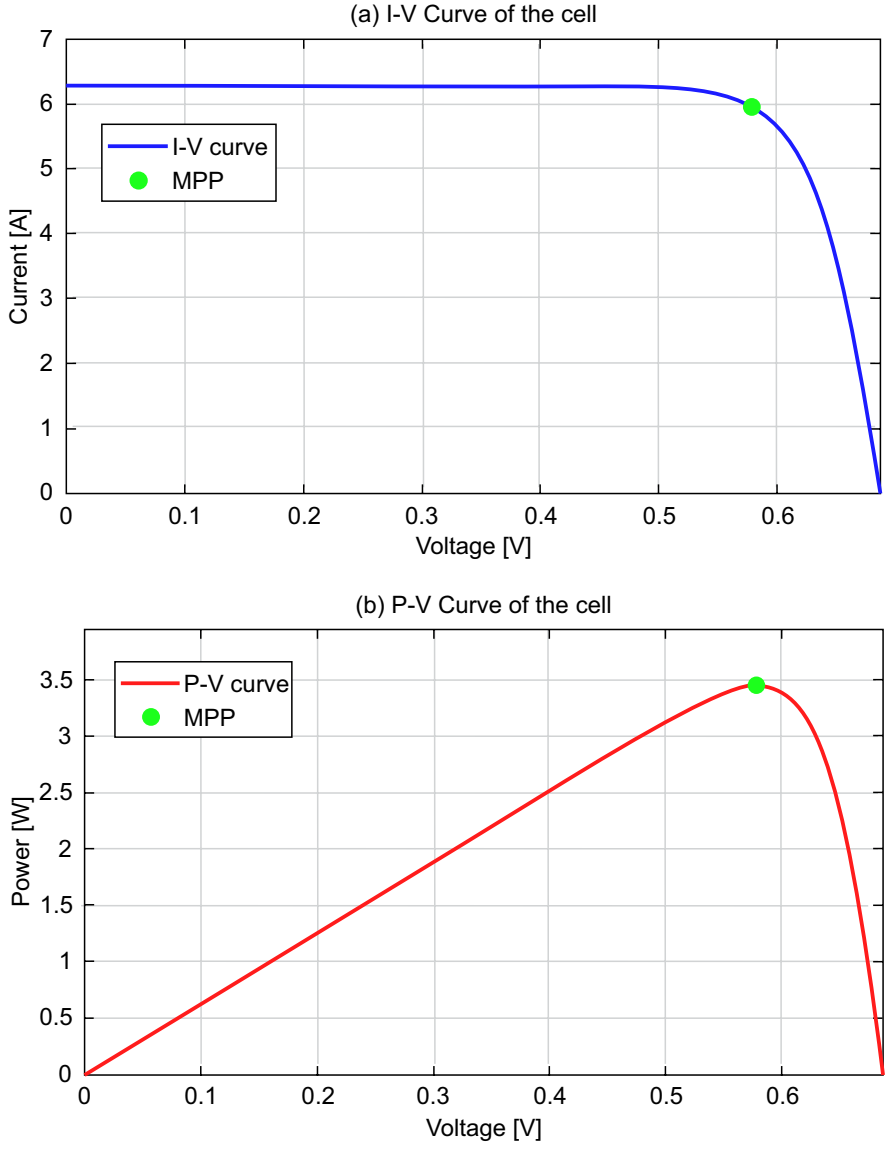

satisfactory accuracy under STC, set at 1000W/m² and 25°C.

The mathematical modeling implemented made it possible to estimate the daily power generated by the photovoltaic cell under different irradiance conditions. As illustrated in Figure 2, the maximum and minimum monthly average daily irradiance values occurred in November (684.4W/m²) and June (461.0W/m²), respectively. These conditions were incorporated into the modeling, resulting in an estimate of the power generated by a photovoltaic cell, with P(mpp,max) = 2.493W and P(mpp,min) = 1.679W.

Figure 4 shows the estimated daily solar energy generated over 5 hours. Under these conditions, the maximum estimated generation was 635.71Wh and the minimum 428.14Wh, considering the system performance of 85% to take into account the losses associated with tracking the MPP and the variations in temperature and irradiance over time.

Based on the estimate of the daily energy generated by the arrangement, it was possible to quantify the contribution of solar generation to the battery recharging system during the flight. In the simulated maximum and minimum irradiance scenarios, the estimated additional autonomy was 4 hours and 14 minutes, and 2 hours and 51 minutes, respectively. These results correspond to maximum and minimum increases of 70.55% and 47.50% in the autonomy of the aircraft.

The insertion of the photovoltaic array showed considerable potential for extending the UAVs operational autonomy. However, the precise quantification of this extension requires the consideration of a more dynamic operational profile, incorporating variables such as flight path, altitude and environmental conditions. Due to the exploratory nature of this study, the estimate of additional autonomy presented should be interpreted as preliminary, and may be progressively refined in subsequent analyses by incorporating more representative operational mission scenarios, including these variables.

The UAV considered in this study was used exclusively as a reference for the trade-off analysis between additional autonomy and the mass impact of photovoltaic integration. The adoption of on-board solar generation requires the architecture of the aircraft to be designed to accommodate the associated structural, aerodynamic and balancing constraints. In this sense, the obtained results regarding autonomy extension provide quantitative support for UAV projects still in

Figure 4. Estimated solar energy generated during 1 hour.

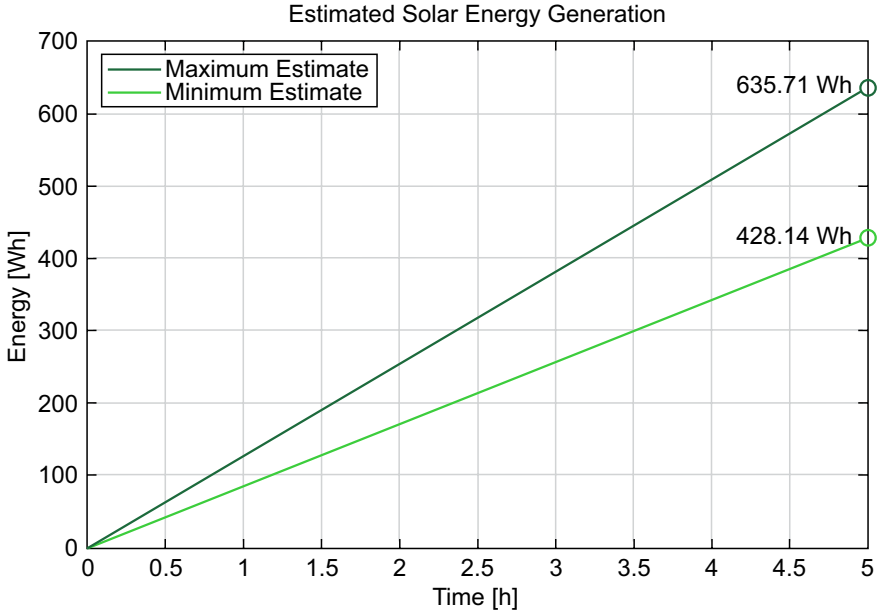

the initial design phase, in which extending operational autonomy constitutes a design guideline and the feasibility of solar energy integration remains under evaluation

The additional mass introduced by the photovoltaic system must be carefully evaluated, given that mass represents a highly sensitive design variable in unmanned aircrafts. In the configuration adopted, the integration of the system resulted in an increase of 575g, corresponding to approximately 1.44% of the UAV weight. Although this percentage may seem small, it represents a significant fraction in the context of aeronautical design, where minimal variations in mass can directly impact the aircraft's performance.

Figure 5 shows the relationship between energy supplied and mass impact, comparing the battery-only configuration with the hybrid configuration consisting of batteries and a photovoltaic system. The results indicate that photovoltaic integration allows the UAVs autonomy to be extended with a smaller increase in mass, since to achieve the same length of autonomy with batteries alone, it would be necessary to install one or two additional units, depending on the irradiance scenario evaluated. Alternatively, replacing the battery considered in the case study with one with a higher nominal capacity would also result in a greater increase in mass compared to the photovoltaic system.

Conclusion

The insertion of on-board solar generation proved to be a viable solution for considerably extending the UAVs energy autonomy. The analysis of the trade-off between the increase in mass and the associated energy gain indicated a favorable relationship, reinforcing the potential of photovoltaic integration as a complementary solution in prolonged missions, especially in UAV projects still in the initial design phase,

Figure 5. Relationship between energy supplied and mass impact.

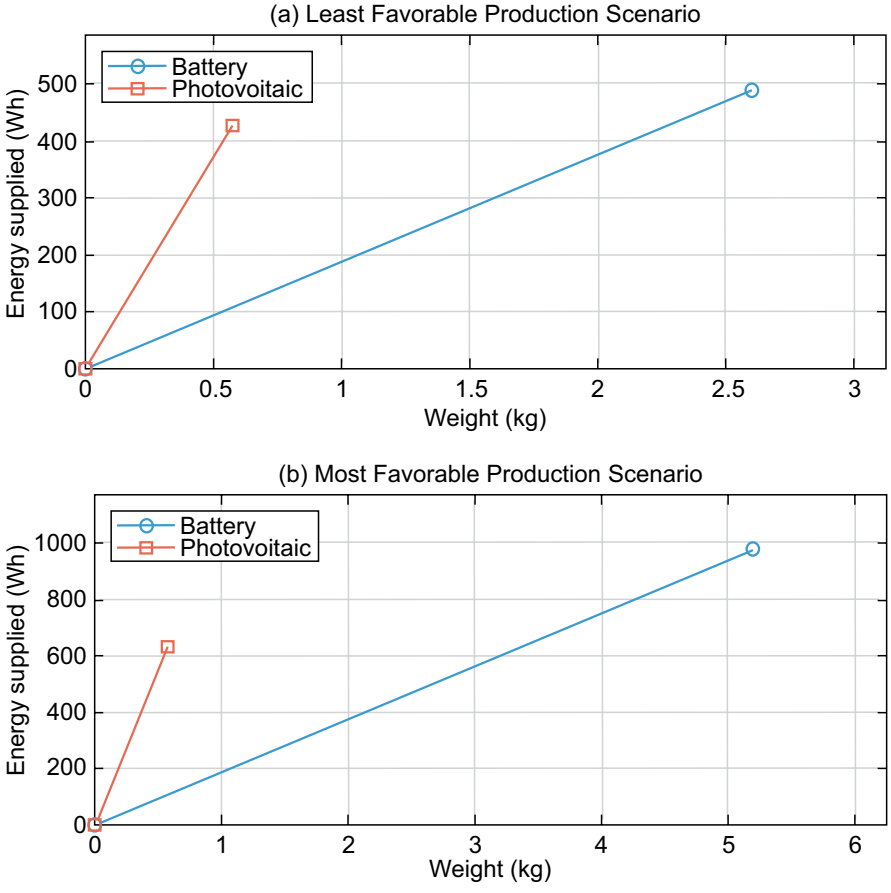

in which the architecture of the aircraft can be adapted to accommodate the incorporation of the photovoltaic system.

The objectives of this work were achieved within the established limitations, and, as prospects for continuity, with highlight on the incorporation of operational scenarios that consider variables such as flight altitude, flight path and environmental conditions throughout the flight. Additionally, technical-structural feasibility analyses should be conducted to evaluate the integration of the photovoltaic system in UAVs during early design stages, allowing the aeronautical project to accommodate such integration, as well as in to existing UAVs of similar class and size.

References

1. Mateja K, et al. energy autonomy simulation model of solar powered UAV. Energies. 2023;16(1):479
2. Quintana J, et al. hybrid powerplant design and energy management for UAVs: enhancing autonomy and reducing operational costs. Energies. 2025;18(12):3101.
3. Elmeseiry N, Alshaer N, Ismail T. a detailed survey and future directions of unmanned aerial vehicles (UAVs) with potential applications. Aerospace. 2021;8(12):363.
4. Souza JC. solar system for a long endurance electric UAV [master's thesis]. Covilhã: University of Beira Interior; 2015.
5. Vidales HM. design, construction and test of the propulsion system of a solar UAV [master's thesis]. Lisbon: Technical University of Lisbon; 2013.
6. Marta A, Gamboa P. long endurance electric UAV for civilian surveillance missions. In: proceedings of the international council of the aeronautical sciences; 2014.
7. Villalva MG, Gazoli JR, Ruppert E. comprehensive approach to modeling and simulation of photovoltaic arrays. IEEE Trans Power Electron. 2009.
8. Treter ME, Mezaroba M, Michels L. mathematical modeling of the electrical behavior of photovoltaic modules: a review. In: anais do congresso brasileiro de energia solar (CBENS); 2020.
9. Rauschenbach HS. solar cell array design handbook: the principles and technology of photovoltaic energy conversion. New York: Springer; 2012.
10. Sera D, Teodorescu R, Rodriguez P. PV panel model based on datasheet values. In: IEEE conference proceedings; 2007.
11. Villalva MG, Gazoli JR, Ruppert E. modeling and circuit-based simulation of photovoltaic arrays. In: brazilian power electronics conference; 2009.
12. De Soto W, Klein SA, Beckman WA. improvement and validation of a model for photovoltaic array performance. Sol Energy. 2006.
13. Bakar A, et al. design of low altitude long endurance solar-powered UAV using genetic algorithm. Aerospace. 2021;8(8):228.
14. Genstattu. tattu plus 22000mAh 6S 25C 22.2V datasheet [internet]. 2021 [cited 2026 Apr 4]. Available from: https://www.genstattu.com/content/Tattu-Plus.pdf
15. SunPower Corporation. C60 solar cell datasheet [internet]. 2010 [cited 2026 Apr 4]. Available from: http://eshop.terms.eu/_data/s_3386/files/1379942540-sunpower_c60_bin_ghi.pdf
16. Sunforge. genasun GVB-8-Li-25.0V MPPT boost charge controller datasheet [internet]. 2021 [cited 2026 Apr 4]. Available from: https://cdn.shopify.com/s/files/1/0062/2959/0114/files/Genasun_GVB-8_datasheet_23.pdf
17. Energy Sector Management Assistance Program (ESMAP). global solar atlas 2.0: technical report [internet]. 2019 [cited 2026 Apr 4]. Available from: https://globalsolaratlas.info/map

Design and Analysis of a Metal Detection System Based on an Inductive Sensor

Akin Santos[1]*, Alexandre da Silva[1], Kauan da Silva[2], Leonardo Trinchão[3], Ludmila dos Anjos[3], Tiago Barretto Sant'Anna[1], João Alberto Castelo Branco Oliveira[4]

[1]SENAI CIMATEC University, Robotics Department; [2]SENAI CIMATEC University, CC Drones; [3]SENAI CIMATEC University, Graduation in Electrical Engineering; [4]SENAI CIMATEC University, Embedded Systems; Salvador, Bahia, Brazil

This article presents the development and analysis of a metal object detection system utilizing an inductive sensor. The project covers everything from the fundamental operating principles of inductive sensors to their practical application within a circuit controlled by an ESP32 microcontroller. A detailed noise analysis of the system was conducted, comparing theoretical quantization noise with experimentally measured noise. This allowed for the identification of predominant interference sources. The results demonstrate the system's effectiveness in metal detection and quantify the measurement errors, thereby validating the application of inductive sensors in industrial automation and process control systems.

Keywords: Inductive Sensor. Metal Object Detection. ESP32 Microcontroller. Noise Analysis. Digital Filtering.

In industrial automation, high-precision detection of metallic objects is fundamental to protecting equipment and maximizing the efficiency of production lines. The advancement of smart sensors and integration with Industry 4.0 paradigms require a deep understanding of physical principles, implementation strategies, and technological limitations. Inductive sensors remain robust and versatile solutions that can be used in both harsh industrial environments and in portable and wearable devices. In wearable and antenna applications, inductive textile sensors made with conductive yarns offer stable performance, low cost, and ease of manufacturing [1], while in industrial environments, shielded construction ensures immunity to dust, dirt, and oil [2].

Inductive sensors operate based on an LC oscillator circuit coupled to a high-permeability coil; the approach of a metal induces eddy currents that drain energy from the oscillator and alter the inductance, allowing for the rapid and precise detection of the object [3]. Due to their robustness and immunity to contaminants such as dust, dirt, and oils [2], these sensors are widely used for position control, parts counting, and speed monitoring. In high-frequency inductive sensors, the switching frequency can reach up to 5 kHz, enabling pulse counting to calculate motor rotation [3].

The integration of these sensors with microcontrollers like the ESP32 requires analog-to-digital conversion (ADC). The ESP32's internal ADC offers a nominal resolution of 12 bits but exhibits non-linearities as it does not differentiate between close voltages, such as 3.3 V and 3.2 V or 0.1 V and 0.1 V [4], and is sensitive to noise. The documentation from Espressif, the developer of the ESP32, recommends using a 0.1 µF decoupling capacitor on the input pin and applying multisampling (multiple samples) to reduce intrinsic noise [5]. Furthermore, different sources of noise, such as quantization, thermal noise, flicker (1/f noise), and electromagnetic interference, can degrade the quality of the measurements [6]. Oversampling and filtering techniques are applied to reduce quantization noise or disperse noise energy to other frequencies. Implementing digital filters improves the signal-to-noise ratio [6].

Spectral analysis using the Fast Fourier Transform (FFT) converts the signal from the time domain to the frequency domain and allows

Received on 10 October 2025; revised 21 December 2025.
Address for correspondence: Akin Santos.Av. Orlando Gomes, 1845, Piatã, Salvador, Bahia, Brazil. Zipcode: 41650-010. E-mail: akinsilva@hotmail.com.

J Bioeng. Tech. Health 2026;9(3):262-271

for the identification of unwanted components and their amplitude [7]. To attenuate components outside the band of interest, digital finite impulse response (FIR) or infinite impulse response (IIR) filters are applied. Low-pass filters are used to remove high-frequency signals; high-pass filters attenuate low-frequency signals; band-pass filters select only the desired range.

Thus, the present work develops and analyzes a system for detecting metallic objects using an inductive sensor coupled with an ESP32 microcontroller. The objective is to reliably measure the rotation of a motor from the passage of a metal plate, quantify the limits imposed by ADC quantization and noise, and apply digital filtering techniques to mitigate interference and increase accuracy.

The following sections present the theoretical foundation of the sensors and filtering techniques, describe the materials used and the mathematical methods employed in the generation and filtering of noise, detail the development of the circuit and the interface with the ESP32, and discuss the experimental results and the performance of the system under test conditions.

Theoretical Framework

This section covers all the material used as a theoretical basis for the project's development, from the operation/actuation of inductive sensors to more specific concepts about signal reading and processing.

Inductive Sensors in Automation

Inductive sensors are widely used in industrial automation for the non-contact detection of metallic objects, offering robustness, durability, and immunity to polluted or humid environments [8-10]. They operate by means of an oscillator that generates an electromagnetic field; the proximity of a metallic object alters this field and, consequently, the inductance, which is detected by the circuit [11,12]. Typical applications include parts counting, position control, and limit switches.

Electrical Inductance in Inductive Sensors

The inductance L of a coil is given by:

$$L = \frac{N^2 \mu A}{l},$$

Where N is the number of turns, μ is the magnetic permeability, A is the cross-sectional area, and l is the length of the coil [11]. In inductive sensors, the approach of metallic objects alters this inductance, enabling detection [13].

Correction Factor and Inductive Coupling

Sensors are calibrated for standard targets like steel (factor ≈ 1) (Table 1), and have a reduced range for aluminum, brass, and copper, among others [11]. Inductive coupling involves eddy currents induced in the metal, which modify the coil's properties and are interpreted by the detection circuit [14].

Table 1. Calibration for standard targets.

Material	Correction Factor
Steel (Fe360)	1.0
Stainless steel	0.7–0.9
Aluminum	0.4–0.5
Brass	0.3–0.4
Copper	0.25–0.35

Noise in Sensor Systems

Noise in sensors can be intrinsic (circuit-related) or extrinsic (environmental), classified according to its source or spectrum [15].

Intrinsic Noise

Among the main sources of signal degradation in measurement systems are electromagnetic and radiofrequency interference (EMI/RFI), which can induce spurious readings and compromise data reliability. Added to this is thermal noise, also known as Johnson-Nyquist noise, originating from the thermal agitation of charge carriers,

whose spectral density is constant and imposes a physical limit on the system's sensitivity. Another relevant factor is quantization noise, introduced during the analog-to-digital conversion (ADC) process due to the discretization of signal levels, which, in high-resolution converters, can be modeled as white noise [16] (Figure 1).

In quantization, the values of an already-sampled analog signal are approximated to a limited number of discrete levels. Essentially, it rounds each sample value to the nearest quantized level, transforming a continuous range of amplitudes into a finite set of digital values that can be represented and stored. Quantization noise can be modeled as white noise because, for most signals, the rounding error of each sample is random and uncorrelated with the signal. This randomness distributes the noise energy uniformly across the entire frequency spectrum, which is the main characteristic of white noise.

Quantization Noise and Standard Deviation

The formulas used to obtain the value of these variables for later analysis are demonstrated below. The standard deviation is relevant for assessing an average rate of variation between the measured and the real value, and the quantization step is for analyzing the signal's digitization.

- Quantization step Δ:

$$Q = \frac{V_{FS}}{2^N} \quad (1)$$

Where VFS is the full-scale voltage and N is the number of bits of the ADC. For a 12-bit ADC with VFS=3.3 V, we get Q≈0.805 mV, a value that indicates the smallest difference detectable by the converter. Variations smaller than this value are rounded to the nearest level, generating what is called quantization error. The standard deviation of the quantization noise allows for estimating the impact of this error on the measurements and is used in precision analyses and the calculation of the signal-to-noise ratio (Figure 2).

- Theoric standard deviation:

$$\sigma_{quant} = \frac{Q}{\sqrt{12}} \approx 0,232 \text{ mV}.$$

- Practical comparison: The measured noise was approximately 32.445 mV, a value about 140 times higher than the estimated theoretical thermal noise. This significant difference indicates that, in addition to thermal noise, there is a relevant contribution from other sources, the main one being electromagnetic interference (EMI), evidenced by the excess magnitude and the measurement environment being subject to inductive and capacitive couplings.

Figure 1. Example of continuous signal quantization.

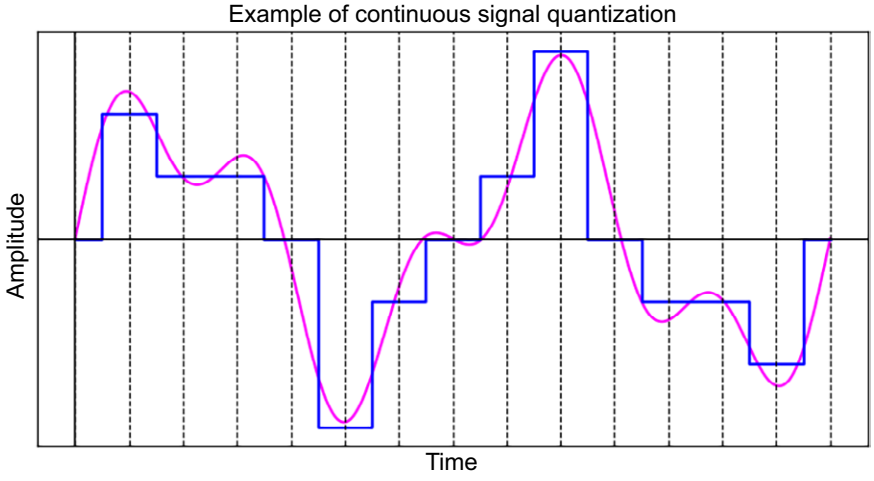

Figure 2 represents the system's baseline voltage signal (without material detection). From its analysis, it was possible to identify the signal's characteristics and obtain the necessary samples to calculate the standard deviation of the actual noise.

Spectral Noise

Classification of noise based on frequency [17]:

- White Noise: Constant spectral density across all frequencies;
- Pink Noise (1/f): Decreasing density (3 dB/ octave or 10 dB/decade), concentrating energy at low frequencies.

Figure 3 shows how a signal's power is distributed across frequencies. For white noise, the Figure is a straight, horizontal line, indicating that the energy is distributed uniformly across all frequencies.

For pink noise, however, the graph has a negative slope of -3 dB per octave. This means that the noise power is greater at lower frequencies and decreases as the frequency increases. Because of this, pink noise is perceived by the human ear as having a more balanced and pleasant sound than white noise.

Detection System with Inductive Sensor

This section covers the constructive aspects of the detection system, including the electrical schematic and the integration of the inductive sensor with the microcontroller.

Following that, an analysis of the noise present in the system is presented, an essential step to ensure the accuracy and reliability of the detection. The electrical schematic of the metallic detection system, illustrated in Figure 4, is based on the integration of an inductive sensor with the ESP32 microcontroller, which is responsible for signal processing and controlling the display interface.

The sensor, positioned near an iron plate coupled to the motor's shaft, is powered and connected to the circuit in a way that provides an output signal compatible with the ESP32's logic level. With each complete rotation of the plate, the sensor generates an electrical pulse, which

Figure 2. Resting voltage signal used to measure the standard deviation of real noise.

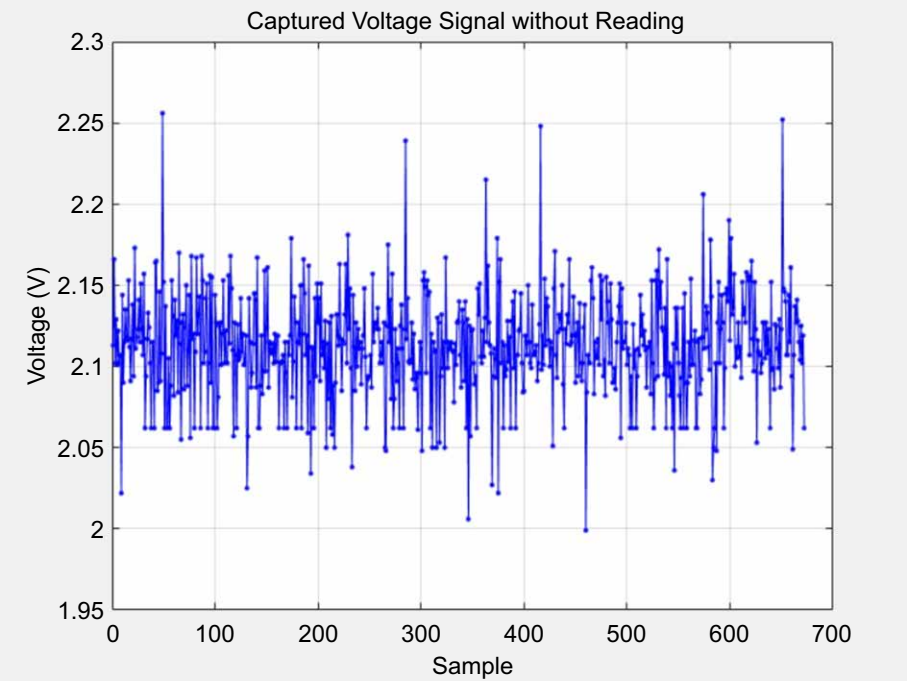

Figure 3. Spectral density for white and pink noise.

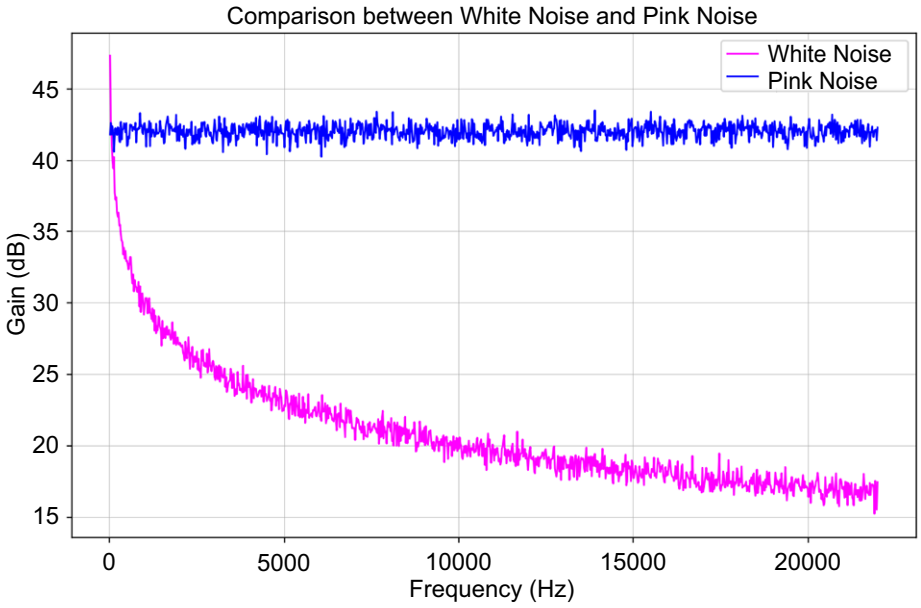

Figure 4. Physical assembly of the prototype in the laboratory.

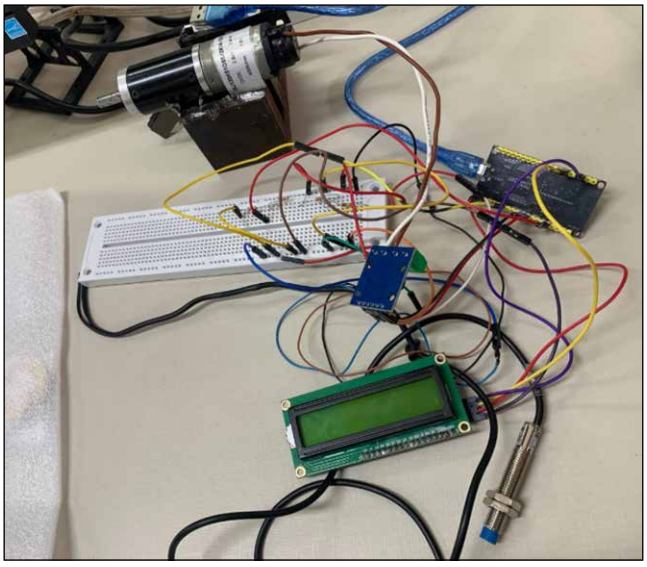

is sent to the microcontroller's digital input. In addition to reading the signal from the inductive sensor, the ESP32 also receives information from a piezoelectric sensor, used for comparisons in additional tests.

The inductive sensor's signal is processed to determine the rotations per minute (RPM) in real-time, while the piezoelectric sensor provides complementary measurements for experimental analysis. The LCD display is connected to the ESP32 to show, in real-time, the RPM and voltage values, enabling direct monitoring during tests.

The electric motor, coupled to the iron plate, constitutes the mechanical element being evaluated, simulating real detection conditions. The physical assembly of the circuit, shown in Figure 5, was carried out on a protoboard, using jumpers and resistors to interconnect the components.

Next, the noise analysis is presented, aiming to improve the precision of the metal detection system.

Noise Analysis Method

To examine the quality of the captured signal and the robustness of the method, the study was divided into two approaches: quantization analysis and spectral analysis with digital filtering.

Quantization Noise Analysis

The ESP32's built-in ADC (12 bits, VFS range = 3.3 V) was considered. The magnitude of the quantization step Q and its theoretical standard

Figure 5. Project schematic showing the sensor actively measuring the metallic object.

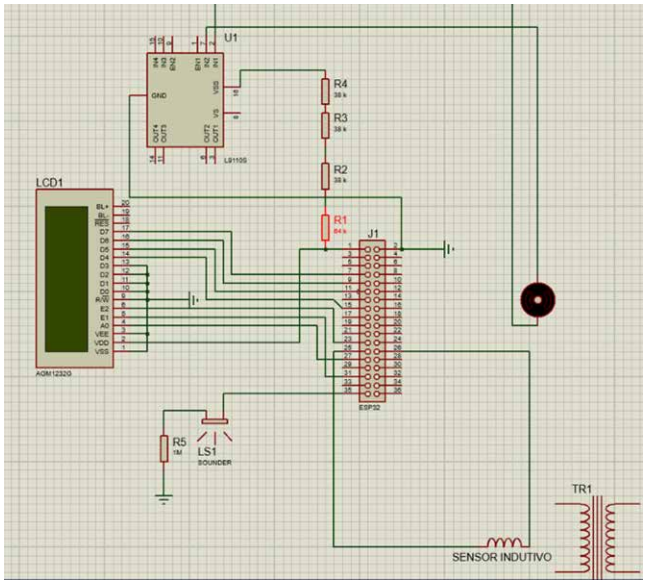

deviation, σquantization, were calculated using Equations 1 and 2, based on the classic model of uniform quantization, as mentioned in the Theoretical Framework section:

$$Q = \frac{V_{FS}}{2^{N_{bits}}} \quad (1)$$

$$\sigma quantizacao = Q \sqrt{12} \quad (2)$$

In the experimental phase, the voltage signal at rest was recorded, without the presence of the plate, to evaluate the system's actual standard deviation and compare it with the theoretical value. The observed deviation in the results was approximately 140 times greater than the estimated theoretical value, highlighting the presence of additional noise sources beyond quantization noise.

Noise Mitigation in the ESP32

Knowing that the ESP32's ADC is sensitive to noise, two additional strategies were applied: (a) the inclusion of a 0.1 µF bypass capacitor at the ADC input, which filters high-frequency noise and stabilizes the circuit's power supply, and (b) averaging by multisampling with 64 samples, as recommended in the official documentation [18,19].

Spectral Analysis and Filtering: For characterization in the frequency domain

To characterize the noise and optimize detection, an analysis was performed in the frequency domain. Synthetic white and pink noises were generated in MATLAB software based on the parameters described in Omron Industrial Automation [12] and PCBgogo [20], allowing for the simulation of the system's noise conditions. Subsequently, both the original signals and those with added noise were subjected to the Fast Fourier Transform (FFT) for the analysis of their frequency components. Observing that the signal of interest was concentrated below 60 Hz, a second-order digital Butterworth filter with a cutoff frequency of 60 Hz was designed, prioritizing stability and lower distortion. Finally, the gain in the signal-to-noise ratio (SNR) before and after filtering was evaluated, verifying a considerable improvement. This approach, which combines the controlled injection of noise with digital filtering, allowed for the quantitative validation of the SNR increase, demonstrating the filter's effectiveness in cleaning the inductive sensor's signal.

Addition of Spectral Noise

For the spectral analysis, two types of synthetic noise—white and pink—were injected into a square wave signal using MATLAB software, as illustrated in Figure 6, which presents the original signal and the same signal after the addition of the noises. Next, the Fast Fourier Transform (FFT) was applied to identify the signal's frequency components, making it possible to compare the spectrum before and after the noise injection.

Figure 7 shows the frequency spectrum of the signals with and without noise, allowing for the observation of the increased spectral density at high frequencies due to the presence of the added noises.

Subsequently, a second-order digital Butterworth filter with a cutoff frequency of 60 Hz was employed to reduce the interference caused by the noise. The result of this filtering is shown

Figure 6. Original signal and with injected white and pink noise.

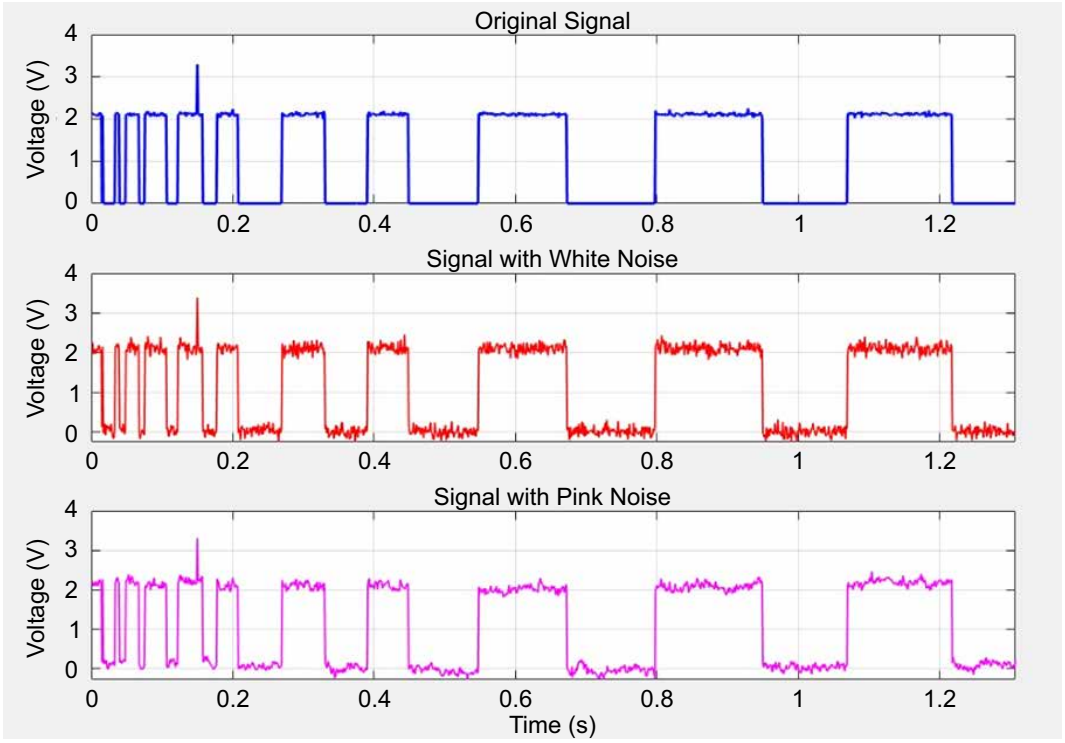

Figure 7. Frequency spectrum of signal without and with noise.

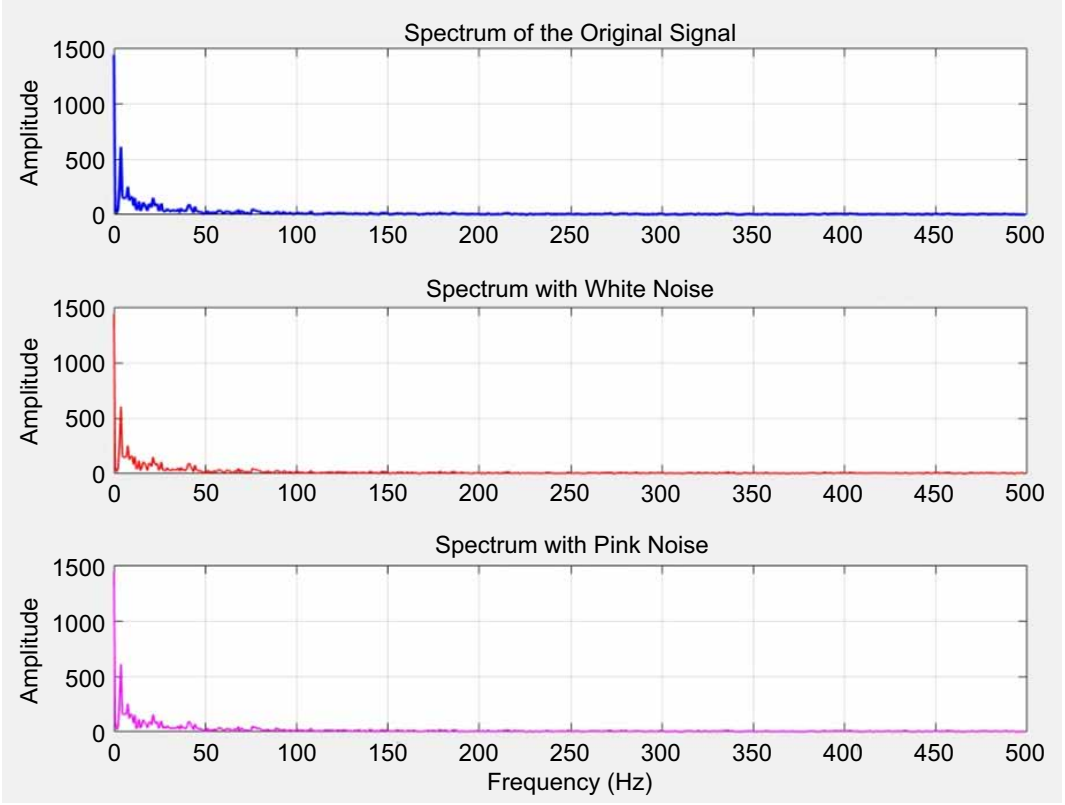

in Figure 8, in which the significant attenuation of high-frequency components can be observed, highlighting the filter's efficiency in cleaning the signal and increasing the signal-to-noise ratio (SNR).

Results

The project's execution allowed for the validation of the detection system. The system was able to identify the presence of the iron plate and measure the motor's rotation with an average of 119.7 ± 1.78 RPM. The average voltage at rest was 2.1134 ± 0.0009 V, thus making it possible to observe the motor's rotation by the delivered voltage, noting how much it differs from the cited rest voltage.

Therefore, upon analyzing the data of: voltage at rest, voltage consumed when the motor is in motion, and the variation detected by the sensor, a satisfactory performance of the sensor was validated.

Comparative Analysis of System Noise

For the analysis of white and pink noise, it was found that the measured standard deviation (32.445 mV) was about 140 times greater than the theoretical quantization noise (0.232 mV).

This indicates a low influence from the inserted noises and that the predominant noise sources are thermal and electromagnetic interference (EMI), not the ADC's limitation.

This concludes which are the main intrinsic sources capable of interfering with the constructed system. These are strengthened by the already known impacts on electrical systems caused by temperature and magnetic/electric fields.

Analysis of Spectral Noise Results

Fast Fourier Transform (FFT): Based on Figure 7, it was possible to identify that its components were concentrated at low frequencies [21].

Figure 8. Signals with white and pink noise after filtering.

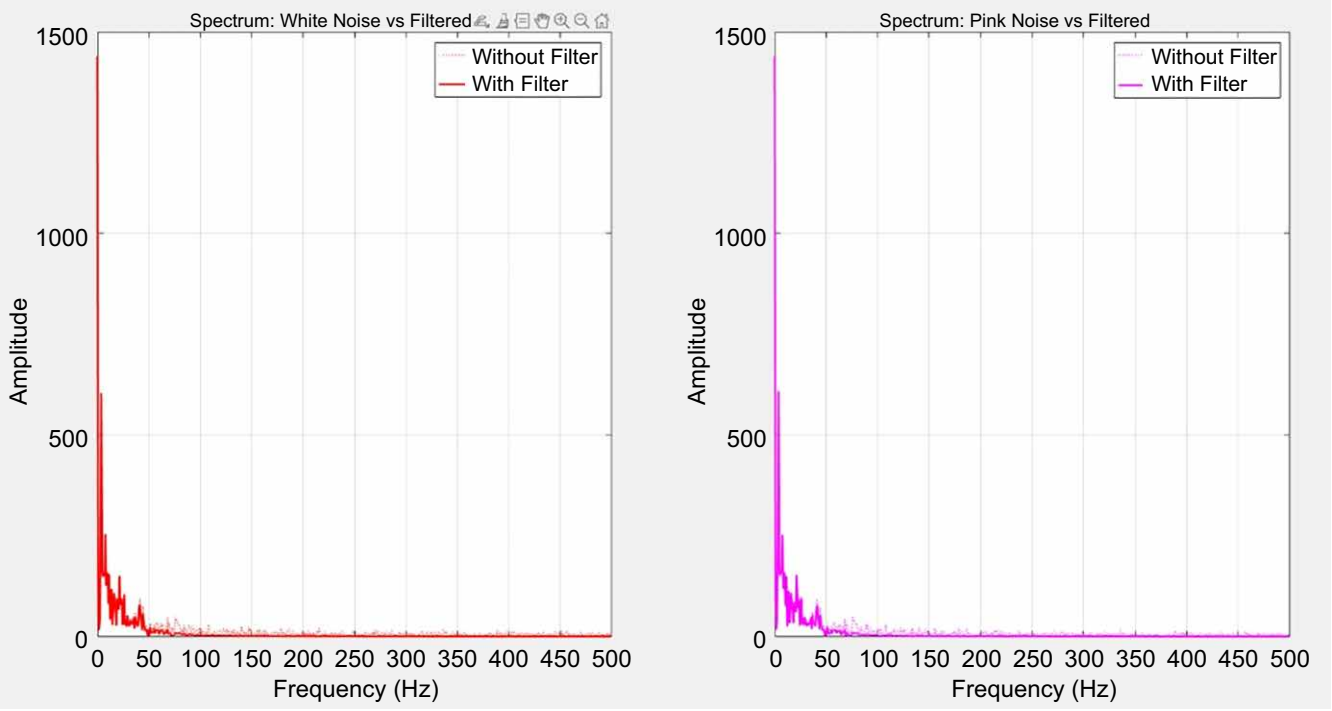

- Low-Pass Filtering: The use of the Butterworth filter resulted in an effective elimination of high-frequency noise, constituting an 80% reduction in its presence and its components.
- Signal-to-Noise Ratio (SNR) Improvement: The attenuation of high-frequency components, as discussed in the development section, resulted in a significantly higher SNR, providing a cleaner and more precise signal—consistent with studies that demonstrate SNR gains using low-pass filters [22].

In summary, the injection of synthetic noise and its spectral analysis, after comparing Figures 6 and 9, allowed for the validation of the filtering process's effectiveness—specifically, in the application of a low-order Butterworth filter—in increasing the SNR, corroborating consolidated practices in signal processing.

Conclusion

This work presented the design, implementation, and analysis of a metallic object detection system, integrating an inductive sensor, embedded processing on an ESP32 microcontroller, and an LCD display for data visualization.

The experimental results demonstrated that the system achieved a measurement error of approximately 1.5% for rotation speed (RPM), meeting the requirements of various control and industrial automation applications. The noise analysis, a central focus of the study, revealed a significant technical finding: the standard deviation of the measured noise in the system (32.445 mV) was approximately 140 times higher than the theoretical quantization noise (0.232 mV).

This finding proves that the main source of imprecision does not lie in the resolution of the A/D converter, but rather in external interferences like electromagnetic noise (EMI), directing optimization efforts towards shielding and signal filtering instead of hardware replacement. The adopted architecture, based on the ESP32, facilitates future expansions and improvements.

As future work, it is suggested to implement real-time digital filters (such as moving average

Figure 9. Frequency spectrum of the signals after filtering.

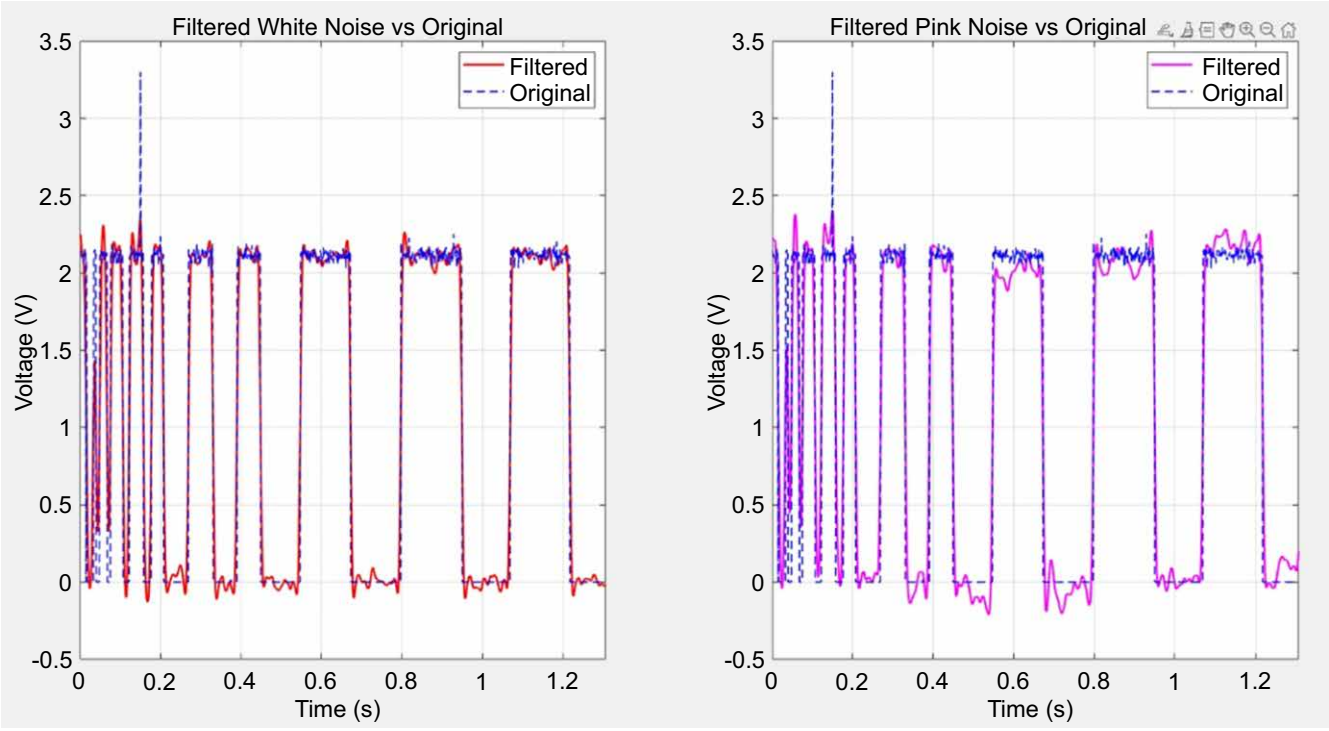

or Kalman) in the firmware to mitigate the measured noise, integrate the system with an IoT platform for remote cloud monitoring, and characterize the sensor's response to different types of metallic materials by exploring correction factors. Additionally, the use of machine learning techniques could be explored for object classification or anomaly detection in the process.

In summary, the proposed system represents a low-cost solution with satisfactory precision and great potential for expansion. It serves as a practical and didactic validation for the application of industrial sensors in embedded systems, contributing to the development of smarter and more connected solutions in the context of Industry 4.0.

References

1. Patiño AG, Mencon C. Inductive textile sensor design and evaluation for a wearable monitoring device. Sensors (Basel). 2021;21(11):225.
2. Micro-Epsilon. Eddy current inductive sensors [Internet]. Available from: https://www.micro-epsilon.com/distance-sensors/inductive-sensors-eddy-current/
3. Baumer. Working principle and technology of inductive sensors. Baumer USA [Internet]. Available from: https://www.baumer.com
4. Santos S. ESP32 analog input with Arduino IDE [Internet]. 2019. Available from: https://randomnerdtutorials.com
5. Espressif Systems. Analog to digital converter (ADC): ESP32 – ESP-IDF programming guide v4.2.5 [Internet]. 2025. Available from: https://docs.espressif.com
6. Hardware and Systems Engineering (HWE). Hardware and systems engineering design: noise and interference [Internet]. 2025 Available from: https://www.hwe.design
7. Eureka. Identifying noise sources with FFT analysis on oscilloscopes [Internet]. 2025 Available from: https://www.eurekamagazine.co.uk
8. Zhang Y, et al. An analog-digital mixed measurement method of inductive proximity sensor. Sensors (Basel). 2016;16.
9. ScienceDirect Topics. Proximity sensor: an overview [Internet]. 2025 Available from: https://www.sciencedirect.com
10. Li X, et al. Differential structure of inductive proximity sensor. Sensors (Basel). 2019;19.
11. Wikipedia contributors. Inductive sensor [Internet]. Wikipedia; 2025. Available from: https://en.wikipedia.org/wiki/Inductive_sensor
12. Omron Industrial Automation. Overview of proximity sensors [Internet]. Available from: https://www.ia.omron.com/support/guide/41/introduction.html
13. TME EU. O que é a indutância e de que ela depende? TME EU News [Internet]. 2025 Mar 21. Available from: https://www.tme.eu
14. Omron. Technical explanation for proximity sensors [Internet]. 2015 Available from: https://www.ia.omron.com
15. Fraden J. Handbook of modern sensors: physics, designs, and applications. New York: Springer; 2015.
16. IEEE. Quantization and thermal noise in ADCs. IEEE Spectrum [Internet]. 2002 Sep 9. Available from: https://spectrum.ieee.org
17. Yamagata M, et al. Effects of subthreshold electrical stimulation with white noise, pink noise, and chaotic signals on postural control during quiet standing. Gait Posture. 2022;94:39–44.
18. Arduino Forum. Fixing the non-linear ADC of an ESP32 [Internet]. Available from: https://forum.arduino.cc/t/fixing-the-non-linear-adc-of-an-esp32/699190
19. Espressif Systems. ADC calibration driver – ESP32 [Internet]. Available from: https://docs.espressif.com/projects/esp-idf/en/stable/esp32/api-reference/peripherals/adc_calibration.html
20. PCBgogo. What you need to know to understand inductive sensors [Internet]. Available from: https://www.pcbgogo.com
21. Cooley JW, Tukey JW. An algorithm for the machine calculation of complex Fourier series. Math Comput. 1965;19(90):297–301.
22. Lee S. Butterworth filter design essentials [Internet]. 2025. Available from: https://www.allaboutcircuits.com

Analysis of the Impact of Homodyne Detection Efficiency on Remote State Preparation

Wagner C. Normando Filho[1]*, Leonardo J. Pereira[1], Alexandre B. Tacla[1]
[1]QuIIN (Quantum Industrial Innovation), EMBRAPII CIMATEC Competence Center in Quantum Technologies, SENAI CIMATEC University ; Salvador, Bahia, Brazil

Continuous-variable quantum key distribution (CV-QKD) is a leading technology for secure communication, whose security guarantees fundamentally rely on the quantum nature of the transmitted states and the measurement process. However, real-world detectors invariably suffer from limitations, such as inefficiency, which affects the overall security and performance of the system. Here, we investigate the impact of detector efficiency on remote state preparation in the context of entanglement-based CV-QKD. Specifically, by using the Wigner function formalism and starting from a two-mode squeezed vacuum state, we derive the analytical form of the quantum state of one mode conditioned on a homodyne measurement performed on the other mode. Our analysis explicitly contrasts the ideal case of unit efficiency (η=1), which prepares a pure, displaced squeezed state, with the non-ideal scenario. For η < 1, we demonstrate that the preparation result is a mixed state characterized by increased noise and degraded squeezing. We calculate the exact analytical expressions for the conditional state's variance and mean displacement, quantifying their dependence on both the efficiency η and the initial squeezing parameter.

Keywords: Wigner Function. Efficiency Detection. Noise Detector.

Abbreviations: CV-QKD, Continous-Variable Quantum Key Distribution. DV-QKD, Discrete-Variable Quantum Key Distribution. EPR, Einstein-Podolsky-Rosen. GG02, Frédéric Grosshans and Philippe Grangier 2002.

Continuous-variable quantum key distribution (CV-QKD) represents one of the most promising approaches in secure quantum communication. Unlike discrete-variable QKD, CV-QKD encodes information in the quadratures of electromagnetic fields. This approach offers significant advantages, such as compatibility with standard telecommunication components, potentially high secret key rates and straightforward integration with existing optical fiber infrastructures [1,2].

In entanglement-based CV-QKD, the protocol begins with the sender, Alice, generating pairs of entangled continuous-variable states, typically twomode squeezed vacuum states. She then keeps one mode to herself and sends the other mode to the receiver, Bob. Both parties independently perform quadrature measurements (homodyne or heterodyne detection) on their respective entangled modes, obtaining correlated measurement results. After this quantum phase, Alice and Bob perform standard post-processing procedures to extract a symmetric secure secret key: they perform parameter estimation, then apply error correction and privacy amplification. Generally, the security and performance of this protocol is affected by the detector's noise and efficiency [1,3].

In this work, we investigate theoretically the impact of Alice's homodyne detection efficiency on the remote preparation of Bob's state. Theoretically, such a detector can be modeled by placing a beam splitter with transmittance η before the homodyne detector [4-8]. For this purpose, we employ the phase-space formalism of the Wigner function, a powerful tool that provides a quasi-probabilistic and intuitive representation of quantum states [9]. We start from a two-mode squeezed vacuum state, a fundamental resource for generating continuous-variable entanglement. We analyze the quantum state of Bob's mode b conditioned on the outcome of a homodyne measurement performed on Alice's mode a. By calculating and visualizing the Wigner function of the conditioned state in mode *b*, we graphically demonstrate how measurement inefficiency modify

Received on 20 December 2025; revised 22 February 2026.
Address for correspondence: Mabel Diz Marques Mota. Av. Orlando Gomes, 1845 - Piatã, Salvador – BA – Brazil, Zipcode: 41650-010. E-mail: mabel.mota@fieb.org.br / mabeldizmarques@gmail.com.

J Bioeng. Tech. Health 2025;9(3):272-276

properties of the state, such as its degree of squeezing. In the ideal case of unit efficiency (η=1), Alice projects Bob's state into a pure, displaced squeezed state. For η < 1, we show that the preparation result is a mixed state characterized by increased noise and degraded squeezing.

Wigner Function Formalism

The Wigner function, W (*x, p*), is the main tool of the phase-space formalism. It is a quasi-probability function that maps the density operator of a quantum state, $\hat{\rho}$, onto a real function in the classical phase space defined by the variables (*x, p*). In the one-dimensional case, it is defined as the Fourier transform of the displaced density operator in the position representation [9,10]:

$$W_{\hat{\rho}}(x,p) = \frac{1}{2\pi\hbar}\int e^{-\frac{ipy}{\hbar}} \langle x-\frac{y}{2}|\,\hat{\rho}\,|x+\frac{y}{2}\rangle\, dy \quad (1)$$

The Equation 1 maps the density matrix, defined in Hilbert space, to a function in the one-dimensional phase space, thus providing an equivalent way of describing the quantum state of the physical system under study [8,9,11]. The Wigner function formalism is complete in the sense that it reproduces all quantum-mechanical results obtained through the traditional Hilbert-space approach [11].

Just as in the traditional formalism, where measurements are described by Hermitian operators, the phase-space formalism also allows such operators to be represented by functions in phase space. This mapping from operators to functions is formally known as the Weyl symbol and is defined as [12]:

$$W_{\hat{A}}(x,p) = \int e^{-\frac{ipy}{\hbar}} \langle x-\frac{y}{2}|\,\hat{A}\,|x+\frac{y}{2}\rangle\, dy, \quad (2)$$

where $\hat{A}$ is an arbitrary operator.

Equations 1 and 2 are structurally very similar. The first includes a constant factor ensuring normalization, as physically realizable states must be normalized.

If $\hat{A}$ is Hermitian, the result of Equation 2 is a realvalued function in phase space [12]. In the literature, the Weyl symbol is also commonly referred to as the Wigner function of an operator. Notably, the Wigner function in Equation 1 is simply the Weyl symbol of the density operator $\hat{\rho}$, multiplied by the factor $\frac{1}{2\pi\hbar}$.

Ideal *vs* Non-Ideal Homodyne Detection

The two-mode squeezed vacuum state (EPR state) can be expressed in the Fock basis as follows [8]:

$$|\psi_{sq}\rangle_{ab} = (1-\lambda^2)^{1/2}\sum_{n=0}^{\infty}\lambda^n\,|n\rangle_a \otimes |n\rangle_b\,. \quad (3)$$

where $\lambda = tanh(\zeta)$ with ζ being the squeezing parameter. In the Wigner function formalism, the EPR state above is expressed as [8]:

$$W(a,b) = Ke^{-\frac{(x_a-x_b)^2}{4\sigma_0 s^2}-\frac{(x_a+x_b)^2}{4\sigma_0^2/s}-\frac{(p_a-pb)^2}{4\sigma_0^2/s}-\frac{(p_a+p_b)^2}{4\sigma_0^2 s}}. \quad (4)$$

Here $a = (x_a, p_b)$ and $b = (x_b, p_b)$ refer to modes *a* and *b*, respectively. Furthermore, $K = 1/(2\pi\sigma_0^2)^2$ is the normalization constant, σ_0^2 is the variance, and *s* is the squeezing factor:

$$s = e^{2\zeta}\,. \quad (5)$$

The effect of a measurement on one of the modes of a bipartite state can be described, in the Wigner function formalism, by the following general relation [8]:

$$W_{\hat{\rho}_{cond,b}}(b) = \frac{\iint_{\mathbb{R}^2} W_{\hat{\Pi}_{x_0}}(a)W_{\hat{\rho}_{ab}}(a,b)da}{\iiint\int_{\mathbb{R}^4} W_{\hat{\Pi}_{x_0}}(a)W_{\hat{\rho}_{ab}}(a,b)dadb} \quad (6)$$

In the equation above, $W_{\hat{\Pi}_{x_0}}$ is the phase-space representation of the measurement operator $\hat{\Pi}_{x_0}$ corresponding to the outcome x_0. Our goal is to use the above integral to determine the result of both ideal and non-ideal homodyne detection on mode *a* of the EPR state given in Equation 4. This system is ilustrated in Figure 1.

In the ideal case, homodyne detection of the quadrature $\hat{x}$ with outcome x_0 is described by the following POVM element [7-9].

$$\hat{\Pi}_{x_0} = |x_0\rangle\langle x_0|\,. \quad (7)$$

In the phase-space representation, the projector above corresponds to a Dirac delta distribution centered at the value x_0 [8,9]:

Figure 1. A two-mode squeezed vacuum state (EPR state) source sends mode a for Alice and mode *b* for Bob. By Alice performing a homodyne measurement on mode *a,* Bob's mode *b* collapse to *a* squeezed state for η = 1, where η is the efficiency of the homodyne detector.

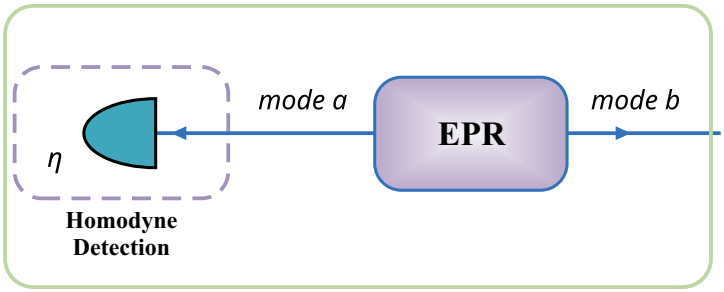

$$W_{\hat{\Pi}_{x_0}}(a) = \frac{1}{4\pi\sigma_0^2}\delta(x_a - x_0). \tag{8}$$

By substituting the expression above together with Equation 4 into Equation 6, and performing the integration, we obtain:

$$W_{\hat{\rho}_{cond,b}}(b) = K' e^{-\frac{(x_0-x_b)^2}{4\sigma_0^2 s^2} - \frac{(x_0+x_b)^2}{4\sigma_0^2/s^2} + (1-\tilde{\lambda}^2)\left[x_0^2 - A p_b^2\right]}. \tag{9}$$

Here, the constants are defined as follows:

$$K' = \frac{A\sqrt{\pi}}{\pi\sigma_0\sqrt{1-\tilde{\lambda}^2}}, \tag{10}$$

$$A = \frac{1}{4\sigma_0^2 s^2} + \frac{1}{4\sigma_0^2/s^2}, \tag{11}$$

$$B = \frac{1}{4\sigma_0^2/s^2} - \frac{1}{4\sigma_0^2 s^2}, \tag{12}$$

$2\tilde{\lambda} = B/A.$

The expression above represents the Wigner function of an EPR state conditioned on an ideal homodyne measurement on mode *a* with outcome x_0.

We now follow the same procedure, but consider *a* non-ideal homodyne measurement characterized by a finite detection efficiency η, which, the phase-space representation of the POVM [8],

$$W_{\hat{\Pi}_{\eta,x_0}}(a) = \frac{e^{\frac{x_a - x_0}{2\sigma_0^2(1-\eta)}}}{4\pi\sigma_0^2\sqrt{2\pi\sigma_0^2(1-\eta)}}, \tag{13}$$

depicted in Figure 2.

Figure 2. Comparison of the Wigner Function of the POVM for different quantum efficiencies η.

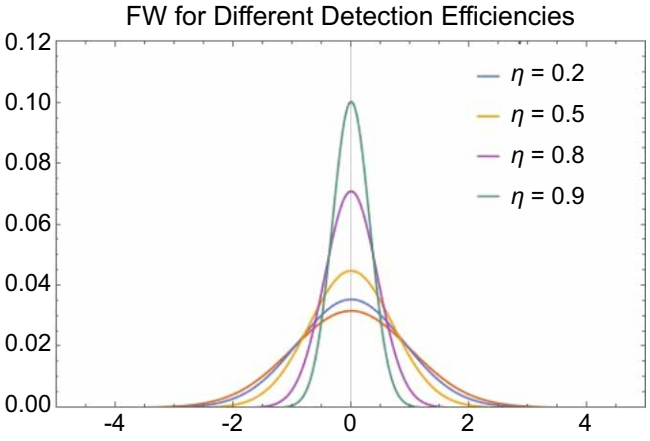

The equation above reduces to Eq.8 in the limit η → 1, which corresponds to the ideal case. By substituting this expression into Eq. 6, together with the EPR state, and evaluating the integral, we obtain the following Wigner function:

$$W^{\eta}_{\hat{\rho}_{cond,b}}(b) = \frac{e^{-\frac{(x_b-\bar{x}_b)^2}{2\sigma_x^2}} e^{-\frac{p_b^2}{2\sigma_p^2}}}{\sqrt{(2\pi\sigma_x^2)(2\pi\sigma_p^2)}}. \tag{14}$$

The variances in position and momentum, after te measurement, are given, respectively, by

$$\sigma_x^2 = \frac{[2s + (1-\eta)(s^2+1)]}{[(s^2+1) + 2(1-\eta)s]}\sigma_0^2, \tag{15}$$

$$\sigma_p^2 = \frac{(s^2+1)}{2s}\sigma_0^2, \tag{16}$$

and the mean displacement is expressed by

$$\bar{x}_b = -\frac{\sqrt{\eta}(s^2-1)}{[(s^2+1)+2(1-\eta)s]}x_0 \,. \qquad (17)$$

Figure 3 shows mode b Wigner function after mode a inefficient homodyne measurement. We see when EPR squeezing s increases, mode b x quadrature squeezes too.

Figure 3. Wigner function of mode-b state, conditioned on the measurement in mode a, for different values of s.

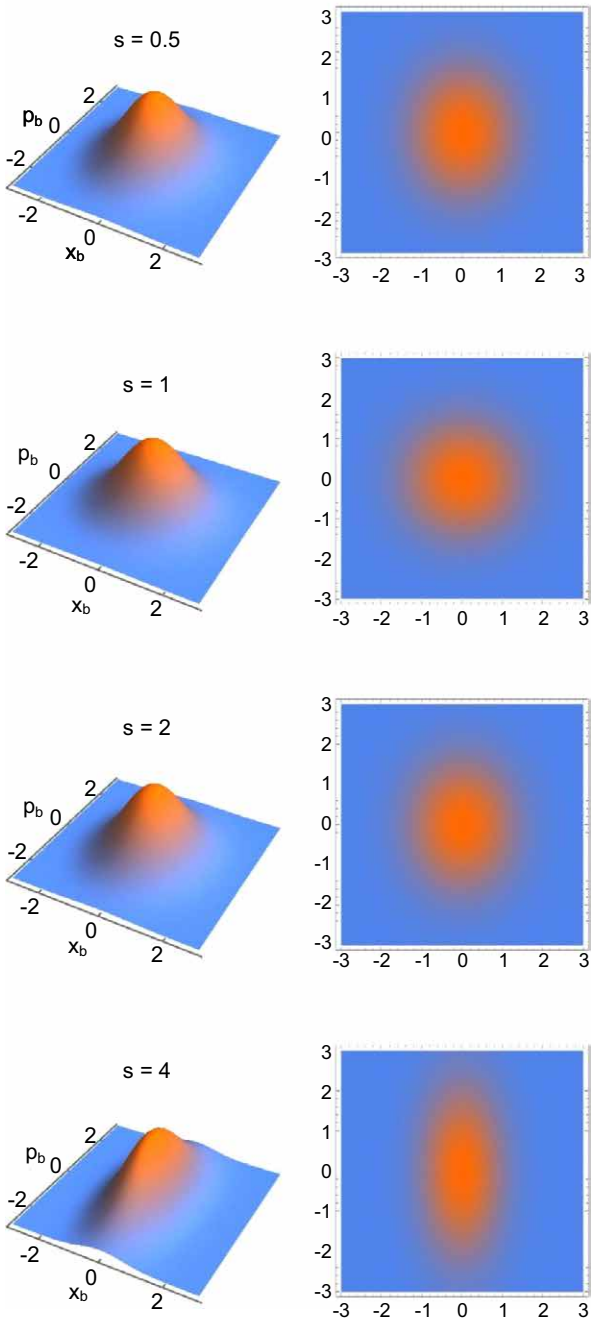

Figure 4 shows mode b amplitude $\bar{x}_b$ as function of inefficiency $(1 - \eta)$. We see inefficiency attenuate the amplitude value and EPR squeezing s increases the amplitude.

Figure 4. Mode b quadrature amplitude $\bar{x}_b$ as function of the inefficiency 1 η for different values of squeezing parameter s.

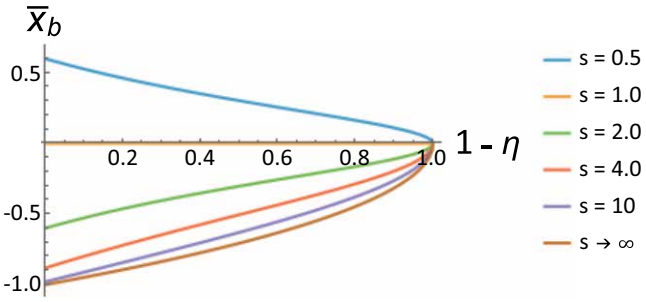

Note when $s = 1$ there is no EPR squeezing, mode b variances and x quadrature become $\sigma_x^2 = \sigma_p^2 = \sigma_0^2$ and $\bar{x}_b = 0$. This means measurement on mode a has no effect on mode b, as it should be, since zero squeezing is equivalent to separable state.

For the maximum efficiency ($\eta = 1$), mode b variances and x quadrature become σ_x^2 $\sigma_p^2 = \sigma_x^4$ and $\bar{x}_b = -x_0\ (s^2-1)/(s^2+1)$. So, when variance p increases, variance x decreases, which is a squeezed state feature (we call this a perfect squeezed state).

Conclusion

In this work, we presented a theoretical and visual analysis of how detector efficiency affects remote state preparation in entangled systems. Using the Wigner function formalism, we derived the analytical form of the conditioned quantum state and demonstrated how homodyne detection inefficiencies on Alice's mode impact the prepared state on Bob's mode. Our results show that while homodyne measurement collapses Bob's mode into a squeezed state regardless of detector efficiency, inefficiencies attenuate the quadrature amplitude and degrade the squeezing. Importantly, when EPR squeezing is absent ($s = 1$), Bob's state remains unaffected by Alice's measurements, confirming the expected behavior for separable states.

These findings provide valuable insights for the practical implementation of CV-QKD protocols, where detector inefficiencies directly impact the amount of shared correlations. By quantifying how detection losses affect state preparation, our analysis establishes a foundation for developing more accurate security models that account for realistic detector performance. This work opens the path toward incorporating detector inefficiency effects into comprehensive CV-QKD security analyses, enabling more precise estimation of achievable secret key rates.

Acknowlegement

This work has been fully funded by the project "Non-conventional Receivers for CV-QKD" supported by QuIIN Quantum Industrial Innovation, EMBRAPII CIMATEC Competence Center in Quantum Technologies, with financial resources from the PPI IoT/Manufatura 4.0 of the MCTI grant number 053/2023, signed with EMBRAPII.

References

1. Usenko VC, Acín A, Alléaume R, Andersen UL, Diamanti E, Gehring T, et al. Continuous-variable quantum communication.
2. Zhang Y, Bian Y, Li Z, Yu S, Guo H. Continuous-variable quantum key distribution system: past, present, and future. Appl Phys Rev. 2024;11(1):011318.
3. Laudenbach F, Pacher C, Fung CHF, Poppe A, Peev M, Schrenk B, et al. Continuous-variable quantum key distribution with Gaussian modulation—the theory of practical implementations. Adv Quantum Technol. 2018;1(1):1800011.
4. Olivares S. Introduction to generation, manipulation and characterization of optical quantum states. Phys Lett A. 2021;418:127720.
5. Hogg D, Berry DW, Lvovsky AI. Efficiencies of quantum optical detectors. Phys Rev A. 2014;90(5):053846.
6. Leonhardt U. Measuring the quantum state of light. Cambridge: Cambridge University Press; 1997.
7. Ferraro A, Olivares S, Paris MGA. Gaussian states in continuous variable quantum information. arXiv [quant-ph]. 2005;0503237.
8. Morin O. Non-Gaussian states and measurements for quantum information [dissertation]. Paris: Université Pierre et Marie Curie; 2013.
9. Schleich WP. Quantum optics in phase space. Hoboken (NJ): John Wiley & Sons; 2015.
10. Wigner E. On the quantum correction for thermodynamic equilibrium. Phys Rev. 1932;40:749-759.
11. Zachos C, Fairlie D, Curtright T. Quantum mechanics in phase space: an overview with selected papers. Singapore: World Scientific; 2005.
12. Gneiting C, Fischer T, Hornberger K. Quantum phase-space representation for curved configuration spaces. Phys Rev A. 2013;88(6):062117.

A Systematic Review of Mobile Soft Robots

Tiago Barretto Sant'Anna[1]*, Lucas Cruz da Silva[1]
[1]SENAI CIMATEC University, Robotics Department; Salvador, Bahia, Brazil

This article presents a comprehensive review of the advancements in mobile soft robotics, highlighting their design, actuation mechanisms, and performance capabilities. The objective is to examine the fastest and most capable mobile soft robots, emphasizing their diverse approaches and technologies for various environments. A systematic literature review was conducted using IEEE Xplore and Scopus databases, focusing on mechanical models, actuation methods, and performance metrics. Results show that the Tunable Dynamic Walking robot, using vibration through soft twisted beams, achieved the highest speed of 156.30 mm/s. Additionally, the Untethered Crawling Robot, employing pneumatic actuation, demonstrated the highest payload capacity of 6000 g. These findings underscore the significant progress in speed, mobility, and payload capacities of mobile soft robots. The study emphasizes the importance of continued research in enhancing the functionality and adaptability of these robots for real-world applications, including inspection, surveillance, and environmental monitoring.

Keywords: Mobile Soft Robots. Actuation Mechanisms. Robotics. Inspection. Surveillance. Pneumatic.

The field of robotics has evolved significantly, introducing innovative concepts such as soft robots, which differ from traditional robots in their flexibility and adaptability [1]. Soft robots are constructed with pliable materials that allow for more natural and safe movements, especially in interactions with humans and delicate structures [1]. This approach contrasts with traditional rigid robots, which, while robust, may be limited in applications requiring subtlety and compliance [2].

Within the vast universe of soft robots, there are various categories, including inflatable robots, robots based on electroactive polymers, and robots that use fluid-based actuation mechanisms. Each of these types has unique characteristics that make them suitable for different applications [3]. For instance, inflatable robots can be used in environments where safety is paramount, while robots using electroactive polymers can be more efficient in tasks requiring precision and detailed control [4,5].

Received on 18 December 2025; revised 10 February 2026.
Address for correspondence: Tiago Barretto Sant'Anna. Av. Orlando Gomes, 1845 - Piatã, Salvador – BA – Brazil, Zipcode: 41650-010. E-mail: tiagobarreto581@gmail.com.

J Bioeng. Tech. Health 2026;9(3):277-282

A distinction within the field of soft robotics is between static soft robots and mobile soft robots. Static soft robots are typically anchored to a fixed position and are designed for tasks such as manipulation, gripping, and interaction with their immediate surroundings. They excel in applications where their soft, adaptive nature can be used to handle delicate objects or perform complex, nuanced movements without the need for relocation [6].

In contrast, mobile soft robots combine the flexibility of soft robots with the ability to move through their environment. This mobility allows them to navigate complex and dynamic spaces, making them ideal for applications such as inspection, surveillance, and environmental monitoring [7]. Pneumatic systems use compressed air to create movement, mimicking the motion of muscles for smooth and adaptive actions [8]. Dielectric elastomers are electrically active polymers that change shape when an electric field is applied, providing lightweight and precise movements. Fluid-based actuation involves using hydraulics or liquid metals to produce strong and stable movements [9]. Additionally, vibration-based mechanisms use controlled vibrations to navigate uneven or complex terrains with precision [5].

This article aims to provide a comprehensive overview of the current state of mobile soft robots,

focusing on their design, actuation mechanisms, and performance capabilities. By examining the fastest and most capable mobile soft robots, we highlight the diverse approaches and technologies developed to enhance robot performance in different environments.

Furthermore, we explore the payload capacities of these robots, emphasizing the practical implications of their ability to carry and manipulate various loads. The diversity in actuation methods and payload capabilities demonstrates the potential of soft robots to address a wide range of tasks, from heavy lifting to delicate handling. The findings presented in this article underscore the importance of continued research and development in the field of mobile soft robotics, aiming to further improve the functionality and adaptability of these innovative machines.

Materials and Methods

This study conducted a comprehensive literature review focusing on mobile soft robots, utilizing two primary academic databases: IEEE Xplore and Scopus. The objective was to identify and analyze mechanical models of mobile soft robots that have been successfully implemented or have the potential to inspire new prototypes.

The following steps were undertaken in the method:

- Database Selection and Search Strategy: A systematic search was performed on IEEE Xplore and Scopus using specific keywords related to mobile soft robotics, such as "mobile soft robot," "soft robotics," "actuation mechanisms," and "locomotion." The search was restricted to articles published within the last ten years to ensure the inclusion of the most recent advancements in the field.
- Inclusion and Exclusion Criteria: The inclusion criteria focused on articles that described mechanical models of mobile soft robots, their actuation methods, and their performance capabilities. Articles were excluded if they did not provide sufficient experimental data or detailed descriptions of the robots' design and functionality.

This analysis can be shown in Figure 1.

- Data Extraction: Relevant information was extracted from the selected articles, including details on actuation methods, speeds, payload capacities, environments in which the robots operate, and their capabilities for forward movement, turning, and vertical motion. This data was systematically organized into tables to facilitate comparison and analysis.
- Quantitative and Qualitative Analysis: A bibliometric analysis was conducted using the Bibliometrix [10] tool to perform both quantitative and qualitative evaluations of the collected data. The quantitative analysis included metrics such as citation counts, publication trends, and the geographical distribution of research. The qualitative analysis focused on identifying common themes, challenges, and innovative solutions in the design and actuation of mobile soft robots.
- Comparison and Evaluation: The extracted data was compared to identify the fastest and strongest actuation methods and design approaches. This comparative analysis provided insights into the strengths and limitations of current mobile soft robotic technologies.
- Critical Review and Future Directions: Based on the analysis, a critical review was conducted to summarize the key findings and highlight the potential areas for future research. Recommendations were made for improving the design, functionality, and adaptability of mobile soft robots, with a focus on enhancing their practical applications in real-world scenarios.

By following this structured methodology, the study aimed to provide a thorough understanding of the current landscape of mobile soft robotics and to identify promising avenues for further innovation and development.

Figure 1. Venn diagram of searched articles.

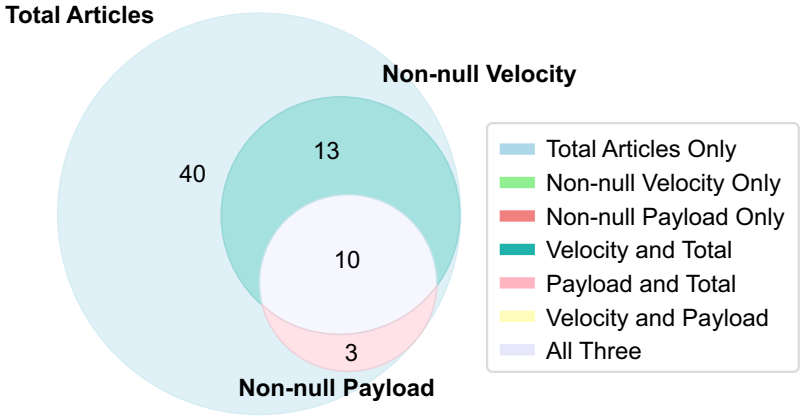

Results and Discussion

Mobile soft robots have shown advancements in speed and mobility, achieved through various actuation methods. However, the maximum speed of a robot can limit its application in different environments, as low-speed robots are not suitable for long-distance navigation. Table 1 provides a comparison of some of the fastest soft robots, highlighting their actuation mechanisms, speeds, and capabilities in different environments.

The Table 1 presents the five fastest soft robots from the articles database, detailing their tethered status, actuation methods, maximum speeds, environments, and capabilities for forward movement, turning, and vertical motion. Tethered robots are connected to external power sources via cables, while untethered robots operate independently with onboard power. Each robot is referenced by its corresponding research article.

The Tunable Dynamic Walking robot (Table 1, item 1) is tethered and utilizes vibration through soft twisted beams for actuation, reaching the highest speed of 156.30 mm/s among the compared robots. Designed for ground environments, it excels in both forward movement and turning, although it lacks vertical motion capability. This robot is referenced in the study by Jiang and colleagues [11].

The Insect-Scale Robot (Table 1, item 2) employs dielectric elastomer actuators and is untethered, achieving a significant speed of 100.00 mm/s. It is also designed for ground environments, capable of forward movement and turning, but does not support vertical motion. This robot is documented in the study by Li and colleagues [12].

A versatile example, the Soft Wall-Climbing Robot (1, item 3), uses dielectric-elastomer artificial muscles for actuation and is untethered. It can achieve speeds of 88.46 mm/s and is capable of forward movement, turning, and vertical motion. This robot's ability to climb walls, in addition to moving on the ground, makes it suitable for various inspection and surveillance applications. This robot is referenced in the study by Gu and colleagues [13].

The DECSO robot (Table 1, item 4) is another untethered robot that uses pneumatic actuation to reach speeds of 75.00 mm/s. It excels in forward movement and turning in ground environments, although it does not support vertical motion. This robot is documented in the study by Johnsen and Tsukagoshi [14].

The Thick Miniatured Mobile Soft Robot (Table 1, item 5) employs pneumatic actuators and, while its speed is lower at 31.50 mm/s, it supports forward movement, turning, and vertical motion. This capability highlights its potential for

navigating complex terrains and environments. This robot is referenced in the study Liu and colleagues [15].

The diversity in actuation methods and capabilities among the fastest mobile soft robots is evident. Each robot brings unique advantages tailored to specific environments and tasks, from ground-based operations to vertical climbing and complex terrain navigation. In terms of speed, the vibration through soft twisted beam type actuation achieved the best results with 156.30 mm/s, and this is probably due to the high operating frequency that this actuator requires.

The payload capacity of mobile soft robots is a critical parameter that defines their practical applications and functional capabilities. This capacity affects their ability to couple with sensors, transport equipment, and determines the amount of batteries the robot can carry. Table 2 provides a comparative analysis of several soft robots based on their tethered status, actuation methods, payload capacities, environments, and movement capabilities, including forward movement and turning.

The Untethered Crawling Robot (Table 2, item 1) is tethered and utilizes pneumatic actuation, boasting the highest payload capacity of 6000g among the listed robots. It is designed for ground environments and supports both forward movement and turning. This robot's significant payload capacity underscores its potential for applications requiring heavy lifting and transportation. The reference for this robot is provided by Dong and colleagues [16]. The pneumatic actuators proved to be more capable of carrying more load than the vibration-actuated ones, suggesting that the load distribution generated by the pneumatic system is more effective, as proven experimentally.

The Laser Pouch Motors robot (Table 2, item 2) also operates tethered and employs a liquid-to-gas phase change mechanism for actuation, with a payload capacity of 750g. Designed for ground environments, it is capable of forward movement but lacks data on its turning capabilities. This innovative actuation method allows the robot to manage substantial loads efficiently. The robot is referenced by Hiraki and colleagues [17]. The Legged Robot (Table 2, item 3) is untethered and uses pneumatic actuation to carry a payload of 620g. It is designed for ground environments and supports both forward movement and turning. This robot's design and functionality highlight its adaptability and robustness in navigating various terrains while carrying moderate loads. The reference for this robot is provided by Drotman and colleagues [18].

The Tripod Mobile Robot appears twice in the table with two different actuation mechanisms. The first instance (Table 2, item 4) uses soft membrane vibration for actuation, enabling it to carry a payload of 500g. It is untethered, designed for ground environments, and supports both forward movement and turning. This robot's soft membrane vibration mechanism offers a unique approach to payload management, making it suitable for delicate handling tasks. The reference for this robot is from Kim and colleagues [19].

In its second instance (Table 2, item 5), the Tripod Mobile Robot employs a vibration mechanism for actuation, with a lower payload capacity of 100g. Like its counterpart, it is untethered and supports both forward movement and turning, designed for ground environments. This configuration highlights the trade-offs between different actuation methods and payload capacities, showcasing the flexibility of design in soft robotics. The reference for this version of the robot is provided by Kim and colleagues [20].

In summary, the payload capacities of these mobile soft robots demonstrate a wide range of capabilities, from carrying heavy loads to managing delicate payloads. The diversity in actuation methods, such as pneumatic actuation, liquid-to-gas phase change, and vibration mechanisms, illustrates the innovative approaches in the field. The pneumatic robot "Untethered Crawling Robot" was able to support more weight, and this is because of this and its actuation system that guarantees better support than "Tripod Mobile Robot".

Table 1. Table 1: Fastest mobile soft robots by speed.

Item	Name	Thethered	Actuation	Speed (mm/s)	Environment	Forward movement	Turn	Vertical motion	Reference
1	Tunable Dynamic Walking	X	vibration through soft twisted beams	156.30	Ground	V	V	X	[11]
2	Insect-Scale Robot	V	dielectric elastomer	100.00	Ground	V	V	X	[12]
3	soft wall-climbing robot	V	dielectric-elastomer artificial muscles	88.46	Ground	V	V	V	[13]
4	DECSO	V	pneumatic	75.00	Ground	V	V	X	[14]
5	Thick Miniatured Mobile Soft Robot	V	pneumatic	31.50	Ground	V	V	V	[15]

Table 2. Mobile soft robots ordered by payload capacity.

Item	Name	Thethered	Actuation	Payload	Environment	Forward movement	Turn	Reference
1	Untethered Crawling Robot	X	Pneumatic	6000 g	Ground	V	V	[16]
2	Laser Pouch Motors	X	Liquid-to-Gas Phase Change	750 g	Ground	V	NaN	[17]
3	legged robot	V	Pneumatic	620 g	Ground	V	V	[18]
4	Tripod Mobile Robot	V	Soft Membrane Vibration	500 g	Ground	V	V	[19]
5	Tripod Mobile Robot	V	Vibration Mechanism"	100 g	Ground	V	V	[20]

Conclusion

This study has provided a comprehensive review of the advancements and current state of mobile soft robotics. By analyzing various mechanical models and their actuation mechanisms, we have highlighted the significant progress made in the field, particularly in terms of mobility, adaptability, and payload capacities. The diversity in actuation methods, such as pneumatic systems, dielectric elastomers, and vibration-based mechanisms, underscores the innovative approaches that have been employed to enhance the performance of mobile soft robots.

The comparative analysis of the fastest and most capable mobile soft robots revealed that each robot brings unique advantages tailored to specific environments and tasks. From ground-based operations to vertical climbing and complex terrain navigation, these robots demonstrate the potential for widespread applications, including inspection, surveillance, and environmental monitoring. This review found that robot Tunable Dynamic Walking with actuation model vibration through soft twisted beams had the fastest performance.

Moreover, the payload capacities of these robots show a wide range of capabilities, from heavy lifting to delicate handling, further emphasizing their versatility. Here it was found that the pneumatic actuation model had the best performance supporting 6000g load. The findings indicate that continued research and development in mobile soft robotics are essential to address the existing challenges and to optimize the design and functionality of these robots.

Future research should focus on exploring new actuation mechanisms, improving multifunctional capabilities, and enhancing the adaptability of mobile soft robots to various real-world scenarios. By building on the current advancements, the

field of mobile soft robots can continue to evolve, offering innovative solutions for a broad spectrum of applications.

In conclusion, the ongoing development and refinement of mobile soft robots hold great promise for the future, with the potential to revolutionize the way we approach tasks in challenging environments. The insights gained from this study provide a solid foundation for future innovations and practical implementations in the field of soft robotics.

Acknowledgement

The authors would like to acknowledge Shell Brasil Petróleo LTDA, the Brazilian Company for Industrial Research and Innovation (EMBRAPII), and Brazilian National Agency for Petroleum, Natural Gas and Biofuels (ANP) for the support and investments in RD&I.

References

1. Rus D, Tolley MT. design, fabrication and control of soft robots. Nature. 2015;521(7553):467-475. doi:10.1038/nature14543.
2. Khan AH, Li S, Zhou X. dynamic manipulation of pneumatically controlled soft finger for home automation. Measurement. 2021;170:108680. doi:10.1016/j.measurement.2020.108680.
3. Lee C, Kim M, Kim YJ, Hong N, Ryu S, Kim HJ, et al. soft robot review. Int J Control Autom Syst. 2017;15(1):3-15. doi:10.1007/s12555-016-0462-3.
4. Oliveira J, Ferreira A, Reis JCP. design and experiments on an inflatable link robot with a built-in vision sensor. Mechatronics. 2020;65:102305. doi:10.1016/j.mechatronics.2019.102305.
5. Kaal W, Herold S. electroactive polymer actuators in dynamic applications. IEEE/ASME Trans Mechatron. 2011;16(1):24-32. doi:10.1109/TMECH.2010.2089529.
6. Shintake J, Cacucciolo V, Floreano D, Shea H. soft robotic grippers. Adv Mater. 2018;30(29). doi:10.1002/adma.201707035.
7. Qin L, Tang Y, Gupta U, Zhu J. a soft robot capable of 2D mobility and self-sensing for obstacle detection and avoidance. Smart Mater Struct. 2018;27(4):045017. doi:10.1088/1361-665X/aaab393.
8. Diteesawat RS, Helps T, Taghavi M, Rossiter J. electro-pneumatic pumps for soft robotics. Sci Robot. 2021;6(51). doi:10.1126/scirobotics.abd3721.
9. Zhao Y, Yin L, Zhong S, Zha J, Dang Z. review of dielectric elastomers for actuators, generators and sensors. IET Nanodielectr. 2020;3(4):99-106. doi:10.1049/iet-nde.2019.0045.
10. Aria M, Cuccurullo C. bibliometrix: an R-tool for comprehensive science mapping analysis. J Informetr. 2017;11(4):959-975.
11. Jiang Y, Chen F, Aukes DM. tunable dynamic walking via soft twisted beam vibration. IEEE Robot Autom Lett. 2023;8(4):1967-1974. doi:10.1109/LRA.2023.3244716.
12. Li T, Zou Z, Mao G, Yang X, Liang Y, Li C, et al. agile and resilient insect-scale robot. Soft Robot. 2019;6(1):133-141. doi:10.1089/soro.2018.0053.
13. Gu G, Zou J, Zhao R, Zhao X, Zhu X. soft wall-climbing robots. Sci Robot. 2018;3(25). doi:10.1126/scirobotics.aat2874.
14. Johnsen LP, Tsukagoshi H. deformation-driven closed-chain soft mobile robot aimed for rolling and climbing locomotion. IEEE Robot Autom Lett. 2022;7(4):10264-10271. doi:10.1109/LRA.2022.3191798.
15. Liu Z, Liu J, Wang H, Yu X, Yang K, Liu W, et al. a 1 mm-thick miniatured mobile soft robot with mechanosensation and multimodal locomotion. IEEE Robot Autom Lett. 2020;5(2):3291-3298. doi:10.1109/LRA.2020.2976306.
16. Dong X, Tang C, Jiang S, Shao Q, Zhao H. increasing the payload and terrain adaptivity of an untethered crawling robot via soft-rigid coupled linear actuators. IEEE Robot Autom Lett. 2021;6(2):2405-2412. doi:10.1109/LRA.2021.3061342.
17. Hiraki T, Nakahara K, Narumi K, Niiyama R, Kida N, Takamura N, et al. laser pouch motors: selective and wireless activation of soft actuators by laser-powered liquid-to-gas phase change. IEEE Robot Autom Lett. 2020;5(3):4180-4187. doi:10.1109/LRA.2020.2982864.
18. Drotman D, Jadhav S, Karimi M, de Zonia P, Tolley MT. 3D printed soft actuators for a legged robot capable of navigating unstructured terrain. In: IEEE international conference on robotics and automation (ICRA); 2017. doi:10.1109/ICRA.2017.7989652.
19. Kim D, Kim JI, Park YL. a simple tripod mobile robot using soft membrane vibration actuators. IEEE Robot Autom Lett. 2019;4(3):2289-2295. doi:10.1109/LRA.2019.2902018.
20. Kim JI, Hong M, Lee K, Kim D, Park YL, Oh S. learning to walk a tripod mobile robot using nonlinear soft vibration actuators with entropy adaptive reinforcement learning. IEEE Robot Autom Lett. 2020;5(2):2317-2324.

Instructions for Authors

The Authors must indicate in a cover letter the address, telephone number and e-mail of the corresponding author. The corresponding author will be asked to make a statement confirming that the content of the manuscript represents the views of the co-authors, that neither the corresponding author nor the co-authors have submitted duplicate or overlapping manuscripts elsewhere, and that the items indicated as personal communications in the text are supported by the referenced person. Also, the protocol letter with the number should be included in the submission article, as well as the name of sponsors (if applicable).

Manuscripts may be submitted within designated categories of communication, including:

- Original basic or clinical investigation (original articles on topics of broad interest in the field of bioengineering and biotechnology applied to health). We particularly welcome papers that discuss epidemiological aspects of international health, clinical reports, clinical trials and reports of laboratory investigations.
- Case presentation and discussion (case reports must be carefully documented and must be of importance because they illustrate or describe unusual features or have important practice implications).
- Brief reports of new methods or observations (short communications brief reports of unusual or preliminary findings).
- State-of-the-art presentations (reviews on protocols of importance to readers in diverse geographic areas. These should be comprehensive and fully referenced).
- Review articles (reviews on topics of importance with a new approach in the discussion). However, review articles only will be accepted after an invitation of the Editors.
- Letters to the editor or editorials concerning previous publications (correspondence relating to papers recently published in the Journal, or containing brief reports of unusual or preliminary findings).
- Editor's corner, containing ideas, hypotheses and comments (papers that advance a hypothesis or represent an opinion relating to a topic of current interest).
- Innovative medical products (description of new biotechnology and innovative products applied to health).
- Health innovation initiatives articles (innovative articles of technological production in Brazil and worldwide, national policies and directives related to technology applied to health in our country and abroad).

The authors should checklist comparing the text with the template of the Journal.

Supplements to the JBTH include articles under a unifying theme, such as those summarizing presentations of symposia or focusing on a specific subject. These will be added to the regular publication of the Journal as appropriate, and will be peer reviewed in the same manner as submitted manuscripts.

Statement of Editorial Policy

The editors of the Journal reserve the right to edit manuscripts for clarity, grammar and style. Authors will have an opportunity to review these changes prior to creation of galley proofs. Changes in content after galley proofs will be sent for reviewing and could be required charges to the author. The JBTH does not accept articles which duplicate or overlap publications elsewhere.

Peer-Review Process

All manuscripts are assigned to an Associate Editor by the Editor-in-Chief and Deputy Editor, and sent to outside experts for peer review. The Associate Editor, aided by the reviewers' comments, makes a recommendation to the Editor-in-Chief regarding the merits of the manuscript. The Editor-in-Chief makes a final decision to accept, reject, or request revision of the manuscript. A request for revision does not guarantee ultimate acceptance of the revised manuscript.

Manuscripts may also be sent out for statistical review ou *ad hoc* reviewers. The average time from submission to first decision is three weeks.

Revisions

Manuscripts that are sent back to authors for revision must be returned to the editorial office by 15 days after the date of the revision request. Unless the decision letter specifically indicates otherwise, it is important not to increase the text length of the manuscript in responding to the comments. The cover letter must include a point-by-point response to the reviewers and Editors comments, and should indicate any additional changes made. Any alteration in authorship, including a change in order of authors, must be agreed upon by all authors, and a statement signed by all authors must be submitted to the editorial office.

Style

Manuscripts may be submitted only in electronic form by www.jbth.com.br. Each manuscript will be assigned a registration number, and the author notified that the manuscript is complete and appropriate to begin the review process. The submission file is in OpenOffice, Microsoft Word, or RTF document file format for texts and JPG (300dpi) for figures.

Authors must indicate in a cover letter the address, telephone number, fax number, and e-mail of the corresponding author. The corresponding author will be asked to make a statement confirming that the content of the manuscript represents the views of the co-authors, that neither the corresponding author nor the co-authors have submitted duplicate or overlapping manuscripts elsewhere, and that the items indicated as personal communications in the text are supported by the referenced person.

Manuscripts are to be typed as indicated in Guide for Authors, as well as text, tables, references, legends. All pages are to be numbered with the order of presentation as follows: title page, abstract, text, acknowledgements, references, tables, figure legends and figures. A running title of not more than 40 characters should be at the top of each page. References should be listed consecutively in the text and recorded as follows in the reference list, and must follow the format of the National Library of Medicine as in Index Medicus and "Uniform Requirements for Manuscripts Submitted to Biomedical Journals" or in "Vancouver Citation Style". Titles of journals not listed in Index Medicus should be spelled out in full.

Manuscript style will follow accepted standards. Please refer to the JBTH for guidance. The final style will be determined by the Editor-in-Chief as reviewed and accepted by the manuscript's corresponding author.

Approval of the Ethics Committee

The JBTH will only accept articles that are approved by the ethics committees of the respective institutions (protocol number and/or approval certification should be sent after the references). The protocol number should be included in the end of the Introduction section of the article.

Publication Ethics

Authors should observe high standards with respect to publication ethics as set out by the International Committee of Medical Journal Editors (ICMJE). Falsification or fabrication of data, plagiarism, including duplicate publication of the authors' own work without proper citation, and misappropriation of the work are all unacceptable practices. Any cases of ethical misconduct are treated very seriously and will be dealt with in accordance with the JBTH guidelines.

Conflicts of Interest

At the point of submission, each author should reveal any financial interests or connections, direct or indirect, or other situations that might raise the question of bias in the work reported or the conclusions, implications, or opinions stated - including pertinent commercial or other sources of funding for the individual author(s) or for the associated department(s) or organizations(s), and personal relationships. There is a potential conflict of interest when anyone involved in the publication process has a financial or other beneficial interest in

the products or concepts mentioned in a submitted manuscript or in competing products that might bias his or her judgment.

Material Disclaimer

The opinions expressed in JBTH are those of the authors and contributors, and do not necessarily reflect those of the SENAI CIMATEC, the editors, the editorial board, or the organization with which the authors are affiliated.

Privacy Statement

The names and email addresses entered in this Journal site will be used exclusively for the stated purposes of this journal and will not be made available for any other purpose or to any other party.

Brief Policies of Style

Manuscript	Original	Review	Birief Comunication	Case Report	Editorial ; Letter to the Editor; Editor' s Corner	Innovative Medical Products	State-of-the-Art	Health Innovation Initiatives
Font Type	Times or Arial	Times or Arial	Times or Arial	Times or Arial	Times or Arial	Times or Arial	Times or Arial	Times or Arial
Number of Words – Title	120	90	95	85	70	60	120	90
Font Size/Space-Title	12; double space	12; double space	12; double space	12; double space	12; double space	12; double space	12; double space	12; double space
Font Size/Space-Abstracts/Key Words and Abbreviations	10; single space	10; single space	10; single space	10; single space	-	-	10; single space	10; single space
Number of Words – Abstracts/Key Words	300/5	300/5	200/5	250/5	-	-	300/5	300/5
Font Size/Space-Text	12; Double space	12; Double space	12; Double space	12; Double space	12; Double space	12; Double space	12; Double space	12; Double space
Number of Words – Text	5,000 including spaces	5,500 including spaces	2,500 including spaces	1,000 including spaces	1,000 including spaces	550 including spaces	5,000 including spaces	5,500 including spaces
Number of Figures	8 (title font size 12, double space)	3 (title font size 12, double space)	2 (title font size 12, double space)	2 (title font size 12, double space)	-	2 (title font size 12, double space)	8 (title font size 12, double space)	8 (title font size 12, double space)
Number of Tables/Graphic	7 title font size 12, double space	2 title font size 12, double space	2(title font size 12, double space)	1(title font size 12, double space)	-	-	7 title font size 12, double space	4 title font size 12, double space
Number of Authors and Co-authors*	15	10	5	10	3	3	15	10
References	20 (font size 10,single space	30(font size 10,single space	15 (font size 10,single space)	10 (font size 10,single space)	10 (font size 10,single space	5(font size 10,single space	20 (font size 10,single space	20

*First and last name with a sequencing overwritten number. Corresponding author(s) should be identified with an asterisk; Type 10, Times or Arial, single space. Running title of not more than 40 characters should be at the top of each page. References should be listed consecutively in the text. References must be cited on (not above) the line of text and in brackets instead of parentheses, e.g., [7,8]. References must be numbered in the order in which they appear in the text. References not cited in the text cannot appear in the reference section. References only or first cited in a table or figures are numbered according to where the table or figure is cited in the text. For instance, if a table is placed after reference 8, a new reference cited in table 1 would be reference 9.1 would be reference 9.

Checklist for Submitted Manuscripts

❑1. Please provide a cover letter with your submission specifying the corresponding author as well as an address, telephone number and e-mail.

❑2. Submit your paper using our website www.jbth.com.br. Use Word Perfect/Word for Windows, each with a complete set of original illustrations.

❑3. The entire manuscript (including tables and references) must be typed according to the guidelines instructions.

❑4. The order of appearance of material in all manuscripts should be as follows: title page, abstract, text, acknowledgements, references, tables, figures/graphics/diagrams with the respective legends.

❑5. The title page must include a title of not more than three printed lines (please check the guidelines of each specific manuscript), authors (no titles or degrees), institutional affiliations, a running headline of not more than 40 letters with spaces.

❑6. Acknowledgements of persons who assisted the authors should be included on the page preceding the references.

❑7. References must begin on a separate page.

❑8. References must be cited on (not above) the line of text and in brackets instead of parentheses, e.g., [7,8].

❑9. References must be numbered in the order in which they appear in the text. References not cited in the text cannot appear in the reference section. References only or first cited in a table or figures are numbered according to where the table or figure is cited in the text. For instance, if a table is placed after reference 8, a new reference cited in table 1 would be reference 9.

❑10. Reference citations must follow the format established by the "Uniform Requirements for Manuscripts Submitted to Biomedical Journals" or in "Vancouver Citation Style".

❑11. If you reference your own unpublished work (i.e., an "in press" article) in the manuscript that you are submitting, you must attach a file of the "in press" article and an acceptance letter from the journal.

❑12. If you cite unpublished data that are not your own, you must provide a letter of permission from the author of that publication.

❑13. Please provide each figure in high quality (minimum 300 dpi: JPG or TIF). Figure must be on a separate file.

❑14. If the study received a financial support, the name of the sponsors must be included in the cover letter and in the text, after the author's affiliations.

❑15. Provide the number of the Ethics Committees (please check the guidelines for authors).